THE
PHYSICAL REVIEW
A Journal of Experimental and Theoretical Physics Established by E. L. Nichols in 1893
VOL. 50, NO. 7 OCTOBER 1, 1936 SECOND SERIES

The Latitude Effect in Cosmic Rays at Altitudes up to 29,000 Feet

I. S. BOWEN, R. A. MILLIKAN, S. A. KORFF AND H. V. NEHER, *Norman Bridge Laboratory of Physics, California Institute of Technology, Pasadena, California*

(Received July 20, 1936)

Accurate measurements with Neher recording electroscopes have been made both in Peru and in the Philippines on the cosmic-ray ionization of the atmosphere up to altitudes of 29,000 feet, with the following results: (1) In both localities the ionization rises essentially exponentially following a coefficient $\mu = 0.50$ per meter of water. This means that in the equatorial belt the ionization at 29,000 feet (two-thirds of the way to the top of the atmosphere) is about 50 ions per cc per sec., or half its value at the same altitude in the temperate zone. (2) If any longitude effect such as that which we have proved to exist at sea level exists at altitudes of 26,000 feet, it is inside the limits of our observational uncertainty, about 5 percent.

THE latitude effect at sea level first announced by Clay in 1927 has since then been made the subject of very extensive investigation by many observers,[1] but our knowledge of the even more important latitude effect at altitudes far above the earth's surface thus far rests upon comparatively meager dependable data. Bowen, Millikan and Neher have published exceedingly consistent observations made with Neher vibration-free electroscopes in airplane flights made in northern Canada (near The Pas, mag. lat. 64° N.), in northern United States (near Spokane, mag. lat. 54° N.), in southern United States (near Pasadena, mag. lat. 41° N.), in Panama, (mag. lat. 21° N.), and in Peru (mag. lat. 1° S.). Some of these flights reached the altitude of 29,000 feet (3.3 m of water or 2/3 of the way to the top) and all of them exceeded the altitude of 22,000 feet. These flights revealed the significant facts that (1) there is no latitude effect at all at altitudes up to 22,000 feet north of Spokane; (2) that at that altitude there is a reduction of 11.5 percent in the cosmic-ray intensity between Spokane and Pasadena; (3) that there is a still farther fall of 25 percent from the Spokane value between Pasadena and Panama, or 36.7 percent all told; and (4) that there is no change at all between Panama and Peru. Also, at very much higher altitudes, up to 55,000 feet (1 m of water or 90 percent of the way to the top of the atmosphere), the observations of Bowen, Millikan and Neher,[2] made with Neher electroscopes in the Fordney-Settle manned-balloon flight, and of Bowen, Millikan and Neher made with self-registering electroscopes sent up with sounding balloons, brought to light a latitude difference at this high altitude amounting to 40 percent between geomagnetic latitudes 52° N. and 42° N. Both of these observations, in magnetic latitudes 52° and 42°, have been twice roughly checked in different years, so that they may be depended

[1] The results obtained by many observers are summarized in an article by A. H. Compton, Phys. Rev. **43**, 387 (1933), and our own elaborate "Precision Survey" is found in Phys. Rev. **50**, 15 (1936).

[2] See curves in Fig. 6, p. 221, *International Conference on Nuclear Physics*, London, 1934; also Fig. 6, Phys. Rev. **46**, 650 (1934).

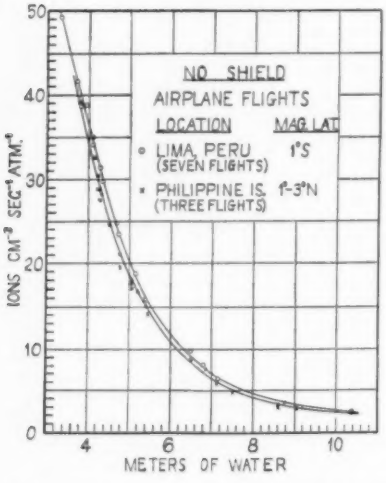

FIG. 1. Comparison between the altitude-ionization curves in Peru and in the Philippines at essentially the same geomagnetic latitude.

upon as to general order of magnitude. Clay has also reported some preliminary high altitude observations in Java.[3]

The present investigation extends the dependable observations on cosmic-ray intensities made with Neher electroscopes up to 29,000 feet in Peru, and, more important, fixes the extent of the longitude effect in the equatorial belt from sea level up to beyond 26,000 feet. The importance of this last observation arises from its bearing upon the much discussed question as to the fraction of the cosmic radiation that enters our atmosphere in the form of charged particles and the fraction that consists of photons. The very existence of the *longitude* effect at sea level discovered[4] independently early in 1934 by Clay and by Millikan and Neher, and shown by the latter observers to be represented by a 4 or 5 percent smaller sea-level cosmic-ray intensity in the equatorial belt on the Asiatic side of the earth than on the South American side, obviously means that a portion, at least, of the "nonfield-sensitive" sea-level intensity is the result of incoming charged particles of sufficient energy (about 10 billion electron volts) to get through the blocking effect of the earth's magnetic field even in the equatorial belt; for this blocking effect is larger on the Asiatic side of the earth than on the South American side, since the earth's magnetic field is known to be stronger in the Singapore region than in the Lima area.

If, then, this longitude difference, small at sea level, is, like the latitude effect, large at high altitudes, the only possible interpretation would be that even the incoming equatorial cosmic rays are chiefly very high energy charged particles. If, on the other hand, it diminishes with altitude instead of increasing, the natural interpretation would be, since photons cannot possibly show either a longitude or a latitude effect at all, that the effect of the incoming photons preponderates over that of the incoming electrons—a result which would of course speak in favor of a large photonic component in the nonfield-sensitive rays that alone can get into the equatorial belt. It was, then, primarily to obtain new light on this point that a comparison was sought between the "altitude-ionization" curves in Peru and, in essentially the same geomagnetic latitude, in the Philippines. The results of this comparison are shown in Fig. 1.

The Peru curve was obtained as the result of seven different flights in which unshielded Neher self-recording electroscopes were taken up to altitudes which reached heights of 29,000 feet, two-thirds of the way to the top of the atmosphere. These flights were arranged for and in some cases made by S. A. Korff in collaboration with the Pan American Airways, the Compania de Aviacion Faucett, and by Mr. Hugh I. Wells, to all of which services we desire herewith to express great appreciation for their assistance. The satisfactory way in which all the points taken on these seven different flights, each point corresponding to a "leveling off" by the pilot for about an hour's time, fall on a smooth curve is evidence enough of the dependability of these measurements. The films corresponding to these flights were shipped back to us at Pasadena and there measured by H. V. Neher.

To obtain the second of the curves shown in Fig. 1, H. V. Neher went to the Philippines in November, 1935, and had an unshielded electroscope like that used in the Peru flights taken up in three flights made by Captain Kirby and Lieutenants Morrill and McGuire through the

[3] J. Clay, Physica **1**, 376 (1934); **2**, 183 (1935).
[4] Millikan and Neher, Phys. Rev. **47**, 206 (1935).

kind cooperation of the U. S. Army air-corps. Here again the consistency of the points attests the dependability of the curve.

The conclusions to be drawn from these two curves may be stated as follows:

1. *Within the uncertainty of the measurements* here estimated at five percent there is at 26,000 feet no difference between the cosmic-ray intensities in Peru and in the Philippines. The sea-level difference of four percent may continue up to the highest altitudes here reached, but the precision of the measurements is insufficient to determine whether it does or not. The difference cannot, however, be appreciably more than that.

2. In the equatorial belt on both sides of the world the cosmic-ray ionization rises essentially exponentially from sea level to an altitude of 29,000 feet with an apparent absorption coefficient of 0.5 per meter of water fitting well the upper part of the depth-ionization curve. In the temperate latitudes the coefficient that must be used to fit the observed curves equally well is only a little larger, namely, 0.55 per meter of water. This difference is sufficient, however, to make the ionization in the equatorial belt at 29,000 feet (about 50 ions cc/sec. in air at 1 atmos.) about 50 percent of its value at the same altitude in the temperate latitude 52, in which the Fordney-Settle flight was made. These results destroy the validity of the chief argument that has been advanced thus far for the great preponderance of the particle component over the photonic component of the cosmic rays which come into the earth's atmosphere in the equatorial belt.

We wish to express our appreciation to the Carnegie Corporation of New York and the Carnegie Institution of Washington as well as to the above-mentioned air services through whose aid the foregoing results have been made possible.

OCTOBER 1, 1936 PHYSICAL REVIEW VOLUME 5

The Heavy Particle Component of the Cosmic Radiation

R. B. BRODE, H. G. MACPHERSON AND M. A. STARR, *Department of Physics, University of California, Berkeley, California*

(Received July 27, 1936)

A large Wilson cloud chamber was used to study the heavy particles in the cosmic radiation. The chamber had a volume of 7 liters and an illuminated section 5 cm deep by 30 cm in diameter, so that there was no danger of confusing alpha-particle tracks with heavy cosmic rays. Heavy tracks made in the 1.5 seconds preceding the expansion were recorded. In 8500 pictures, about 80 heavy tracks were observed. Of these, 21 were made by particles of about the ionization of slow protons. Their paths could be seen in the illumination for distances equivalent to path lengths of from 13 to 45 cm in air. 45 less dense old tracks were observed that had an ionization noticeably greater than an electron track. Of the tracks that appeared to have tripped the counters causing the expansion, 14 were considerably heavier than electron tracks. Three disintegrations with heavy tracks apparently arising from the wall of the chamber were observed. Most of the other old heavy tracks were also probably of secondary origin. It is estimated that about one percent of the sea-level cosmic ionization is due directly to heavy particles.

INTRODUCTION

THE analysis of the variation of the cosmic-ray intensity with altitude led Compton and Bethe[1] to propose that the primary cosmic radiation consisted in part of very high energy protons and alpha-particles. However, the Wilson cloud chamber photographs of the cosmic radiation did not seem to give much support to their hypothesis. Blackett[2] showed that the frequency of appearance and the magnitude and range of most of the heavy particles observed in cloud chamber photographs could be accounted for as contamination alpha-particles emitted from the walls of the chamber. Blackett and Occhialini,[3] reported two heavy tracks which were probably due to protons. In a large chamber located on

[1] A. H. Compton and H. A. Bethe, Nature **134**, 734 (1934).

[2] P. M. S. Blackett, Proc. Roy. Soc. **A146**, 281 (1934).

[3] P. M. S. Blackett and G. P. S. Occhialini, Proc. Roy. Soc. **A139**, 699 (1933).

the Jungfrau (3500 meters elevation) Herzog and Scherrer[4] observed one probable proton track in 165 pictures. Rieder and Hess[5] in 1200 pictures taken in a chamber at an elevation of 2300 meters found 3 tracks with a range of 5 cm which they concluded were not due to contaminating alpha-particles. Most of the proton tracks reported by Kunze[6] are undoubtedly positrons but a few of his tracks appear to be due to heavy particles. Anderson[7] has recently reported the results of his cloud chamber experiment on Pike's Peak (elevation 4300 meters) in which he observed a number of heavy particle tracks. The existence of heavy particles in the cosmic radiation at very great altitude has also been verified by the tracks left in photographic emulsion.[8,9]

Montgomery, Ramsey and Swann[10] attempted to identify heavy particles as a component of the cosmic radiation at sea level by measurements with an ionization chamber combined with a coincidence counter. From their measurements they concluded that if heavy particles existed at sea level they were present in negligible numbers. Clay,[11] however, concluded that heavy particles were occasionally present in an ionization chamber as the result of some disintegration phenomena occurring in the walls of the chamber.

In a chamber where the illuminated region is only 1 or 2 cm broad it is not possible to distinguish an alpha-particle track that passes perpendicularly through the light beam from a cosmic heavy particle. However, if the depth of the chamber is considerably greater than the range of an alpha-particle it can easily be identified. In the chamber used in this experiment the depth corresponded to 20 cm range and it was possible to observe particles with ranges up to 60 cm in the chamber. All tracks shorter than 10 cm range were not counted as possible heavy cosmic particles.

[4] G. Herzog and P. Scherrer, J. de phys. et rad. (VII) **6**, 489 (1935).
[5] F. Rieder and V. F. Hess, Nature **134**, 772 (1934).
[6] P. Kunze, Zeits. f. Physik **83**, 1 (1933).
[7] C. A. Anderson and S. H. Neddermeyer, Phys. Rev. **49**, 415 (1936).
[8] T. R. Wilkins and H. St. Helens, Phys. Rev. **49**, 403 (1936).
[9] L. H. Rumbaugh and G. L. Locher, Phys. Rev. **49**, 889 (1936).
[10] C. G. Montgomery, D. D. Montgomery, W. E. Ramsey and W. F. G. Swann, Phys. Rev. **49**, 890 (1936).
[11] J. Clay, Physica **2**, 111 (1935).

Apparatus

The Wilson cloud chamber used in these experiments was not essentially different from the chamber designed by Blackett. The chamber was 30 cm in diameter and 10 cm deep. It had a front glass of half-inch "Tufflex" glass and in the back a wire gauze covered with black velvet. The piston was a thin aluminum sheet attached to a rubber ring at the edges. The face of the aluminum sheet was covered with a thin layer of paraffin to keep the gas of the chamber from contact with the aluminum. Compressed air pushed the piston up against stops whose position could be adjusted to vary the expansion ratio. With nitrogen in the chamber at two atmospheres pressure and a mixture of 3 parts ethyl alcohol and one of water, an expansion ratio of 1.125 gave good tracks. To keep a more uniform distribution of vapor in the chamber a small dish of the mixed liquids was placed above a lead shelf at the top of the chamber. The lead shelf was introduced to study the showers produced in the lead.

The chamber was tripped by a coincidence beween a Geiger-Müller counter above and one below the chamber. The thyratron that was tripped by the counter sent a current through the moving coil of a dynamic loudspeaker. This speaker coil pulled a small roller bearing trip from under a valve and released the air from the chamber. The breadth of the tracks of the cosmic rays indicated a delay of 0.015 second from the arrival of the cosmic ray to the full expansion. 0.035 second later the illumination began and continued for about 0.1 second. As a source of light eight 150-watt 110-volt type C Mazda lamps were used on 220 volts d.c. They were focused through the chamber by cylindrical lenses. To prevent the breaking of the lamps at the seal-in a choke was placed in the supply line to limit the current until the filaments became hot. The first set of lamps was destroyed by an accident but the present set show no signs of wear after over 6000 pictures.

A pair of Kodak Retina cameras with Schneider-Kreuznach f: 3.5 lenses were used to photograph the chamber. The cameras were set on opposite sides of the normal to the plane of the chamber at angles 15° to the normal. The photographs were taken on Eastman Super X

film which was developed two minutes in Eastman D-8 developer. The lenses were tested[12] by photographing straight lines through the front glass of the chamber and were found to introduce fictitious curvatures of about 40 meters radius in lines 7 cm from the center. This distortion was negligible compared with a distortion of 10 meters radius of curvature introduced by turbulence in the chamber. The chamber turbulence was however sufficiently consistent so that tracks could be measured to a radius of curvature of 20 meters.

The operation of the chamber was entirely automatic. To eliminate the turbulence that followed an expansion, the chamber was allowed to stand from 40 sec. to 1 min. after an expansion. No slow or clearing expansions were required. The average time elapsed in waiting for a coincidence was two minutes. 75 percent of the pictures showed a cosmic-ray track that passed through the two counters. A clearing field of 45 volts was applied between the front and back of the chamber. This clearing field did not cause a measurable separation of the ions in the track of the cosmic ray that tripped the chamber. The tracks produced in the second before the expansion are still visible but because of their diffuseness they do not interfere with the study of the sharp tracks.

The apparatus was located on the top floor of a 3-story reinforced concrete building. Directly over the apparatus was only a thin sheet iron roof. Although the Lawrence cyclotron was located in a building 200 feet away, no correlation between its operation and the appearance of heavy particles in the chamber was observed.

Identification of Proton Tracks

Heavy particles are recognizable in a cloud chamber by the fact that at moderate and slow speeds they produce greater ionization than an electron. It is possible to estimate the relative ionizing power of a particle from the apparent breadth of its track if the length of time between the passage of the particle and the completion of the expansion is known.[2] The ionizing particle leaves ions in its path concentrated in a very narrow column. The ions will rapidly diffuse away from the center of this column, producing a broadening of the track. The diffusion of the tracks will be effectively stopped at the completion of the expansion when each ion becomes the nucleus of a relatively heavy water drop. Although the distribution of ions in any track will be of a Gaussian character, the photographic film will show a complete blackening in the case of a heavy track to a point where the density of water drops reaches a certain minimum critical value, and will show a rapidly fading shaded edge outside this region. The distance from the center at which the critical density of ions is reached will be a function of the total number of ions in the track. In measuring the width of a track it is convenient to measure to the point where the blackness shades off rapidly at about the critical density of droplets for blackening of the film.

The superficial density of ions at any distance x from the center of the column of ionization at a time τ after the passage of the ray is[2]

$$\rho(x) = [N_0'/(4\pi D\tau)^{\frac{1}{2}}]e^{-x^2/4D\tau}, \qquad (1)$$

where D is the diffusion coefficient for the ions and N_0' is the total number of ions per cm path length after allowing for the effect of recombination. From this, the distance from the center of the track to the point where the superficial density of ions is ρ_1 is given by

$$x_1 = (4D\tau \ln [N_0'/\rho_1(4\pi D\tau)^{\frac{1}{2}}])^{\frac{1}{2}}. \qquad (2)$$

The diameter or effective track width is twice this. The breadth of track for a particle of given ionizing power is then nearly proportional to the square root of the time between the passage of the particle and the formation of the droplets on the ions. In cases where the separation of the positive and negative ion columns can be measured this time can be calculated from the strength of the clearing field and the mobility of the ions. The width of the track is also a function of the ionizing power of the particle, varying as the square root of the logarithm of the number of ions formed per cm path. The value of ρ_1 will vary with the intensity of illumination and position of the track in the chamber. An average value can, however, be calculated by fitting the data for alpha-particles of known age to a curve of the type given by Eq. (2).

[12] P. M. S. Blackett and R. B. Brode, Proc. Roy. Soc. **A154**, 573 (1936).

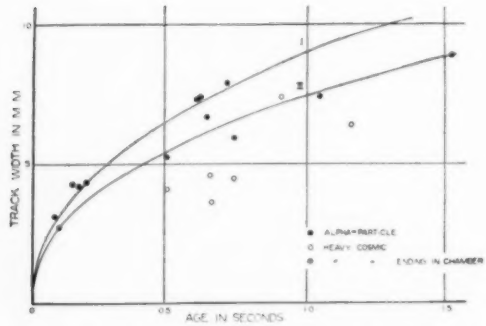

FIG. 1. Breadth of tracks as a function of age. Curve I is a theoretical curve fitted to the 4 cm range alpha-particle data by suitable choice of one constant. With the same constant, curve II is calculated for 2-million-volt protons.

In calculating the age of the tracks an average mobility for the positive and negative ions was used. The presence of alcohol vapor in the nitrogen gas of the chamber reduces the ion mobility considerably.[13] For 2.2 percent alcohol vapor a mobility constant k of 1 cm²/volt sec. is obtained. The relation k/D=constant gives for the diffusion coefficient a value of 0.0207 cm² sec.$^{-1}$.

The value of N_0' used in Eq. (2) must be calculated taking into account the effect of recombination of the ions before the positive and negative columns are separated. This problem has been considered by Jaffé.[14]

The amount of recombination will depend on the initial density of the ions, the rate of diffusion, and the length of time that the positive and negative ion clouds are allowed to overlap each other as they are pulled apart by the clearing field. For alpha-particles of 4 cm range an average of about 8×10^4 ion pairs are formed per cm path at 1.8 atmospheres pressure. About 4.16×10^4 ions/cm path are calculated to be present after recombination has been taken into account. We have measured the widths of alpha-particle tracks and calculated their age by the separation of their positive and negative ion clouds in the clearing field. The alpha-particle data are represented by the black dots in Fig. 1. Curve I is calculated from Eq. (2), and is fitted to the data at one point by choosing a suitable value of ρ_1, the critical superficial density of water droplets to blacken the film. The value of ρ_1 used is 1250 ions/cm². Curve II is calculated for an agent producing 15 percent of the ionization of an alpha-particle. This is the average ionization density in the last 16 cm of a proton's range. The circles in Fig. 1 represent the data for long heavy tracks of cosmic origin for which the time of formation could be calculated from the separation in the clearing field. It is to be seen that curve II fits the maximum track widths observed quite well. The two circles with crosses in them represent tracks that ended in the gas of the chamber. Since any ionizing particle has its maximum density of ionization at its end, it seems probable from the observed widths that these at least are protons.

The ionization to be expected from a proton goes down as the energy of the particle increases, until at 5×10^8 volts a proton has about the same ionization as an electron.[15] Since a fast proton has a less dense ionization, the photographically

FIG. 2. Heavy cosmic-ray track with a length of 15 cm showing in the chamber at 1.8 atmospheres of nitrogen. The positive and negative ion columns have been pulled apart by the clearing field, enabling the age of the track to be determined. Stereoscopic measurements show that this track ended in the gas of the chamber. Its apparent width indicates that it is probably a proton. The fine vertical line in the center of the picture is a stretched wire used as a reference line for position measurements.

[13] L. B. Loeb, Int. Crit. Tables **6**, 110 (1929).
[14] G. Jaffé, Ann. d. Physik, **42**, 303 (1913).
[15] H. Bethe, *Handbuch der Physik*, vol. 24/1, 2nd ed., (1933), p. 522.

FIG. 3. Tracks of heavy particles producing intense ionization. The tracks in Figs. 3 and 4 are all due to particles that passed through the chamber a short time previous to the expansion.

observed track will be narrower than that calculated for a slow proton. This means that any tracks of width less than that calculated for slow protons are to be ascribed to higher speed particles. In fact the width of the tracks could be used to calculate the ionization per cm path for particles whose age is known from the clearing field separation and the approximate energy of the particles could then be obtained from ionization-energy relations. However, the error of an individual observation is so great as to make this method of obtaining energies very approximate. Such a calculation involves the assumption of the nature of the ionizing particle.

From the range-energy relations given by Bethe one can calculate the maximum ionization to be expected in the track of a proton that trips the Geiger counters and expands the chamber. The glass wall of the chamber, the glass wall of the Geiger counter tube and the side of the copper cylinder which forms its outside electrode have a combined absorbing power equivalent to that of 21 meters of air. Consequently, for a particle to penetrate to the

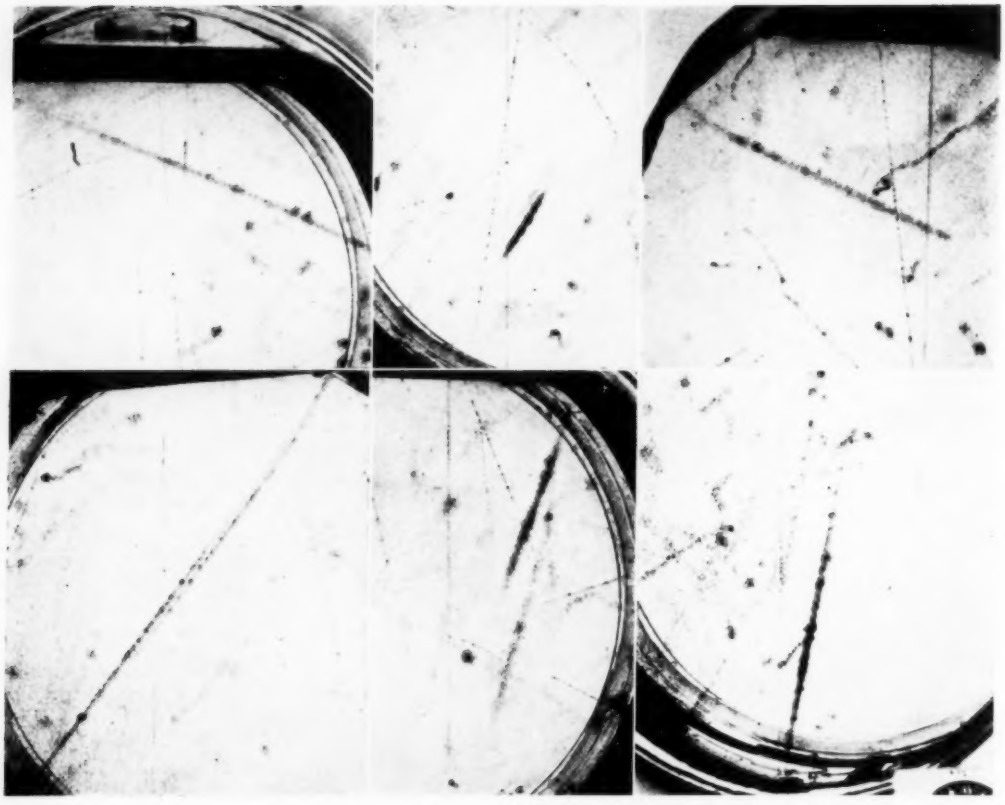

FIG. 4. Heavy cosmic-ray tracks of medium and light ionization. These tracks are presumably made by high speed protons or alpha-particles.

lower counter it must have a range of at least 21 meters of air while in the chamber. A proton of this range would have an energy of 5.6×10^7 volts, and an alpha-particle would have 2.6×10^8 volts. These are the minimum energies that a particle could have while in the chamber and still get into the bottom counters to cause the expansion. Corresponding to these minimum energies there is a maximum ionization to be expected for counter tripping tracks. From Bethe's tables a proton at 5.6×10^7 volts has an energy loss per cm path about 6 times that for a high speed electron, and an alpha-particle of 2.6×10^8 volts loses energy about 25 times as fast as an electron. If the same proportion of energy loss goes into ionization in the case of the electron, proton and alpha-particle, the maximum ionization to be expected from a counter tripping proton is only about 6 times the ionization of an electron while a counter tripping alpha-particle could have up to 25 times the ionization of an electron.

SUMMARY OF RESULTS

In the 8500 photographs, a total of 80 tracks were observed that showed a markedly heavier ionization than an electron track. Of these 21 were estimated to have an ionization of more than 50 times that of an electron, appearing to be almost as dense as an alpha-particle or a proton track. They are clearly distinguished from alpha-tracks however by their lengths. The longest alpha-particle ranges are less than 9 cm, while the sections of the ranges of these very heavy tracks made visible in the illuminated portion of the chamber varied from 13 to 44 cm, with an average range of 25 cm visible. Only

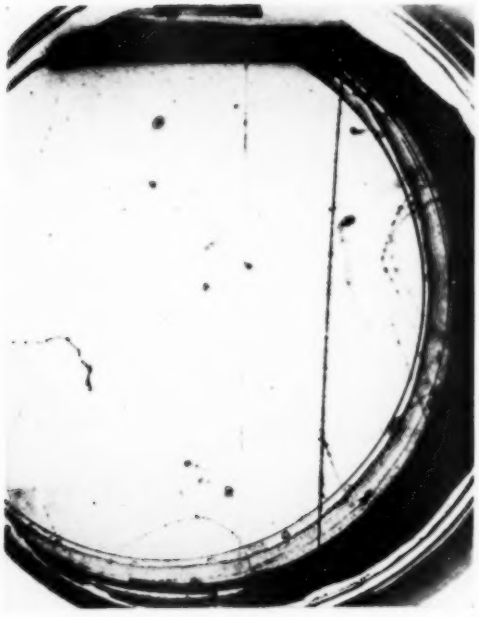

FIG. 5. A heavy cosmic ray that apparently tripped the counters and caused the expansion. It is estimated to have between 5 and 20 times the ionization of a fast electron.

(a) (b) (c)

FIG. 6. (a) Enlarged track of a heavy particle that apparently tripped the counters. (b) Electron track taken under identical conditions. (c) Track of a fresh alpha-particle. (Magnification 3×.)

two of these tracks appear certainly to terminate in the gas of the chamber. One of these is shown in Fig. 2. In most of the tracks both ends fade out of the illuminated section or end at a wall of the chamber, indicating that only a portion of the total range was observed. The longest range observed, 44 cm, corresponds to an energy loss in the chamber of 5.8 million volts for a proton and of 25 million volts for an alpha-particle. Fig. 3 shows several of these heavy tracks at 0.31 scale.

24 old tracks occurred with a density of ionization estimated to be between 10 and 50 times the ionization in an electron track. Such tracks could be made only by very fast particles, whatever their nature. These tracks show no signs of terminating except at the walls of the chamber and without question are capable of passing entirely through the gas of the chamber. There were 21 old tracks of density of ionization of from 3 to 10 times the ionization of an electron. Tracks of this density older than 0.2 second cannot easily be distinguished from old electron tracks, while the heaviest tracks as old as 1.5 seconds can be seen readily. Consequently the ratio of lightly ionizing tracks to very heavy tracks must be corrected for the difference in collecting time. Fig. 4 shows several tracks of medium and light ionization.

In addition to these tracks that occurred in the chamber at any time during the 1.5 seconds preceding the expansion, there were 14 tracks of particles of higher ionizing power than an ordinary electron that appeared to have passed through both Geiger counters and caused the expansion of the chamber. Seven of these are estimated to have an ionization of from 5 to 20 times that of an electron. Such a track is shown in Fig. 5. Fig. 6 (a) shows an enlarged section of another track of this nature. The track (b) of Fig. 6 is an electron track enlarged to the same scale. It was taken in the same region of the chamber under identical conditions on the same day. A fresh alpha-track is shown in (c) for comparison. The other seven of the 14 heavy

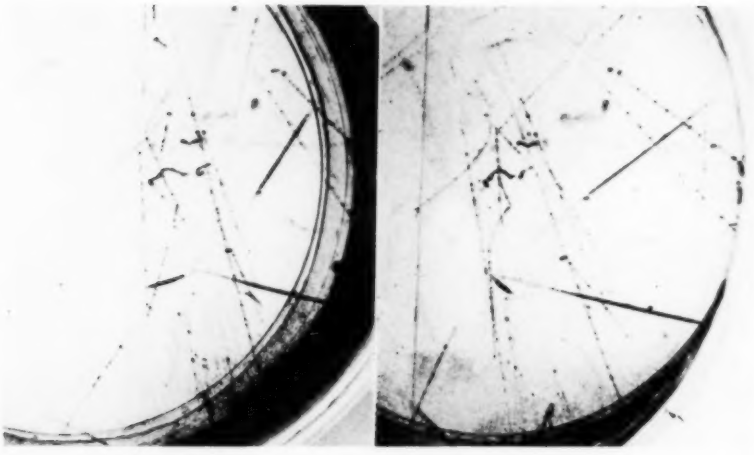

FIG. 7. Stereoscopic views of a disintegration in which three heavy particles are ejected from the front glass of the chamber.

counter tripping tracks are estimated to have had from 2 to 5 times the ionizing power of a fast electron.

Three pictures of disintegrations were obtained in which heavy particles were emitted. They apparently originated in the front glass of the chamber. One showed 3 heavy tracks, one two, and one had two heavy tracks and three electron tracks coming from a point. The disintegration with three heavy particles is shown in Fig. 7.

CONCLUSIONS

It can be seen from the calculation of Bethe that it is not easy to distinguish by ionization alone between a proton and an electron of energies over 5×10^8 electron volts. Probably all of the 80 heavy tracks observed are due to protons of energies less than 3×10^8 electron volts. To penetrate the earth's atmosphere a primary cosmic proton would require an energy of over 4×10^9 electron volts. Unless the cloud chamber happened to be just at the end of the range of a primary cosmic-ray proton it would probably not be distinguished from an electron by its ionization. The 44 particles observed with the heaviest ionization are very likely secondary particles resulting from a disintegration similar to the 3 disintegrations observed. The random distribution in direction is also consistent with the probable secondary origin of these particles. Their energies are insufficient to permit the particle to penetrate the glass walls of the chamber. There seemed to be no evidence of any association of the heavy particles with showers or other cosmic-ray tracks. Two of the disintegrations seem to be associated with a shower and the third disintegration is too old to identify electron tracks.

The chamber was sensitive to heavy tracks for over 1.5 seconds and had a volume of over 7 liters. The amount of cosmic ionization in this volume due to the heavy particles in the 10,500 seconds included in the photographed observations is roughly estimated as about one percent of the total ionization. This contribution to the ionization although small is not to be considered as negligible. The heavy particles whose tracks are only slightly denser than an electron track might be either primary or secondary particles. It is not possible to conclude from these tracks that the primary cosmic radiation contains high speed protons as one of its components. It is now, however, not possible to say that the failure to observe heavy particles in the cosmic radiation in a cloud chamber is evidence against the existence of primary protons.

Measurements of the Effect of Paraffin and Lead on the Rate of Production of Very Large Cosmic-Ray Bursts

D. HEYWORTH, *Wellesley College, Wellesley, Mass.*
AND
RALPH D. BENNETT, *Massachusetts Institute of Technology, Cambridge, Mass.*

(Received July 20, 1936)

Observations have been made at sea level of burst frequency and magnitude for bursts larger than 15×10^6 ion pairs, using a Model C cosmic-ray intensity meter. The effects of the following on the rate of production of bursts of different magnitudes have been investigated: (*a*) degree of shielding of the ionization chamber; (*b*) heavy building structure above the instrument; (*c*) lead placed immediately above the ionization chamber; (*d*) paraffin placed immediately above the ionization chamber. The results on the enhancement of burst production by lead agree with, and extend the range of, those already reported. Paraffin has a much smaller effect than lead on the rate of production of large bursts.

INTRODUCTION

EARLY tests made with the Model C type[1] of cosmic-ray intensity meter of the Carnegie Institution of Washington indicated its usefulness in the collection of data on the frequency and magnitude of large bursts of ionization[2] caused by cosmic rays. These studies have been extended by Doan[3] at the University of Chicago for several similar meters operating side by side and for various degrees of shielding.[4] During the past seven months the authors have operated one of these meters at the Massachusetts Institute of Technology at a point near sea level, and have assembled further data on the effect on large burst frequency of the amount and material of the shielding and its proximity to the ionization chamber. The purpose of this paper is to report the results of these observations.

In Table I we have summarized our results, omitting all bursts smaller than 15×10^6 ion pairs.

It will be recalled that the 1.6 cm thick steel spherical ionization chamber in the Model C meter is normally surrounded by a uniform layer of lead shot whose effective thickness is about 10.7 cm. The shot space may be filled to any desired level, and if half-filled or less, the upper half of the 3 mm thick outer shell of the shot chamber may be removed. We have operated the meter under three degrees of shielding as follows:

1. "Full shield," with all shielding in place.
2. "Three-quarter shield," when the shot level is even with the top of the spherical ionization chamber.
3. "Half-shield," with the upper half of the shot and its thin enclosing shell removed.

We have also operated the meter in two locations as follows:

1. In Building No. 10 where the instrument had above and around it the equivalent of about eight stories of a building of heavy concrete and steel construction.
2. In Building No. 20, which is a light frame structure with thin wooden roof.

EFFECT OF DIFFERENT DEGREES OF SHIELDING

Fig. 1(a) shows the burst frequencies for different magnitude groups for different degrees of shielding in Building No. 10. We have used as a measure of the uncertainty in each observed frequency a quantity obtained by dividing each mean rate by $\sqrt{n}$, where n is the number of bursts on which the rate is based. We have indicated this measure of uncertainty by the length of the vertical line associated with each mean rate in Fig. 1(a).

Because of the limited number of observations the uncertainties are so great that it is difficult to draw detailed conclusions, but the indication is that the rate of production of bursts is definitely greater for the "3/4 shield" condition than

[1] Compton, Wollan and Bennett, Rev. Sci. Inst. **5**, 415 (1934).
[2] Bennett, Brown and Rahmel, Phys. Rev. **47**, 437 (1935).
[3] R. L. Doan, Phys. Rev. **49**, 107 (1936).
[4] R. L. Doan, Phys. Rev. **48**, 470 (1935).

for either "half-shield" or "full shield." This is in accord with the observations of Doan.[5]

Effect of a Heavy Structure Over the Meter

We have made comparative tests of burst frequency in Buildings No. 10 and No. 20 with the meter in the "half-shield" condition, to determine the effect of a massive structure above the meter. In Building No. 10 the nearest mass above the instrument was a reinforced concrete floor some five meters distant. Supposedly the material above the instrument would give rise to bursts of all sizes, but most of the rays from such bursts would not be expected to pass through the heavy concrete floor immediately above the meter.[6] As a result, most of the burst enhancement observed might be expected to come from this floor. However, the spread of the rays in passing over the five meters intervening between floor and instrument is probably considerable, so that even though a large burst was produced, only a part of the rays from it would pass through the chamber and a comparatively small burst would be recorded. The data for the tests in the two buildings are plotted in Fig. 1(b) and show the very considerable enhancement of burst rate in the smallest magnitude group, while the rates in the larger groups are hardly significantly affected. These same data are plotted logarithmically in Fig. 2(a) with the uncertainty indicated in a way similar to that used in Fig. 1(a). In the lower part of Fig. 2(c) these logarithmic plots are again reproduced and superposed in order to show the effect more clearly. The divergence of the lines at the left indicates the greater enhancement by the heavy structure for bursts of smaller magnitudes.

Table I. *Summary of data.*

(1) Building	(2) Shield	(3) Hours	(4) Burst size ($\times 10^6$ ions)	(5) No. of bursts	(6) Rate in bursts/hr.	(7) Average size
No. 10	Full shield	843	15–30	117	0.1388	29.5
			30–45	20	.0237	
			45–60	9	.0107	
			60–75	6	.0071	
			75–90	5	.0059	
			90–105	1	.0012	
			180–195	1	.0012	
				159	0.1886	
No. 10	¾ shield	208	15–30	35	.1681	30.6
			30–45	11	.0528	
			45–60	7	.0336	
			60–75	2	.0096	
			75–90	2	.0096	
				57	0.273	
No. 10	½ shield	301	15–30	37	.1230	25.7
			30–45	5	.0166	
			45–60	4	.0133	
			60–75	1	.0033	
				47	0.156	
No. 20	½ shield	987	15–30	45	.0456	32.3
			30–45	15	.0152	
			45–60	4	.0041	
			60–75	4	.0041	
			75–90	0	.0000	
			90–105	2	.0020	
			105–120	1	.0010	
				71	0.072	
No. 20	½ shield+23 kg lead	503	15–30	38	.075	46.4
			30–45	9	.0175	
			45–60	9	.0175	
			60–75	5	.010	
			75–90	2	.004	
			90–105	2	.004	
			105–120	1	.002	
			150–165	1	.002	
			180–195	1	.002	
			210–225	1	.002	
			445–460	1	.002	
				70	0.138	
No. 20	½ shield+23 kg paraffin	1335	15–30	45	.0337	41.4
			30–45	16	.0120	
			45–60	9	.0067	
			60–75	4	.0030	
			75–90	3	.0022	
			90–105	2	.0015	
			105–120	1	.0007	
			120–135	1	.0007	
			135–150	2	.0015	
			360–375	1	.0007	
				84	0.0627	

Effect of Material Placed Immediately Above the Ionization Chamber

After a long series of observations to determine the natural rate of burst occurrence in the meter under the half-shield condition in Building No. 20, we made a series of tests to determine the effect of different materials placed immediately above the ionization chamber. The materials tried were first, 23 kg of lead in the form of shot in bags laid directly on the chamber, and second, 23 kg of paraffin in the form of a cube placed face downward directly on the spherical ionization chamber. Since the lead was in the form of a layer a few centimeters thick, while the paraffin formed a cube of nearly 30 cm on a side, the space occupied by the materials was different and thus the results of these tests are only qualitatively comparable. The results are plotted in Fig. 1, (c) and (d), and logarithmically in Fig. 2 (b) and (c). In Fig. 2 (b) the data are given,

[5] Reference 3, p. 122.

[6] Froman and Stearns, Phys. Rev. **49**, 474 (1936).

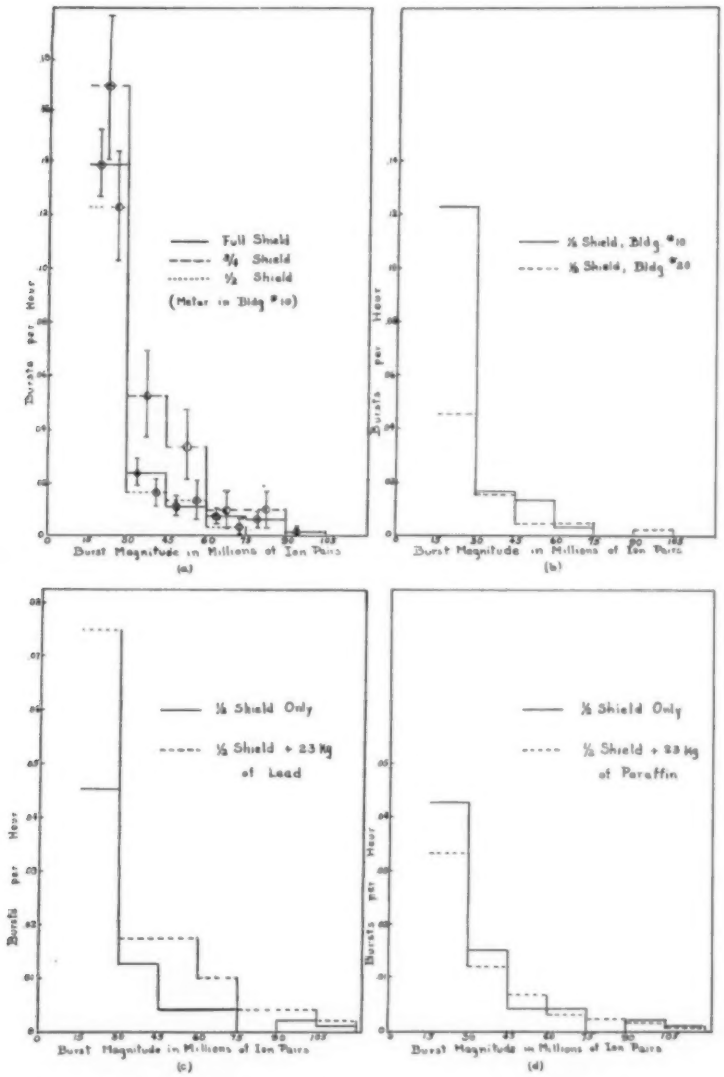

FIG. 1. (a) Effect of different degrees of shielding on burst rate. (b) Effect of placing meter beneath a heavy structure. (Upper half of shield removed.) (c) Effect of 23 kg of lead placed immediately above the ionization chamber. (Upper half of shield removed.) (d) Effect of 23 kg of paraffin placed immediately above the ionization chamber. (Upper half of shield removed.)

together with the uncertainties of the various points calculated as for Fig. 2 (a). In Fig. 2 (c) the three curves of Fig. 2 (b) are reproduced and superposed.

These curves indicate that the burst rate is little affected by the presence of the paraffin. There is an indication of slight enhancement in burst rate for the smaller bursts with a possible small decrease in burst rate for the larger bursts. However, for the lead there is a definite, significant, and approximately uniform enhancement of burst rate for all sizes. From Table I it can be seen that this average rate is nearly doubled by the presence of the 23 kg of lead. Using the

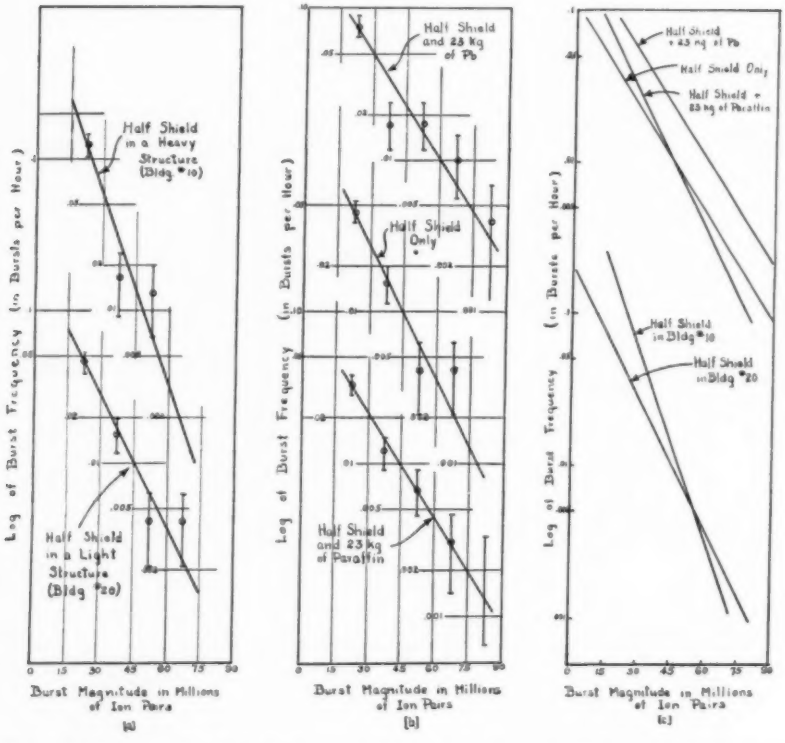
Half Shield in a Heavy Structure (Bldg #10)
Half Shield in a Light Structure (Bldg #20)
Log of Burst Frequency (in Bursts per Hour)
Burst Magnitude in Millions of Ion Pairs
(a)
Half Shield and 23 kg of Pb
Half Shield Only
Half Shield and 23 kg of Paraffin
Log of Burst Frequency (in Bursts per Hour)
Burst Magnitude in Millions of Ion Pairs
(b)
Half Shield + 23 kg of Pb
Half Shield Only
Half Shield + 23 kg of Paraffin
Half Shield in Bldg #10
Half Shield in Bldg #20
Log of Burst Frequency (in Bursts per Hour)
Burst Magnitude in Millions of Ion Pairs
(c)

FIG. 2. (a) Showing the effect of a heavy structure above the meter on burst frequency (with upper half of shield removed). (b) Showing the effect of 23 kg lead and 23 kg paraffin placed immediately above the ionization chamber. (Upper half of shield removed.) (c) Summary of (a) and (b) with axes not displaced.

values from these curves, we can calculate the burst rate per gram of lead in the range of burst magnitudes studied. These values are given in Table II.

It should be borne in mind that the rates obtained in this manner are dependent on the type of instrument used, and that values obtained with a very thin walled ionization chamber, because of the smaller absorption in the walls, might differ considerably from those found here. A similar study has been made by C. G. and D. D. Montgomery[7] using a light Dow-metal chamber, but a direct comparison is not possible, since their rates apply only to bursts smaller than the smallest we have considered.

We have made no attempt to include in our rate analysis bursts whose magnitude exceeds 90×10^6 ions because the number observed was too small to give rates which are significant. However, the effect of material above the ionization chamber on burst production in this region of magnitudes can be seen in its influence on the average burst size as given in Table I, column 7. These figures indicate that the heavy structure above the meter has little effect on the average magnitude of the bursts recorded, but that material placed directly on the ionization cham-

TABLE II. *Burst rate per gram of lead for different burst magnitudes.*

Burst size $\times10^{-6}$	Burst rate/hr. half-shield	Burst rate/hr. half-shield +23 kg Pb	Burst rate/hr./gm of lead
15–30	0.046	0.074	1.22×10^{-6}
30–45	.0165	.0335	0.74×10^{-6}
45–60	.0059	.0155	$.42\times10^{-6}$
60–75	.00215	.0068	$.20\times10^{-6}$
75–90	.00075	.0030	$.10\times10^{-6}$
15–90			2.68×10^{-6}

[7] Montgomery and Montgomery, Phys. Rev. **47**, 429 (1935).

ber enhances the average magnitude. Thus the average burst size is increased nearly 50 percent by the presence of the 23 kg of lead, and while the paraffin had little effect on burst frequency in the lower ranges, it increased the average size by nearly 30 percent.

Analysis of these average values shows that in the "half-shield" condition less than 10 percent of the total ionization in large bursts is contributed by those greater than 90×10^6 ions, but when the paraffin is added these large bursts contribute more than 25 percent of the total, and with the lead the fraction goes up to nearly 40 percent. Thus it becomes evident that the material above the chamber increases by many fold the number of bursts in the very high ranges. If sufficient data were available to give significant rates in these regions, the slopes of our curves in Fig. 2 (c) might be considerably changed. There is also an indication that more than one exponential would be necessary to express the distribution, as was found in earlier work[2] with the meter fully shielded.

If bursts are conceived as consisting of many rays originating in and diverging from a small volume, then the size of the burst as recorded by an ionization chamber will depend on its proximity to the point of origin of the rays. The evidence to date indicates that material is necessary for the production of bursts. Therefore the placing of material directly on the ionization chamber is equivalent to bringing the chamber near to a source of bursts, with a resulting increase in average burst size. From this point of view our results may be interpreted as further evidence that bursts originate in material, and that they consist of many rays originating in and diverging from a small volume.

OCTOBER 1, 1936 PHYSICAL REVIEW VOLUME 50

Beta-Ray Spectra of Radioactive Manganese, Arsenic and Indium

M. V. Brown and Allan C. G. Mitchell, *Department of Physics, New York University, University Heights, New York, N. Y.*

(Received July 24, 1936)

The beta-ray spectra of radioactive manganese, arsenic and indium was obtained by measuring tracks produced in a cloud chamber situated in a magnetic field. Manganese and arsenic give spectra which can be resolved into two components. The end points of the two components are: for Mn, 1.2 and 2.9 MEV; for As, 1.09 and 3.4 MEV. The endpoint for In is 1.45 MEV.

IN view of the importance of the study of the beta-ray spectra of natural and artificially radioactive substances we have investigated the energy distribution of the electrons emitted from radioactive manganese, arsenic and indium produced by the capture of slow neutrons. It is of interest to see whether the energy distribution of the disintegration electrons fits the theory of Konopinski and Uhlenbeck[1] and also to determine the endpoints of the spectra. While this work was in progress the results of a similar investigation were published by Gaerttner, Turin and Crane.[2] These investigators studied, among other elements, radio-indium and radio-manganese, and their results will be discussed in relation to those obtained by us.

Apparatus

The beta-ray spectra of radio-manganese, arsenic and indium were studied by analyzing the tracks obtained in a Wilson cloud chamber situated in a magnetic field. The chamber, a modification of the magnetically operated one described by Dahl, Hafstad and Tuve,[3] was driven by two electromagnets, one of which compressed and the other expanded the chamber from its equilibrium position. This reduced the load on the magnets and increased the pressure range which could be used. The active part of the

[1] E. J. Konopinski and G. E. Uhlenbeck, Phys. Rev. **48**, 7 (1935).

[2] E. R. Gaerttner, J. J. Turin and H. R. Crane, Phys. Rev. **49**, 793 (1936).

[3] O. Dahl, L. R. Hafstad and M. A. Tuve, Rev. Sci. Inst. **4**, 373 (1933).

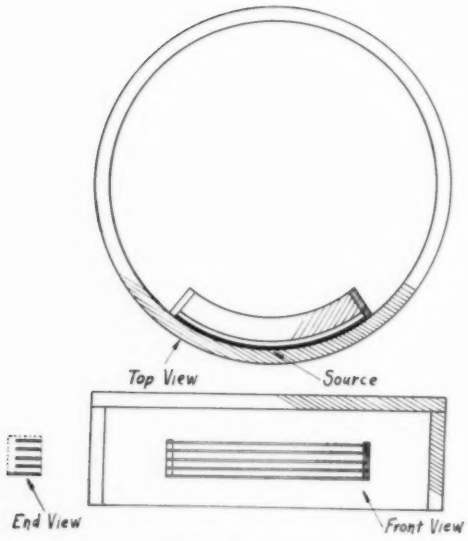

FIG. 1. Cloud chamber and slit system.

chamber, 13 cm in diameter and 4 cm deep, was separated from a secondary volume by a rubber diaphragm. When hydrogen was used in the chamber the secondary volume was also filled with hydrogen to cut down loss by diffusion.

The magnetic field was produced by a Helmholtz coil 15 cm in mean radius enclosed in a water-cooled brass case. The coil was capable of a maximum field of 800 gauss, constant to ± 1 percent throughout the volume of the chamber. The coil was calibrated by means of two different flip coils which agreed to two percent. The expansion and compression magnets produced a field of only one gauss in the chamber space and any inhomogeneity caused by them could be neglected. The electrostatic distortion of the tracks was minimized by grounding out the 90-volt sweeping potential at the instant of expansion.

A Sept camera with an f: 3.5 lens was mounted to photograph along the axis of the coil. Light was furnished by four mercury discharge tubes containing, in addition to the mercury vapor, about 7 cm of helium. Originally 10 mf at 4000 volts was discharged through each, but the tubes were found to burst quickly, sometimes at the first discharge. At present each is operated on 3.5 mf at 7000 volts. This represents nearly as large an energy as before, yet the present tubes have already withstood several thousand discharges without breaking. Sometimes a fresh tube would not fire at 7000 volts, in which case the tube was activated by an ignition coil. The ignition coils were excited by the discharge of 28 mf at 350 volts. Contactors for both the 7000 and 350-volt condenser banks were carried by the same relay. Aluminum mirrors were fixed to the backs of the discharge tubes and short focus cylindrical lenses were mounted on the tube holders to concentrate the light into a nearly parallel beam which illuminated only a narrow region in the chamber.

The radioactive samples were placed in the chamber behind a system of Soller slits, made of aluminum, and fastened to the periphery of the chamber (see Fig. 1). About one-half of the data on indium and manganese were obtained using slits which limited the electron beams to $\pm 5°$. The remaining half of the manganese data and all of that on arsenic were obtained from beams limited to $\pm 10°$. Only such tracks were recorded which were long enough to allow one to measure their curvature to ± 0.5 cm and which showed no deflection preceding the measurable portion of the track. Measurements were made by projecting the photographs on a card bearing a series of concentric circles spaced at 0.5 cm intervals.

In order to reduce the number of crooked tracks, the chamber was flushed with hydrogen which had been bubbled through isopropyl alcohol. This also aided in clearing the chamber after inserting a new sample. Tracks could be obtained after as few as ten expansions.

TREATMENT OF THE DATA

From the measured values of the radii of curvature of the tracks and the value of the magnetic field, a histogram was drawn showing the number of tracks in a given $H\rho$ interval as a function of $H\rho$. Care was taken, of course, to choose such a value of the field that there was no overlapping of intervals in the histogram. A Konopinski-Uhlenbeck plot, as suggested by Kurie, Richardson and Paxton[4] was then made from the data of the histogram. This was accomplished by plotting $(N/f)^{\frac{1}{2}}$ against $(1+\eta^2)^{\frac{1}{2}}$,

[4] F. N. D. Kurie, J. R. Richardson and H. C. Paxton, Phys. Rev. **48**, 167 (1935).

where N is the number of tracks in an interval, $(1+\eta^2)^{\frac{1}{2}}$ the total energy expressed in terms of m_0c^2, and $\eta = H\rho/1700$. It can be shown that[5]

$$f(Z, \eta) = \eta^2(2\pi y/(1-e^{-2\pi y})), \quad (1)$$

where

$$y = Z[(1+\eta^2)^{\frac{1}{2}}/137\eta]. \quad (2)$$

If one plots $(N/f)^{\frac{1}{2}}$ against the total energy one should obtain a straight line, provided that the theory is correct. In certain cases we have found that a straight line could not be fitted to the data. In this case we have been able, by trial, to fit two straight lines to the data, which results in a beta-ray spectrum of two components, the sum of which gives the original histogram.

Manganese

Radio-manganese was prepared by irradiating solutions of $KMnO_4$ or $NaMnO_4$ with neutrons and filtering off the MnO_2 which contained practically all of the activity. The filter paper was washed with distilled water until the wash water showed no purple color, indicating the absence of MnO_4 ion, and hence the absence of occluded Na and K ions. The data taken using $KMnO_4$ agreed to within the experimental error of about ten percent with that obtained using $NaMnO_4$, showing that there were no complications arising from K or Na. From one to two hours was required for filtering, drying and getting the chamber into sensitive operation so that the 3.75 minute period due to vanadium should have practically disappeared.

In order to minimize possible systematic errors, particularly those due to warping of the film on reprojection, half of the data were taken with a magnetic field of 378 gauss and the rest with a field of 490 gauss. The two sets of data agreed to within the experimental error.

The results of the experiments are shown as a histogram and K. U. plot in Fig. 2. The crosses of the K. U. plot correspond to the best curve which can be put through the histogram, and it will be seen that they deviate considerably from a straight line. On the other hand, one can try to resolve the data into two components by passing a straight line through the points of the K. U. diagram for values of $(1+\eta^2)^{\frac{1}{2}}$ greater than 3.0. The difference curve (lower energy component) then gives the straight line passing through the circles. Curve B, on the histogram, corresponds to the circles of the K. U. plot, while curve A corresponds to the straight line placed through the crosses for values of $(1+\eta^2)^{\frac{1}{2}}$ greater than 3.0. The sum of the two curves gives the original histogram, C. The two endpoints thus obtained are 2.9 MEV and 1.2 MEV.

The mean energy of the beta-ray spectrum is 0.56 MEV and one-half of the particles have energies less than 0.44 MEV. Amaldi, d'Agostino, Fermi, Pontecorvo, Rasetti, and Segrè[6] found, for the 2.5-hour period of manganese, a half-value thickness of 0.14 g/cm² of aluminum which corresponds to 0.45 MEV. Gaerttner, Turin and Crane reported a single group with a limit at

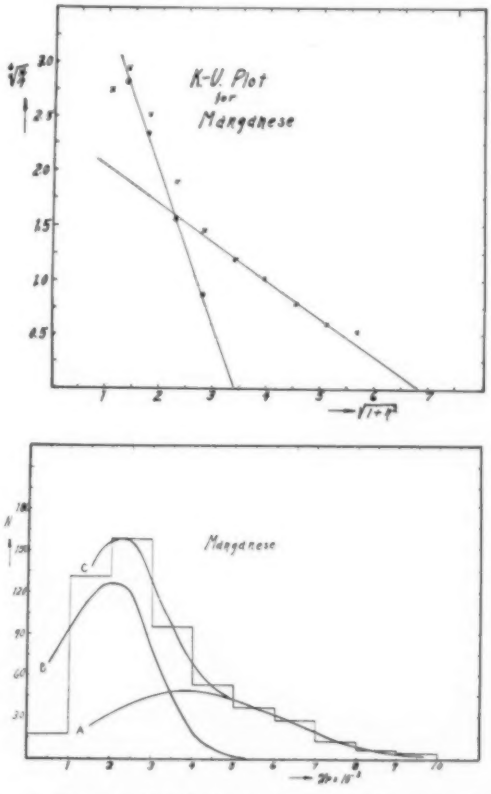

FIG. 2. Konopinski-Uhlenbeck plot and $H\rho$ histogram for the β-particles from radioactive manganese.

[5] The expression (1) for $f(Z, \eta)$ is true only for not too large values of Z. Dr. Harvey Hall has kindly worked out the exact expression for $f(Z, \eta)$ and we have found that for indium, $Z = 49$, the correction to (1) is about 1 percent and can therefore be neglected in our calculations.

[6] E. Amaldi, O. d'Agostino, E. Fermi, B. Pontecorvo, F. Rasetti and E. Segrè, Proc. Roy. Soc. **A149**, 522 (1935).

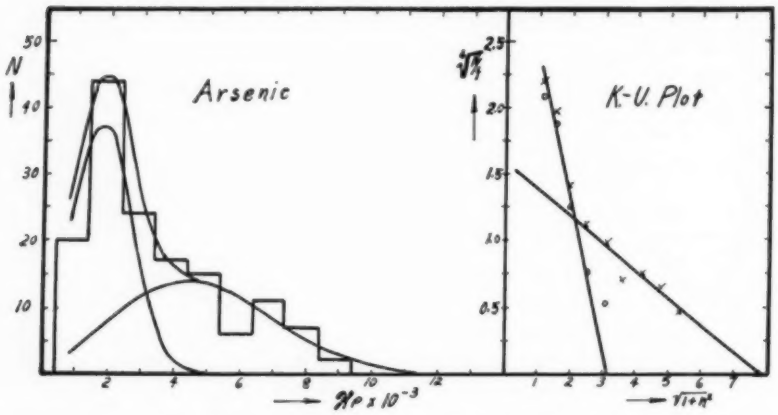

FIG. 3. $H\rho$ histogram and Konopinski-Uhlenbeck plot for the β-rays from radioactive arsenic.

2.8 MEV, while Alichanow, Alichanian and Dzelepow,[7] using a beta-ray spectrograph, reported an upper limit at 3.2 MEV.

The possibility that the high energy group might have a shorter period than the lower energy group was investigated by taking the ratio of the number of tracks having an $H\rho > 4900$ to those having an $H\rho < 4900$ as a function of the time after irradiation for any given sample. The results were erratic, due to statistical fluctuations, so that no exact conclusions could be drawn. The evidence, such as it is, is in favor of the two groups having the same period. It is known that radio-manganese emits gamma-rays but their energy has not been measured. It is possible that the difference in energy of the two beta-ray groups may be connected with the emission of the gamma-ray.

Arsenic

Radio-arsenic was formed by irradiating a solution of cacodylic acid with neutrons. After irradiation, a small amount of $AsCl_3$ was added, and the arsenic precipitated with H_2S. The results of the cloud chamber investigation are shown in the histogram and K. U. plot of Fig. 3. Following the procedure used in the case of manganese we denote by crosses on the K. U. plot the data taken directly from the histogram. As in the case of manganese the crosses do not fall on a single straight line. The K. U. plot can again be resolved into two straight lines, giving the two distribution curves which add together to reproduce the original histogram. The two groups show no difference in period.

The two endpoints obtained by this method are 3.4 MEV and 1.09 MEV, respectively. The mean energy is 0.62 MEV and one-half of the tracks have energies less than 0.45 MEV. For the 26-hour period of arsenic, Amaldi *et al.*[6] give a half-value thickness of 0.16 g/cm² of aluminum, which corresponds to 0.5 MEV.

Indium

Foils of indium, 0.1 g/cm² thickness, were irradiated by slow neutrons obtained by surrounding a 250-millicurie radon-beryllium source with 6 cm of paraffin. About half of the data were taken using the slit system and a vertical camera. The other half were taken without defining slits and with a pair of cameras inclined at 45° to the magnetic field. This arrangement yields much denser photographs, but seriously distorts tracks which are not in a horizontal plane, making them appear elliptical when projected. Relying on the collimation of the light beam to act as an effective slit and choosing only the longest tracks, it was found that the data obtained in this way were in agreement with those obtained using a slit system.

In view of the fact that a solid emitter was used whose stopping power varied from zero to 0.1 g/cm² it is clear that a K. U. plot of the uncorrected data can have no definite meaning. For example, a group of beta-rays, of approximately the same energy, coming from some

[7] A. I. Alichanow, A. I. Alichanian and B. S. Dzelepow, Nature **136**, 257 (1935).

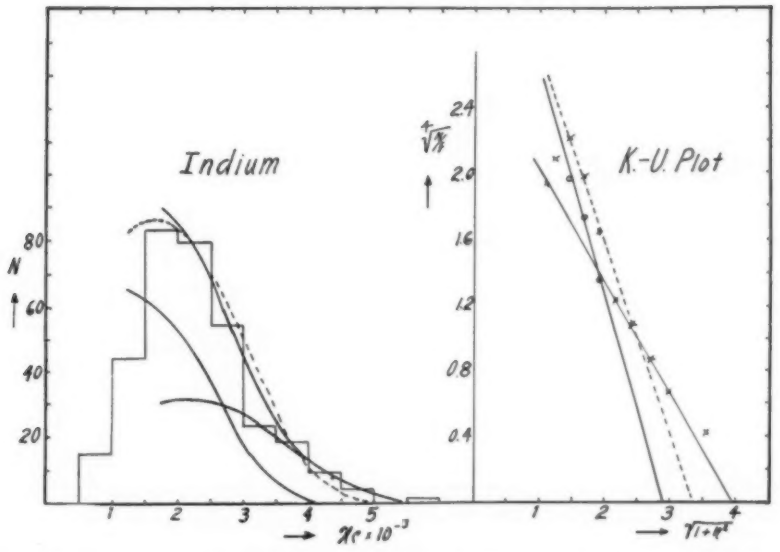

FIG. 4. $H\rho$ histogram and Konopinski-Uhlenbeck plot for the β-rays from radioactive indium.

place, a distance x from the surface of the emitter, would suffer a loss in energy in getting out of the emitter and there would also result a distribution in energy due to straggling.[8] The observed curve could then only be obtained by integrating the product of the true distribution function and the distribution function due to straggling. An overall correction, such as that applied by Gaerttner, Turin and Crane, will probably not give a very accurate reproduction of the true distribution curve from the observed one. On the other hand, it is reasonable to assume that the very fast particles near the end point come from the surface layers of the emitter. We have, therefore, tried to locate the endpoint of the beta-ray spectrum by passing a straight line through the high energy points of the K. U. plot given in Fig. 4. The endpoint thus obtained is 1.45 MEV, in reasonable agreement with that obtained by Gaerttner, Turin and Crane. It is clear from the diagram that no single straight line can be put through all the points of the K. U. curve. A resolution of the data, according to the method previously adopted, makes no improvement and is of no particular significance, since straggling is probably playing a large role at the lower energies.

[8] Rutherford, Chadwick and Ellis, *Radiation from Radioactive Substances* (Cambridge University Press, 1930), p. 424 *et seq.*

DISCUSSION

The use of hydrogen in the chamber reduced the number of crooked tracks to a small fraction of the total number. All tracks were recorded which presented an arc long enough to give an unambiguous measurement. The least definitive slit system used passed only particles lying within $\pm 10°$ to the horizontal. The horizontal component of such a path has more than 98.5 percent of the total energy. All tracks were assumed to lie in the same plane. The depth of the chamber illuminated was about 2 cm and the camera object distance was 40 cm, so that the maximum error from this source was about two percent, and the average error much less. The magnetic field was constant to one percent over the volume of the chamber and was known to one percent. The distortion due to turbulence was not determined, but it seemed to be small. The error in fitting a curve to any given track was less than 5 percent for $\rho = 5$ cm and should largely average out. The plausible spread within which the K. U. curves can be interpreted was not greater than ten percent. The effect produced by stray beta-particles caused by contamination, gamma-rays from the radon etc. which might be mistaken for disintegration electrons, was small. During the course of these

experiments a total of 180 have been measured. These showed a peak near $H\rho = 1500$ and, by inspection, an upper limit at $H\rho = 7500$ (1.8 MEV). Since the source holder covered only one-fourth of the circumference of the chamber wall, it does not seem likely that more than 45, or four percent of the "disintegration" tracks were spurious, and when the fourth root of the number of tracks is plotted, this would mean only a one percent change in a point on the K. U. plot.

In the case of manganese and arsenic the active sources were deposited chemically on filter paper. The amount of deposit was small so that the straggling of the beta-particles was presumably negligible. That this assumption was approximately correct is borne out by the fact that several sources, prepared from $KMnO_4$ and $NaMnO_4$, in which the amount of deposit varied, gave the same results to within ten percent. Furthermore, since the active sources were placed directly in the chamber, no corrections had to be made for the passage of the particles through metallic foils.

The two beta-ray components observed in manganese and arsenic may be connected with the emission of a gamma-ray. It is, of course, possible that the K. U. theory may not be correct and that a plot of $(N/f)^{\frac{1}{2}}$ against $(1+\eta^2)^{\frac{1}{2}}$ should not give a straight line. The theory, however, appears to fit existing data on other radioactive elements. The difference in results obtained in the present paper and those obtained by Gaerttner, Turin and Crane may be accounted for by the fact that they used thick emitters. This is somewhat borne out by the fact that the endpoint obtained by us for indium, using a thick emitter, is in substantial agreement with theirs. It should be pointed out that the procedure adopted by them, namely plotting $(N/f)^{\frac{1}{2}}$ for $Z=0$ is not correct for elements of atomic number as high as manganese (25) and may lead to erroneous results. We have replotted their results for indium and find that, while the shape of the curve is considerably changed when the correct value of Z is used, the extrapolated endpoint is not seriously effected.

The authors are indebted to Dr. D. P. Mitchell and Mr. G. A. Fink of Columbia University for preparing for us one of the sources of radio-manganese. We are indebted to Dr. C. B. Braestrup of the Department of Hospitals of the City of New York for many favors, and also to the American Association for the Advancement of Science for a grant to one of us (A. C. G. M.) with the help of which apparatus has been purchased.

OCTOBER 1, 1936 PHYSICAL REVIEW VOLUME 50

On X-Ray Satellites, Relative Intensities and Line Widths

LYMAN G. PARRATT,* *Cornell University, Ithaca, New York*

(Received July 13, 1936)

Preliminary data are reported on the $L\alpha_{1,2,3,4,5,6,7}$ lines for Ag(47) and on the $M\alpha, \beta$ lines for Au(79) recorded with a two-crystal spectrometer. But the primary purpose of this note is to indicate some of the difficulties in interpreting these and similar data. The disagreement between the present and earlier interpretations and results is large: a factor of about 2.5 in widths of M series lines, a factor or about 2 in α_2/α_1 relative intensities, and a factor of about 4 in the satellite relative intensities. These discrepancies are due to differences in (1) the effective resolving power of the instruments used and in (2) the assumed shapes of the component lines comprising an unresolved complex structure.

RADIATIONLESS transitions, or Auger effects, are assuming a major role in explaining and correlating several perplexing x-ray phenomena: the observed widths of x-ray emission lines and absorption limits,[1] and the relative

* The author is indebted to the Carnegie Foundation for a grant-in-aid (made to Professor F. K. Richtmyer) of this research.

[1] G. Wentzel, *Handbuch der Physik*, Vol. 24, Part 1 (1933), 768; F. K. Richtmyer, S. W. Barnes and E. G. Ramberg, Phys. Rev. **46**, 843 (1934); E. G. Ramberg and F. K. Richtmyer, Phys. Rev. **47**, 805A (1935); L. G. Parratt, Phys. Rev. **50**, 1 (1936); and others.

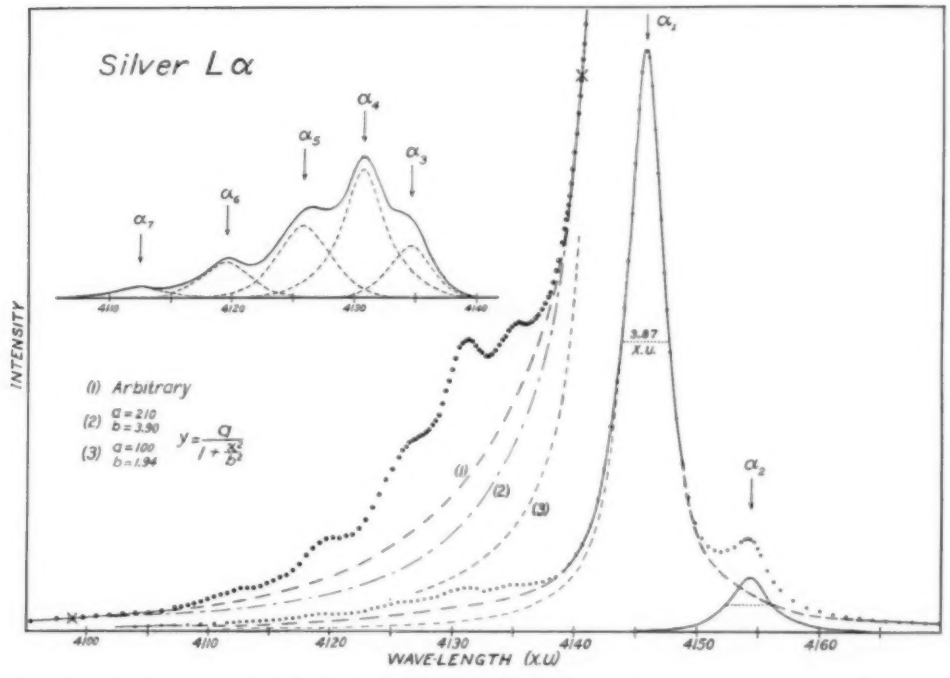

FIG. 1. Ionization curve of the Ag $L\alpha$ region recorded with a two-crystal vacuum spectrometer. The upper satellite region, on the short wave-length side of the α_1 peak, is replotted with an intensity scale increased 6.3 times. The uncertainty of the background of this satellite region is illustrated by the three possible backgrounds sketched in, each defined as indicated in the figure and discussed in the text. The satellite contour and component structure in the upper left part of the figure is determined with background (1).

intensities of x-ray lines, especially of the so-called satellite lines.[2] This development has brought about a rejuvenation of interest in these phenomena and promises to increase considerably our knowledge of subatomic dynamic structure.

To keep pace with this development the experimentalist is hard-pressed to refine his techniques in obtaining quantitative data. Creditable progress has been made by means of the photographic method but the well-known uncertainties inherent in this method make it a treacherous one when quantitative results, involving an accurate intensity scale, are sought. More reliable information has been obtained with the ionization method. The two-crystal spectrometer seems best adapted to this work because of the comparative ease with which a satisfactory compromise between intensity and resolving power can be attained. The present note presents some preliminary data on the $L\alpha_{1,2,3,4,5,6,7}$ lines for Ag(47) and on the $M\alpha$, β lines for Au(79), but the primary purpose of this note is to indicate some of the difficulties in interpreting quantitatively these and similar data.

Figs. 1 and 2 are reproductions of ionization curves of the Ag $L\alpha$ and Au $M\alpha$ regions.[3] We are interested in obtaining from such curves (1) widths at half-maximum intensity (and possibly shapes) of *all* the component lines, (2) intensities of the lines relative to one another, and eventually, (3) the wave-length position of the maximum ordinate of each component line.

Firstly, to obtain these data, we must record the curves with an instrument of as high resolving power as is practical, and we should have a

[2] D. Coster and R. de L. Kronig, Physica **2**, 13 (1935); D. Coster and K. W. de Langen, Physica **3**, 282 (1936); F. R. Hirsh, Jr., Phys. Rev. **50**, 191 (1936); and others.

[3] The two-crystal vacuum spectrometer, calcite crystals A_1B_4, and accessory equipment used in recording these curves have been discussed elsewhere. See Phys. Rev. **50**, 1 (1936).

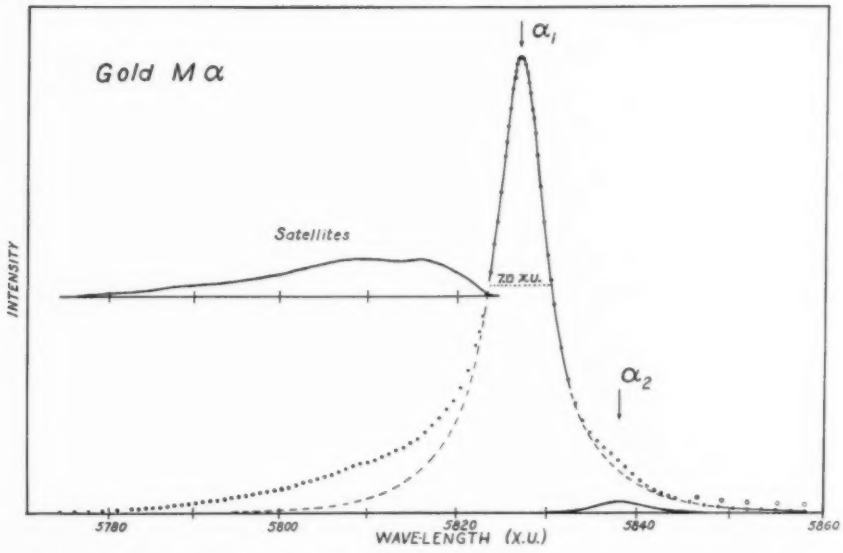

FIG. 2. Ionization curve of the Au $M\alpha$ region. The open circles at the extreme lower right part of the curve are calculated from the dispersion expression matched at the maximum and half-maximum ordinates of the α_1 line. The satellite background in this curve is determined from the assumptions that the α_1 line is symmetrical, that the shape (and width) of the α_2 line is about the same as of the α_1 line, and that the α_2 intensity is about 2.5 percent of the α_1 intensity.

good notion as to the magnitude of the effective resolving power. The "practical" choice of resolving power is a compromise between two factors: (1) the emergent intensity, or, rather, the accuracy and ease with which the intensity readings are to be made, and (2) the accuracy desired in the final results. (The concepts of resolving power and dispersion must not be confused.) Numerically, the resolving power used in recording the curves of Figs. 1 and 2 is of the order of 11,000; the $d\lambda$ interval (full width at half-maximum intensity of the diffraction pattern) is about 1/10 of the full width of the Ag $L\alpha_1$ line and about 1/14 of the full width of the Au $M\alpha_1$ line. We may assume that the resolving power is infinite but if we do we introduce thereby a first error in our interpretation and in our final results.[4] Actually, for some measurements, the correction for a resolving power as high as 11,000 is negligible (compared with a subsequent uncertainty soon to be discussed) but it is to be emphasized that this correction *is not* negligible when the effective $d\lambda$ interval is a much larger fraction of the true widths of the lines being studied. By way of illustration we may refer to the excellent pioneer work of Molin[5] on M series lines. This work, with an ionization single-crystal spectrometer, deals primarily with relative intensities but for the purpose of illustrating resolving power we shall consider certain line width measurements only. Molin's observed full widths of the Au $M\alpha_1$ and $M\beta_1$ lines are 19.7 and 18.6 X.U., respectively; the present full widths of the same lines are 7.0 and 6.5 X.U. In obtaining true component structure, the need for high resolving power is obvious. This need is increasingly greater for L and K series lines because the intrinsic widths of these lines are correspondingly less, being approximately 2/3 and 1/3 as wide as the M series lines for the same wave-length.

Assuming for the present that we have infinite resolving power, we meet an insurmountable difficulty when we attempt to draw in *uniquely* the component structure. We know very little

[4] See L. G. Parratt, Rev. Sci. Inst. **6**, 387 (1935) and Phys. Rev. **50**, 1 (1936).

[5] K. Molin, Inaugural-Dissertation, Upsala, 1927, and M. Siegbahn, *Spektroskopie der Röntgenstrahlen*, second edition (1931), pages 362–368.

about the true shapes of these x-ray lines. Many lines are unquestionably *not* symmetrical (about their maximum ordinates). Furthermore, we cannot with impunity assume that the width or shape of one component line is the same as the width or shape of an adjacent component line in an unresolved structure.

In drawing in component structure, many investigators have gained help, at least for the sake of reproducibility, from the assumption that the shape of the component line (or lines) is given by the Gaussian error curve, $y=ke^{-\alpha x^2}$, or, more recently by the classical dispersion curve, $y=a/(1+x^2/b^2)$. There is good theoretical support (as far as the theory has been developed[6]) for this use of the latter curve and, in fact, the shapes of many x-ray lines have been found experimentally to agree with the dispersion shape.[6] But this assumption, of definite help in some cases, is not a panacea. In Fig. 1 three attempts are made to draw in the short wave-length side of the α_1 line, or what amounts to the satellite background. Background (3) is a sketch of part of the dispersion curve when the constants a and b are chosen to match the α_1 line at the maximum and half-maximum ordinates on the short wave-length side of the α_1 peak. (The α_1 line is not symmetrical at half-maximum intensity, excess energy being found on the *long* wave-length side of the α_1 peak.) This background is obviously inadequate unless one is willing to define as satellites *everything* above such a background *and also* be content either with rather peculiar component shapes or with a large number of components, satellites perhaps, almost approaching a continuum.[7] Background (2) is another attempt to use the above expression, this time the constants a and b are determined by matching the curves on either side of, and adjacent to, an arbitrary but more "reasonable" satellite region. (The curves are matched at the two points indicated by crosses in the figure.) The values of the constants used in cases (3) and (2) are indicated in the figure. Background (1) is entirely arbitrary. The writer believes that a "reasonable" background must lie between (1) and (2).

The satellite contour and structure in the upper left part of Fig. 1 is determined with background (1). It may be in point to say that the shapes of the satellite component lines are in better agreement with Gaussian error curves than with dispersion curves. Although considerable latitude is present in the component shapes the author believes that it is not possible to draw in component lines, each having the dispersion shape, whose sum is equal to the observed unresolved satellite contour without introducing additional components for which there are no specific irregularities in the observed ionization curve. This statement holds when either background (1) or (2) is used.

The total $L\alpha$ satellite intensity (area) relative to the intensity (area) of the α_1 line is 0.16, 0.09 and 0.06 for the three backgrounds, respectively. *As a consequence of the background uncertainty, the satellite relative intensity is uncertain by some 35 percent.*[8]

Because the observed $M\alpha_1$ and $M\beta_1$ lines for Au(79) are each practically symmetrical at half-maximum intensity they may be *arbitrarily* assumed to be entirely symmetrical. Both observed curves approach the base line more quickly than does the expression $y=a/(1+x^2/b^2)$, and more slowly than does the Gaussian error curve. The α_2 background may be arbitrarily determined and, then, the short wave-length side of α_1 may be drawn in with the above assumption of symmetry. With such a dividing line between satellites and parent line the ratios of intensities are 0.19 for the total satellite struc-

[6] See references given in L. G. Parratt, Phys. Rev. **50**, 1 (1936).

[7] A judiciously over-exposed photographic plate may be remarkably sensitive to the number of satellite lines, and, if the effective resolving power is not too low, permits fairly accurate measurements of their wave-length positions. Compare, for example, Fig. 1 with Fig. 1 of a paper by F. K. Richtmyer and R. D. Richtmyer, Phys. Rev. **34**, 574 (1929). (The continuous spectrum on the short wave-length side of the satellites reported by Richtmyer and Richtmyer for the Ag $L\alpha$ region is not found in the present work, but this negative result is conclusive only in setting an upper limit of the total intensity, about 2 percent of the α_1 line, which is about the present experimental error due to the uncertainty of the base line intensity. Because of the difficulties in transposing the ordinate scale of the Richtmyers' densitometer curve to a scale which is linearly proportional to intensity, one cannot say what one might expect for the relative intensity of this continuous spectrum.)

[8] This estimate of the uncertainty in relative intensities varies, of course, with line and with element. For the $K\alpha$ satellite lines this uncertainty is about 5 percent for S(16) and increases with atomic number to perhaps more than 50 percent for Pd(46). See reference 6 and C. H. Shaw and L. G. Parratt, Phys. Rev. to be published.

ture to the α_1 line and 0.21 for the total satellite structure to the β_1 line. In appearance the satellite contours of Au $M\alpha_1$ and $M\beta_1$ are very similar. As yet, neither contour (from these curves) has been satisfactorily resolved into satellite components.[9]

The background of the α_2 line can be drawn with somewhat more assurance than the satellite background because of the smaller extent of the uncertain part of the α_1 line. As the present backgrounds are drawn, the ratio of intensities of the α_2 to α_1 lines are 0.065 and 0.025 for Ag $L\alpha$ and Au $M\alpha$, respectively. *It is to be noted that these values are considerably less than those predicted by the Burger-Dorgelo sum rules, 0.11 and 0.05, respectively.* The writer recognizes that he may be criticized for his particular choice of backgrounds which result in such low relative intensities for the α_2 lines. In fact previous investigators have chosen to draw in the α_1 line in such a manner that much better agreement is found with the sum rules.[10] While these rules have been found valid for many multiplets for some atomic number ranges, the writer is convinced that they do not apply in this simple manner in the present cases.

As stated above,[7] a good notion of wavelength positions of relatively weak lines which are closely adjacent to an intense line can be obtained from photographic plates. The lack of adequate effective resolving power, however, is apt to introduce considerable uncertainty. As an example we may refer to measurements of the Au $M\alpha_{1,2}$ separation. Lindberg[11] measures 14 X.U.; Hirsh,[9] 10.2 X.U.; the separation obtained from the curve of Fig. 2 is 11.1 X.U. Furthermore, from Fig. 2, it is obvious that the α_2 background may be drawn in, with increasing α_2/α_1 relative intensity, so that the $\alpha_{1,2}$ wavelength separation may be either slightly increased or decreased, depending upon the α_1 shape one wishes to assume.

The disagreement between the present and earlier interpretations and results is large: a factor of about 2.5 in widths of M series lines, a factor of about 2 in α_2/α_1 relative intensities, and a factor of about 4 in the satellite relative intensities.[12]

The ultimate accuracy of proposed quantitative measurements on component lines, resolved from contours as illustrated in Figs. 1 and 2, is limited essentially by the large *true* line widths, unknown line shapes, and the particular line groupings. It appears that ultimately we must resort to the observer's judgment as to the "reasonableness" of the component line shapes. But *nevertheless* a great deal of uncertainty and ambiguity can be eliminated by recording the line contours with high resolving power, with an accurate intensity scale (and, of course, intensity readings), and also, possibly in some respects, by comparing measurements on as many similar regions of adjacent elements as possible. As stated above, the data of this note are preliminary, and more measurements are now in progress.

[9] See F. R. Hirsh, Jr., Phys. Rev. **38**, 914 (1931), and references. That distinct satellite lines are observed on carefully exposed (over-exposed) photographic plates is due to the physiological or psychological effect of the eye in seeing contrast.

[10] For example, see A. Jönsson, Zeits. f. Physik **46**, 383 (1928); R. C. Spencer, Phys. Rev. **38**, 630 (1931); F. R. Hirsh, Jr., Phys. Rev. **48**, 722 (1935); M. Siegbahn, reference 5, page 366 and pages 356–362; A. H. Compton and S. K. Allison, *X-Rays in Theory and Experiment* (1936), pages 646 to 654; and references.

[11] E. Lindberg, Nova Acta Reg. Soc. Sci. Upsaliensis, Ser. IV, Vol. 7, No. 7, 1931.

[12] F. R. Hirsh, Jr., Phys. Rev. **48**, 722 (1935).

Band Spectra of MgCl, MgBr and MgI in Absorption

FRANK MORGAN, *Mendenhall Laboratory of Physics, Ohio State University, Columbus, Ohio*

(Received July 22, 1936)

The band spectra of MgCl, MgBr and MgI have been studied in absorption. Single systems of four-headed bands, lying between 3600 and 3950A for MgCl and between 3800 and 4000A for MgBr, have been observed. All of the bands degrade toward the violet. A vibrational analysis has been made for each of these systems. These vibrational analyses are consistent with the respective isotope shifts. The analysis of the system for MgCl is not in agreement with that proposed by Parker. A band system, lying between 4040 and 4200A and degrading toward the violet, was also observed for MgI. This system is insufficiently developed for a vibrational analysis.

OLMSTED[1] photographed the flame spectrum of MgCl, MgBr and MgI, but the bands were weak and overlapped by the magnesium oxide bands. Walters and Barratt[2] obtained the bands in absorption with a prism instrument but did not make a vibrational analysis. Parker[3] reported a vibrational analysis for the well-developed system of MgCl bands lying between 3600 and 3950A and also analyzed a weaker system lying in the same region and consisting of three bands, on the assumption that both systems have a common lower state.

EXPERIMENTAL

To obtain the band spectra of MgCl, MgBr and MgI in absorption, gaseous chlorine, bromine or iodine, respectively, was passed over magnesium metal that was heated in an open graphite tube about 30 cm in length in a carbon resistor furnace to a temperature of approximately 1600°C. Nitrogen gas was passed into the furnace to prevent, as far as possible, the oxidation of the magnesium and the burning of the graphite combustion tube. Light from a 500-watt incandescent lamp was passed through the graphite tube containing the vapor under investigation.

Preliminary observations were made on a Hilger E-1 quartz spectrograph, but all measurements were made on spectrograms taken on a 10-ft. concave grating which has a dispersion of approximately 2.7A per mm in the second order. Photographs were taken in the first, second and fourth orders, but most of the measurements were made on second-order plates.

MgCl BANDS

In MgCl only one system of bands was found in absorption. The bands degrade to the violet and apparently have four heads, but the heads are not of equal intensities. Table I shows the Deslandres arrangement of the heads of the bands due to $Mg^{24}Cl^{35}$ and Table II gives the vibrational quantum numbers, the observed wave numbers and the difference between the observed and calculated wave numbers for the Q_2 heads. Within the error of observation these Q_2 heads are represented by the equation:

$$\nu = 26{,}521.0 + 491.6u' - 2.54u'^2 - 0.025u'^3 - 466.0u'' + 2.10u''^2,$$

where $u' = v' + \frac{1}{2}$ and $u'' = v'' + \frac{1}{2}$.

These tables contain the data on three strong sequences, $\Delta v = \pm 1$ and 0, and on two weak ones, $\Delta v = \pm 2$. In the $\Delta v = 0$ sequence the P_1 heads are considerably weaker than the P_2 heads and the P_2 heads are somewhat weaker than the heads due to the Q branches. In the -1 sequence the P_1 heads are stronger while in the $+1$ sequence they are weaker with respect to the Q heads than was the case in the $\Delta v = 0$ sequence. In both the $+1$ and -1 sequences an overlapping of the P heads occurs.

Each strong band due to $Mg^{24}Cl^{35}$ in the $+1$ or -1 sequence is accompanied by a weaker band due to $Mg^{24}Cl^{37}$ and $Mg^{25}Cl^{35}$. In favorable cases a still weaker band due to $Mg^{26}Cl^{35}$ and $Mg^{25}Cl^{37}$ was observed and in one case a band

[1] C. M. Olmsted, Zeits. f. wiss. Phot. **4**, 293 (1906).
[2] O. H. Walters and S. Barratt, Proc. Roy. Soc. **A118**, 120 (1928).
[3] A. E. Parker, Phys. Rev. **47**, 349 (1935).

TABLE I. *MgCl bands.*

	v''	0	1	2	3	4	5	6	7	8
v'										
0	P_1	26455.5	25998.9							
	Q_1	26478.6	26016.9							
	P_2	26516.6	26057.3							
	Q_2	26533.9	26071.5							
1	P_1	26939.0	26480.7	26028.0	25577.7					
	Q_1	26964.1	26503.6	26046.1	25592.2					
	P_2	26998.1*	26541.3	26086.0						
	Q_2	27019.2	26558.0	26100.5	25646.7					
2	P_1				26057.3	25611.9				
	Q_1	27447.8	26985.1	26528.0	26074.8	25625.6				
	P_2	27473.8	27017.5	26565.3	26115.3	25666.9				
	Q_2	27502.5	27039.5	26581.4	26129.0	25678.8				
3	P_1						25643.3			
	Q_1		27459.5	27004.8	26551.8	26103.2	25657.7			
	P_2			27036.1	26587.7	26142.2	25697.2			
	Q_2		27514.6	27057.7	26604.7	26155.5	25710.0			
4	P_1									
	Q_1			27476.8	27024.2	26575.3	26131.1	25688.5		
	P_2					26609.7	26167.1	25727.3		
	Q_2			27529.3	27076.2	26626.7	26180.2	25739.6		
5	P_1									
	Q_1				27487.0	27041.4	26597.1	26155.5	25718.2	
	P_2								25756.0	
	Q_2				27539.8	27092.5	26646.2	26205.0	25767.8	
6	P_1									
	Q_1					27497.0	27057.7	26617.5	26180.2	25746.5
	P_2									
	Q_2					27550.1	27104.6	26663.3	26226.6	
7	P_1									
	Q_1							27069.6	26634.7	
	P_2									
	Q_2							27113.7	26676.5	26242.2

* Overlapped by (3,2) $Mg^{24}Cl^{37}$ band.

was found which should probably be attributed to $Mg^{26}Cl^{37}$. The bands due to $Mg^{24}Cl^{37}$ and $Mg^{25}Cl^{35}$ appeared as one because the values of $(1-\rho)$ are 0.011 and 0.012, respectively, where ρ is the square root of the ratio of the reduced masses of $Mg^{24}Cl^{35}$ and $Mg^{24}Cl^{37}$ or $Mg^{24}Cl^{35}$ and $Mg^{25}Cl^{35}$, and consequently the heads should be separated by only about 0.5 cm^{-1} in either the $+1$ or -1 sequence. Only the heads of the bands due to the molecule $Mg^{24}Cl^{35}$ were strong enough to be measured in the $+2$ or -2 sequence. The average measured isotope shift for the $Mg^{24}Cl^{35}$ and $Mg^{24}Cl^{37}$ or $Mg^{25}Cl^{35}$ molecules for the -1 sequence is 5.0 cm^{-1}, while for the $+1$ sequence it is 6.3 cm^{-1}. The corresponding values, calculated from theory for the vibrational isotope shift, are 4.7 cm^{-1} for $Mg^{24}Cl^{37}$ for the -1 sequence and 5.8 cm^{-1} for $Mg^{24}Cl^{37}$ or 6.3 cm^{-1} for $Mg^{25}Cl^{35}$ for the $+1$ sequence. In the -1 sequence the $Mg^{25}Cl^{35}$ heads should not be observed because of overlapping by the stronger $Mg^{24}Cl^{37}$ bands. This overlapping should not occur in the $+1$ sequence. The agreement of the observed with the calculated isotope shift is very good.

In order to fix the notation appropriate for the head forming branches, the method of Jevons[4] was followed. He showed that for bands that degrade toward the violet, the separation between the P and Q heads increases as v'' decreases and also as v' increases. The separation of the first and second heads and that of the second and fourth heads of each band in $Mg^{24}Cl^{35}$ have been recorded in Table III for the different

[4] Jevons, *Report on Band Spectra of Diatomic Molecules*, p. 55.

vibrational quantum numbers. From this table it is evident that separation of the first and second heads increases as v'' is decreased and as v' is increased, indicating that the first is a P head and the second is a Q head. Also it is seen from the table that the separation of the second and fourth heads do not systematically increase or decrease with an increase or decrease of v' or v''. Hence the second head cannot be a P head and has accordingly been designated as a Q_1 head.

We have attributed this four-headed band system to a $^2\Pi \leftarrow {}^2\Sigma$ transition. This identification is not in agreement with that of Parker[3] who attributes it to a $^2\Sigma \rightarrow {}^2\Sigma$ or a $^2\Pi \rightarrow {}^2\Pi$ transition. His identification is based primarily on the fact that he observed only two heads for each band. We prefer our assignment for the following reasons:

1. This system resembles the $^2\Pi \rightleftarrows {}^2\Sigma$ system of MgF for which Jenkins and Grinfeld[5] have given a rotational analysis.

2. There is also a marked similarity between it and the $^2\Pi \rightarrow {}^2\Sigma$ system of BeCl which has been analyzed by Fredrickson and Hogan.[6]

3. The electronic structures of MgF, MgCl and MgBr are similar and this fact suggests that the same ground state might be expected in each case. In the MgBr system each band has four heads, suggesting that the transition should be $^2\Pi \leftarrow {}^2\Sigma$ or $^2\Sigma \leftarrow {}^2\Pi$. On a frequency scale the band system of MgCl lies between the band system of MgF and the band system of MgBr. This fact suggests that the three systems should have the same upper and lower states. If the transition for MgF is $^2\Pi \rightleftarrows {}^2\Sigma$, as suggested by Jenkins and Grinfeld, it seems highly probable that the band system of MgBr and that for MgCl should be attributed to a $^2\Pi \leftarrow {}^2\Sigma$ transition.

4. The correctness of this assignment is further indicated by the fact that all of the observed heads of the MgCl system are included in this analysis without assuming large perturbations and that the intensities of the bands vary in a regular manner.

TABLE II. *Analysis of MgCl bands.*

v'	v''	ν(observed)	ν(obs.)-ν(calc.)	v'	v''	ν(observed)	ν(obs.)-ν(calc.)
1	3	25646.7	0.4	4	4	26626.7	1.7
2	4	678.8	−0.4	5	5	646.2	1.9
3	5	710.0	0.1	6	6	663.3	1.4
4	6	739.6	0.4	7	7	676.5	−1.2
5	7	767.8	0.9	8	8	688.3	−3.1
0	1	26071.5	−0.4	1	0	27019.2	−0.9
1	2	100.5	−0.2	2	1	039.5	0.1
2	3	129.0	0.5	3	2	057.7	0.3
3	4	155.5	0.6	4	3	076.2	2.0
4	5	180.2	0.2	5	4	092.5	3.2
5	6	205.0	1.5	6	5	104.6	1.9
6	7	226.6	1.3	7	6	113.7	−0.6
7	8	242.2	−3.2	2	0	502.5	1.3
0	0	533.9	0.2	3	1	514.6	−0.5
1	1	558.0	−0.3	4	2	529.3	1.7
2	2	581.4	−0.4	5	3	539.8	1.3
3	3	604.7	0.6	6	4	550.1	2.4

[5] F. A. Jenkins and R. Grinfeld, Phys. Rev. **45**, 229 (1934).

[6] W. R. Fredrickson and M. E. Hogan, Phys. Rev. **46**, 454 (1934).

MgBr Bands

In MgBr a single band system, lying somewhat farther toward the red than the system for MgCl, was found. These bands also degrade toward the violet, but in this case each sequence is separated into two parts. Four sequences, the ± 1, 0 and -2 were observed. Table IV shows the Deslandres arrangement of the observed bands and Table V gives the vibrational analysis, the observed wave numbers and the difference between the observed and calculated wave numbers of the Q_1 heads. Within the error of observation, the following formula represents the wave numbers of the Q_1 heads.

$$\nu = 25{,}765.2 + 393.8u' - 2.05u'^2 - 0.040u'^3 - 373.2u'' + 1.34u''^2,$$

where $u' = v' + \frac{1}{2}$ and $u'' = v'' + \frac{1}{2}$.

The Q_2 heads appear to converge and for the sequences, $\Delta v = 0$ and $\Delta v = 1$, the heads crowd together in such a way that they give the appearance of a broad absorption band. For the $\Delta v = 0$ sequence this absorption band extends from about 25,895 to 25,900 cm^{-1}. The heads designated as P heads are stronger in comparison to the Q heads than they were in the case of MgCl.

TABLE III. *Head-origin separations for MgCl bands.*

	v''	0	1	2	3	4	5
v'							
0	Q_1-P_1	23.1	18.0				
	Q_2-Q_1	55.3	54.6				
1	Q_1-P_1	25.1	22.9	18.1	14.5		
	Q_2-Q_1	55.1	54.4	54.4	54.4		
2	Q_1-P_1				17.5	13.7	
	Q_2-Q_1	54.7	54.4	53.4	54.2	53.2	
3	Q_1-P_1						14.4
	Q_2-Q_1		55.1	52.9	52.9	52.3	52.3

TABLE IV. *MgBr bands.*

v'		v'' 0	1	2	3	4	5	6
0	P_1	25762.5	25393.8					
	Q_1	25775.3	25404.4					
	P_2	25872.1	25503.9					
	Q_2	25886.4	25514.8					
1	P_1	26147.1	25780.9	25415.4	25052.0			
	Q_1	26164.6	25794.5	25425.8	25060.1			
	P_2	26245.2	25880.7					
	Q_2	26263.6	25895.6	25527.6				
2	P_1		26161.0	25798.1	25435.1	25074.7		
	Q_1		26179.1	25811.8	25446.3	25083.9		
	P_2		26254.1	25887.7				
	Q_2		26265.3	25896.9	25531.9			
3	P_1			26173.1		25453.5	25095.7	
	Q_1			26191.5	25827.2	25464.8	25105.0	
	P_2			26258.8				
	Q_2				25898.1			
4	P_1				26185.0		25469.3	25113.7
	Q_1				26201.4	25840.6	25480.9	25123.9
	P_2							
	Q_2							
5	P_1					26196.3		
	Q_1					26206.4	25847.3	25490.7
	P_2							
	Q_2							

Since $(1-\rho)$ for the molecules $Mg^{24}Br^{79}$ and $Mg^{24}Br^{81}$ is only 0.003, the heads due to the different isotopes of bromine have not been resolved completely, although in the second order of the 10-ft grating the heads of the -2 sequence appear to be double and in the fourth order the heads of the $+1$ and -1 sequences also appear to be double. Band heads due to $Mg^{25}Br$ and $Mg^{26}Br$ have been observed under favorable conditions.

In the case of MgBr as in the case of MgCl, the method of Jevons was used to distinguish between the P and Q branches.

MgI BANDS

In MgI there appeared three regions of nearly continuous absorption, lying slightly to the red when compared to the bands found for MgBr. In these regions some band heads appear. In addition to these three regions of nearly continuous absorption there was, farther toward the red, a band system consisting of a few bands that degrade toward the violet. The observed wave numbers of three short sequences, probably $\Delta v = \pm 1$ and 0, of this system are recorded in Table VI. The bands appear to be double headed, but since the heads lie so close together it has not been possible to classify them. If the first head of each sequence is a P head, ω'' should be approximately the difference between the first head of the 0 sequence and first head of the -1 sequence, while ω' should be approximately the difference between the first heads of the $+1$ and 0 sequences. Thus ω'' should be about 312 cm^{-1} and ω' about 318 cm^{-1}.

While the short wave-length sides of the regions of continuous absorption are not sharply defined, they are sharper than the long wave-

TABLE V. *Analysis of MgBr bands.*

v'	v''	ν(obs.)	ν(obs.)-ν(calc.)	v'	v''	ν(obs.)	ν(obs.)-ν(calc.)
1	3	25060.1	−0.3	0	0	25775.3	0.0
2	4	083.9	−0.1	1	1	794.5	0.1
3	5	105.0	0.4	2	2	811.8	0.1
4	6	123.9	0.9	3	3	827.2	0.3
5	7	136.2	−2.6	4	4	840.6	0.7
0	1	404.4	−0.4	5	5	847.3	−3.0
1	2	425.8	−0.8	1	0	26164.6	−0.3
2	3	446.3	−0.2	2	1	179.1	−0.4
3	4	464.8	0.4	3	2	191.5	−1.1
4	5	480.9	0.8	4	3	201.4	−1.0
5	6	490.7	−2.5	5	4	206.4	−3.7

length sides and are in the neighborhood of 24,980, 25,290, and 25,594 cm^{-1}. If the three regions correspond to the -1, 0, and $+1$ sequences, respectively, the difference between the first two numbers should give an approximate value of ω'', while the difference between the second and third numbers should correspond roughly to ω'. Thus ω'' for this system may be expected to be about 310 cm^{-1}, and ω' about 304 cm^{-1}. This value of ω'' is in good agreement with the value, 312 cm^{-1}, for the other system.

TABLE VI. *MgI bands.*

$v'-v''$	-1	0	$+1$
	24010.6	24322.2	24640.2
	16.4	29.0	45.5
	19.2	36.3	50.7
	26.2		
	28.9		
	36.0		

The author wishes to express his appreciation to Professors Alpheus W. Smith and R. V. Zumstein for valuable discussions and suggestions given during the course of this investigation.

OCTOBER 1, 1936 PHYSICAL REVIEW VOLUME 50

The Spectrum of Indium Oxide

WILLIAM W. WATSON AND ARTHUR SHAMBON, *Sloane Physics Laboratory, Yale University*

(Received July 27, 1936)

A rather complex spectrum of InO lying between the two In resonance lines at 4102A and 4511A is described. Most of the band heads are assigned to a $^2\Pi \rightarrow {}^2\Sigma$ system with the frequencies of the main $(R_2+Q_2^2)$ heads given by the formula $\nu = 23{,}595.10+626.66(v'+\frac{1}{2})-3.40(v'+\frac{1}{2})^2 -703.09(v''+\frac{1}{2})+3.71(v''+\frac{1}{2})^2+0.285(v''+\frac{1}{2})^3$. ν_e for the other spin component is at 23,033.10. The large cubic term causes rapid convergence of the few band sequences, giving rise to prominent "tail" bands.

IN a report of the analysis of a band system due to the GaO molecule, Marjorie L. Guernsey[1] discussed briefly a complex spectrum of indium oxide lying largely between the two In resonance lines at 4102A and 4511A. Although the experimental conditions indicated the InO molecule to be the emitter, no obvious regularities in the distribution of bands were noted. And since among the band heads degrading predominantly to the red there occur a number of violet degrading heads, it was suggested that there are two InO band systems overlapping in this region. A reproduction of this spectrum is given in Fig. 1.

Spectra are known[2] for the diatomic oxides of all the other elements of Group III of the periodic table excepting Tl and Ac. These band systems are all transitions between $^2\Pi$ and $^2\Sigma$ electronic states, with a $^2\Sigma$ state lying lowest in the level scheme for each molecule. Similarly we find that the vast majority of the InO band heads constitute either a $^2\Pi \rightarrow {}^2\Sigma$ or a $^2\Sigma \rightarrow {}^2\Pi$ system, with the former designation preferred because of the energy level arrangement of the related molecules. The complexity of the spectrum arises from the near equality of the doublet interval in the $^2\Pi$ state with many of the $\Delta G(v)$ values in both states, producing interlacing of the band sequences, as well as the rapid convergence of these sequences to cause "tail" bands. We give the details below.

A Tl arc burning in air gives rise to no oxide band spectrum in the region of the resonance lines of Tl I. We conclude that one or both of the corresponding Tl O levels are unstable repulsion states, a situation harbingered by the fairly low stability of the lower state of the InO band system discussed in the present paper. This instability is to be contrasted with the apparently rather large dissociation energy of the ground state and the relative abundance of electronic levels in the intervening LaO molecule[3] in this group.

[1] M. L. Guernsey, Phys. Rev. **46**, 114 (1934).

[2] Cf. W. Jevons, *Report on Band Spectra of Diatomic Molecules*, or H. Sponer, *Molekülspektren*, for constants of the known energy levels and references to original papers.

[3] W. Jevons, Proc. Phys. Soc. **41**, 520 (1929).

TABLE I. *Wave numbers, quantum assignments and intensities of band heads in the InO spectrum. at. denotes obliteration by the strong continuum associated with the In resonance lines.*

v', v''	$\nu(cm^{-1})$	Int.	v', v''	$\nu(cm^{-1})$	Int.	v', v''	$\nu(cm^{-1})$	Int.	v', v''	$\nu(cm^{-1})$	Int.
	22994.1	1		*at.*			22668.4	2		23215.5	5
0,0	23057.2	2	2,3	*at.*		5,5	22728.2	0	7,6	23254.9	4
	23557.0	9		22735.0	3		23231.5	4		23771.9	1
	23619.2	7		———			23284.3	4		23817.5	1
	22340	2		24150.0	1		*at.*			22604.0	
0,1	———		3,1	24178.8	6	5,6	*at.*		7,7	22666.3	5
	22864.2	2		24703.9	1		22604	1		———	
	22940.5	0		———			22668.4	2		23215.5	5
	23616.4	9		23463.5	2		*at.*			*at.*	
1,0	23666.7	9	3,2	———		6,3	*at.*		7,8	*at.*	
	24178.8	6		24016.2	7		25121.2	1		———	
	24227.2	6		24061.0	10		———			22635.0	1
	22922.4	3		22784.1	1		23905	1		*at.*	
1,1	22983.0	2	3,3	22840.4	2	6,4	———		8,5	*at.*	
	23481.7	7		23344.7	10		*at.*			24968.8	0
	23542.8	0		23399.6	2		*at.*			———	
	at.			*at.*			———			*at.*	
1,2	*at.*		3,4	*at.*		8,6	———		10,7	*at.*	
	22784.1	0		22682.4	1		*at.*			24860.9	1
	22866.4	2		22750.5	5		*at.*			24887.8	1
	24227.2	6		24053.6	0		———			23711.3	3
2,0	24258.0	5	4,2	24083.5	2	8,7	———		10,8	———	
	———			24609	1		23732.7	5		*at.*	
	24825.3	3		24647.6	0		———			*at.*	
	23542.8	0		23386.2	6		22591.6	2		23151.0	1
2,1	———		4,3	———		8,8	———		10,9	———	
	24095.3	3		23939.8	4		———			———	
	24132.7	1		23985.2	4		———			———	
	22850.2	2		22724.5	1		*at.*			22604.0	2
2,2	22910.1	0	4,4	22781.7	1	9,6	*at.*		10,10	22666.3	5
	23410.9	10		23283.3	4		24904.9	2		23157.3	6
	23476.6	1		23342.6	10		24928.9	0		———	
	at.			23261.8	1		23743.6	4		———	
4,5	*at.*		6,5	23306.2	4	9,7	23771.9	1	11,10	———	
	22635	2		23817.5	0		*at.*			23709.6	1
	22709.0	0		23865.3	3		*at.*			———	
	24647.6	0		22626	1		23157.3	6		———	
5,2	24663.6	1	6,6	22682.4	1	9,8	23204.6	1	12,11	———	
	25203.1	0		23189.3	1		23708.3	2		23735.1	3
	25217.1	0		23241.2	7		23751.6	1		———	
	23971.8	0		*at.*			22591.6	2			
5,3	24001	4	6,7	*at.*		9,9	———				
	at.			———			———				
	at.			22635	2		———				
	23311.7	4		23843.1	2		*at.*				
5,4	23353.3	0	7,5	23865.3	3	9,10	*at.*				
	23875.8	3		*at.*			———				
	———			*at.*			22666.3	5			

EXPERIMENTAL PROCEDURE

The light source was a 220-volt d.c. arc in air carrying 3 amperes between an anode of indium metal packed into a shallow copper cup and a water-cooled copper cathode. The indium metal was kindly supplied to us by Professor H. S. Uhler.[4] Gallium was present to such a slight extent as to make the GaO bands of negligible intensity. By using In_2O_3 in the anode of this

[4] H. S. Uhler and P. E. Browning, Am. J. Sci. **42**, 389 (1916).

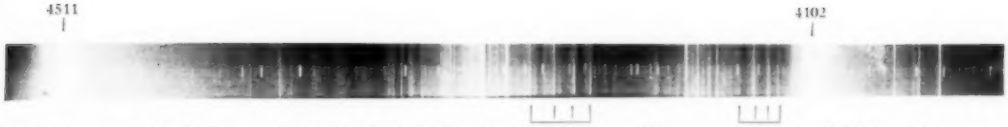

FIG. 1. Spectrum of InO. Corresponding bands in the bracketed groups have the constant spacing of 560 cm^{-1} interpreted as the interval between the two spin components of a $^2\Pi$ state.

arc the same InO spectrum could be produced but with considerably lowered intensity. Spectrograms were taken in the second and third orders of the 21-foot grating in a stigmatic mounting, the dispersion being 2.45 and 1.43A/mm.

INO SPECTRUM

Band heads in this system are observed from 3847A to 4763A, the strong bands being confined to the region between the In resonance lines as exhibited in Fig. 1. Although the majority of the heads degrade to the red, some are diffuse and a number degrade definitely to the violet. Quantum analysis is rendered difficult because of the considerable interlacing of band structure and the lack of evident regularity of spacing of the heads. Also the continuum extending out from each of the In resonance lines on its high frequency side (evidence probably of the existence of quasi-stable In_2 molecules) obliterates a considerable portion of two of the band sequences. However, it is evident that the principal band heads fall roughly into three main groups, with a similar arrangement of successive strong heads (those bracketed in Fig. 1) on the high frequency sides of the two more intense groups.

Between band heads in these two brackets a constant frequency difference of 560 cm^{-1} was found to exist. Both the magnitude and the constancy of this interval suggested that it represented the multiplet spacing in a $^2\Pi$ state of InO. With this and the lower state vibrational frequency which could be approximately predicted for InO as guides, vibrational quantum assignments of most of the heads of appreciable intensity were made. These assignments are presented in Table I. The four heads assigned to each pair of vibrational quantum numbers are probably the heads formed by the Q_1, R_1, R_2+Q_2, and ${}^sR_{21}$ branches of a $^2\Pi\rightarrow{}^2\Sigma$ transition. For many of the bands, structure representing the remaining branches of this type of band is present, but due to incomplete resolution and overlapping the analysis of this structure cannot be made. This frequent overlapping and fusion of band heads also considerably perturbs the intensity distribution in some of the bands.

The following formula gives quite accurately the frequency of the third (R_2+Q_2?) head of each of the bands listed in Table I. $\nu = 23{,}595.10 + [626.66(v'+\frac{1}{2}) - 3.40(v'+\frac{1}{2})^2] - [703.09(v''+\frac{1}{2}) - 3.71(v''+\frac{1}{2})^2 - 0.285(v''+\frac{1}{2})^3]$. The ν_e for the first (Q?) heads is at 23,033.10. ω_e'' is just about that predicted by comparison with the values for other third group diatomic oxide molecules. Of most interest is the large negative cubic term in the lower state. This reduces the successive $\Delta G(v''+\frac{1}{2})$ values at an accelerated rate, causing the sequences to converge at fairly low vibrational quantum numbers with consequent production of "tail" bands degrading to the violet. The $\Delta v = -1$, 0 and $+1$ sequences have convergence points at $v''=6$, 8 and 10, respectively, and the two most markedly violet degrading heads 23,157.3 and 23,735.1 fit very well according to the formula into the (10, 10) and (12, 11) bands, respectively. Early in this investigation we tried without success to place the violet degrading heads into a separate band system. The assignment of most if not all of these heads as "tail" bands in this $^2\Pi\rightarrow{}^2\Sigma$ system is indicated by our analysis, but we cannot positively exclude the existence of another fragmentary band system interlaced with the one here described.

Because of the more rapid decrease in $\Delta G(v''+\frac{1}{2})$ values with increasing v, there is near equality throughout most of the v', v'' matrix scheme of the $\Delta G(v'+\frac{1}{2})$, the $\Delta G(v''+\frac{1}{2})$ and the electronic multiplet interval at every point. This produces a considerable amount of overlapping of band sequences and partial fusions of various band heads. Together with the presence of "tail" bands, this coincidence in intervals makes for the general irregularity in band distribution which proved so puzzling in the earlier investigation.[1]

An Investigation of Irregularities in Thermionic Emission from Tungsten

FELIX L. YERZLEY, *Department of Physics, Cornell University*

(Received June 26, 1936)

A tube employing a moving electrode is used to investigate variations in emission density over the length of a straight tungsten filament. After a critical temperature range is exceeded positive ion emission is shown to be limited to narrow regions near the lead wire connections. Electron emission, even after the filament is carefully aged, is not uniform from point to point, but occurs in a stable though irregular pattern. The irregularity is attributed to differences in work function or to differences in actual area covered by the slit or to a combination of both.

INTRODUCTION

IN a recent paper on emission patterns of cylindrical filaments, R. P. Johnson and W. Shockley[1] reported results obtained photographically from a tube employing a fluorescent screen and circumferential magnification. Photographic recording has also been used by other workers[2, 3] employing flat emitting surfaces and electron microscopes. Pinhole cameras have also found limited application.[4, 5] Quantitative measurements and systematic studies of both electron and positive ion emission from the same filament have not been reported in the literature, however, and the present paper will describe an experimental method developed for this purpose and used in a study of irregularities in the emission of electrons and impurities from tungsten.

EXPERIMENTAL TUBE

A slit arrangement was used, by which emission from selected small areas of a cylindrical filament could be measured. Values of the emission density computed from these measurements, when plotted against position along the filament length, showed longitudinal distribution of emission density. Data on either electrons or positive ions could be obtained by applying proper plate potentials. The principal features of the tube construction are covered in Fig. 1. Both the stationary and the sliding plates were made of seamless nickel tubing. The stationary plate had the diametral dimensions, 0.500-inch inside diameter and 0.520-inch outside diameter, maintained by the manufacturer. To form the sliding plate some of the same stock was forced over an enlarging mandrel to increase the inside diameter to 0.530 inch and was then annealed in a hydrogen furnace. The window was cut in the stationary plate by means of a sharp scribing point. The 0.008-inch slit in the sliding plate was made with a milling cutter.

The filament was accurately centered at the axis of the plate by means of special beryllia insulators supported in nickel spiders. Two quartz beads of the type used in FP-54 pliotron tubes supported the collector on the sliding plate and two others supported a trolley wire in back of the stationary plate. Special precautions were taken to have reliable contact between the collector and the trolley wire. Two connections were made, one a coil of 0.00175-inch nickel wire, the other a spring contact of 0.010-inch nickel wire. Throughout the duration of the tests both contacts remained intact.

Four 0.007-inch thoriated filaments were mounted in a side tube for better purposes and an ionization gauge was permanently connected to the tube to provide a check of vacuum conditions throughout the test.

A scale and vernier arrangement, by which the position of the slit relative to the filament was determined, could be read to 1/20 mm of any desired position. The scale was engraved on the stationary plate and the vernier on the sliding plate.

All parts were carefully designed to facilitate bakeout in the induction furnace. Regardless of how carefully the plates were polished before assembly to permit easy sliding, however, it was found that bakeout roughened the surfaces so

[1] Johnson and Shockley, Phys. Rev. **49**, 436 (1936).
[2] Bruche and Scherzer, *Geometrische Elektronen Optik* (1934).
[3] W. H. Brattain, cf. Becker, Rev. Mod. Phys. **7**, 118 (1935).
[4] H. Seemann, Zeits. f. Physik **79**, 742 (1932).
[5] A. J. Dempster, Phys. Rev. **46**, 165 (1934).

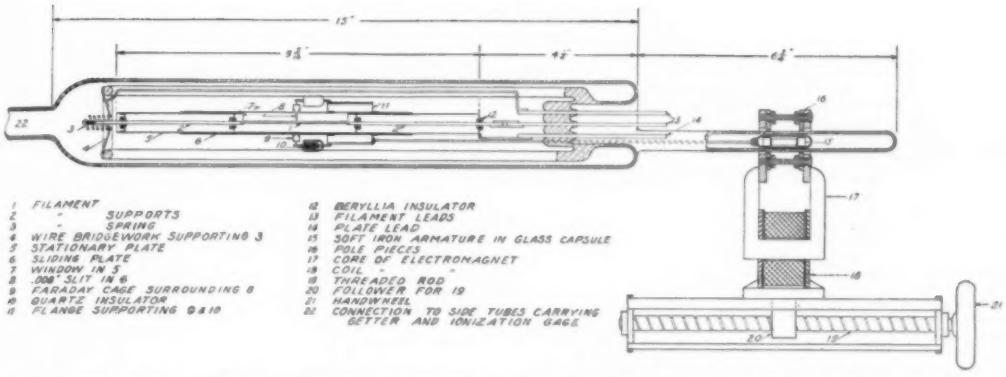

FIG. 1. Layout of the experimental tube and magnetic control. The flexible lead from 9 is not shown, but extends through a seal on the back of the tube.

badly that the full force of the magnetic control was necessary. This amounted to a pull of about a pound.

Throughout the test, the pressure in the tube as indicated continuously by the ionization gauge, was maintained at 2×10^{-7} millimeters of mercury or less. Any gas evolved was taken up by burning the thoriated filaments.

THE MEASURING CIRCUIT

The major features of the tube circuit are shown in Fig. 2. The filament current was accurately controlled and measured with a Leeds and Northrup Type K potentiometer, and could be reversed by means of the switch shown. The voltmeter was used to make occasional checks on the IR drop through the filament to verify the dimensional constancy of the wire. Appreciable evaporation of tungsten would, of course, increase the voltmeter reading for a given value of the filament current. The sliding and stationary plates of the experimental tube were at the same potential by virtue of their metallic contact. The potential of both relative to the filament was maintained by "B" batteries whose connections could be reversed to accelerate either electrons or positive ions as required. For all measurements reported in this paper the plate to filament potential was 200 volts. Currents to the collector were distributed over a range from 10^{-4} to 10^{-16} ampere necessitating an extremely flexible measuring circuit. For the small currents a DuBridge-Brown pliotron circuit[6] was used to measure the drop across one of three high resistors of different values. For the larger currents a shunted galvanometer was used. Actually the same galvanometer served for the pliotron circuit and for direct measurements, a reversing switch being provided in addition to permit the change from positive ion to electron measurement.

POSITIVE ION RESULTS

Temperature gradient along the length of filaments is the most easily recognizable cause of longitudinal differences in emission density. At low filament temperatures the lead connections are near room temperature and a maximum occurs near the half-way point on the length of the filament. As the filament current is increased the maximum value of the temperature increases and gradually stretches out into a plateau region of more or less constant value. The maximum may be determined to a sufficient degree of accuracy for most requirements from

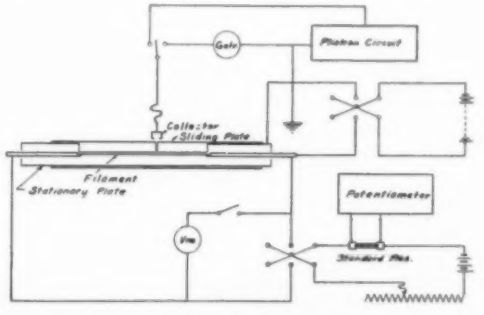

FIG. 2. Wiring diagram.

[6] DuBridge and Brown, Rev. Sci. Inst. **4**, 532 (1933).

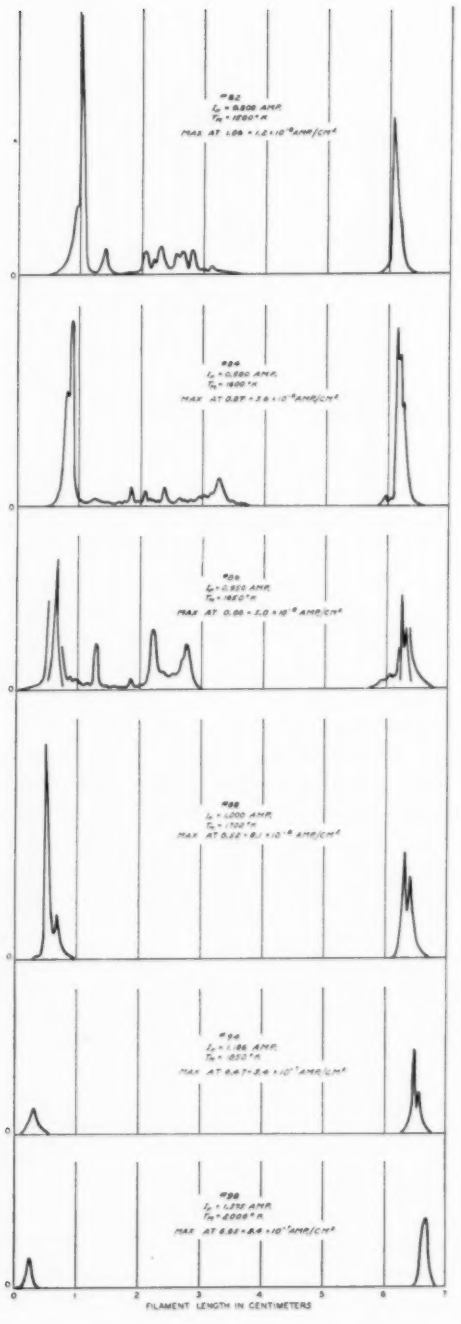

FIG. 3. Longitudinal distribution of positive ion emission at various stages of the aging process. The maxima of curve 86 are plotted to 1/10 the scale of other points.

the data of Jones and Langmuir.[7] At the ends, thermal conduction by the lead wires causes a temperature gradient from the plateau value to the temperature of the leads as described by Langmuir, McLane and Blodgett.[8] Neither the maximum temperature nor the end losses can be precisely calculated, however, since emission currents are frequently appreciable in comparison with the heating current, and because the temperature of the lead wire connection is normally indeterminate experimentally.

For regular thermal emission of electrons or of characteristic ions[9] the emission density is an increasing function of the temperature. The emission of ions of impurities, on the other hand, is not an increasing function over the entire temperature range, but increases to a maximum and then decreases as the temperature is raised further.

The phenomenon behaves as though a critical temperature exists at which ion emission is a maximum. Thus as the temperature of an unaged filament is increased, emission of ions of impurities will increase until the critical temperature is reached and will then decrease with further increases in temperature. Regardless of the influence of other factors it is likely that the principal reason for the critical temperature is the cleaning of the wire in the hotter regions. Above the critical temperature the surface coating is very thin or nonexistent, whereas it may give rise to very strong currents at or below the critical temperature. This lends considerable weight to the assumption that tungsten can be adequately cleaned for experiments on electron emission, a conclusion which will be substantiated by electron data to be given later.

Experimental results for a 0.0048-inch Fansteel tungsten wire are shown in Fig. 3 for various temperatures. The filament had not been burned previously above 1400°K, hence the distributions represent successive stages in the aging of a raw filament.

Curve 82 represents the distribution of ion emission corresponding to a temperature maximum of 1500°K and a temperature gradient beginning near the center and extending to a

[7] Jones and Langmuir, General Electric Reprint, 1927.
[8] Langmuir, McLane and Blodgett, Phys. Rev. **36**, 478 (1930).
[9] L. P. Smith, Phys. Rev. **35**, 390 (1930).

minimum at the lead connections. The regions of greatest emission density show irregularities such as that at 0.97 cm which may be evidence either of different chemical components in the surface coating or of irregular distribution of the surface film. A surface coating of more durable nature is indicated by the emission from 1.2 to 3.6 cm. No emission was observed between 3.6 and 5.8 cm with a sensitivity that would have detected emission densities of 10^{-11} amp./cm^2.

The sequence of curves following 82 represents emission distributions at successively higher temperatures. It can be seen that as the temperature is increased and the region of relatively uniform temperature widens out into a more extensive plateau, the increasing temperature near the lead wires causes the maxima to shift progressively toward the ends.

In addition to temperature dependence, two other factors are important in considering emission of positive ions from the cooler portions of filaments. The first of these is variation with time, and the second is the influence of the applied electric field.

Before beginning the set of observations shown in Fig. 4, to illustrate the change of ion emission with time, the filament was maintained at 1700°K for several hours with an electron accelerating voltage of +200 volts. The ion collector was set to receive ions from the "6.5 cm" region of the filament and the potential was reversed to −200 volts at the time $t=0$. It is therefore clear that the intensity of ion emission is subject to great changes with time, and in a negative field will decrease. From the rapidity of the initial decay it is seen that a curve such as 94 cannot be obtained until the decay has leveled off to relatively stable values, since a single traverse for ion distribution over the end regions involves about a hundred and fifty experimental points and takes about two hours time. Hence, the distribution curves do not represent maximum values, and do not represent instantaneous distributions. Thus, on curve 94 for example, the crest at 6.47 cm does not accurately correspond to the crest at 0.31 cm since the two were not obtained simultaneously. Furthermore, the shapes of the peaks are subject to some distortion for the same reason.

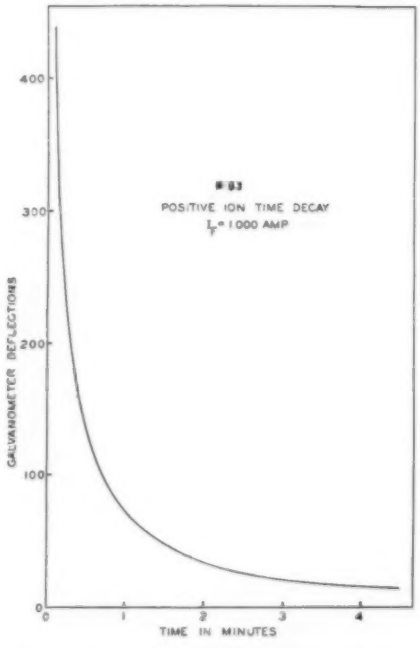

FIG. 4. Decay of positive ion emission with time.

The second factor is dependence upon field conditions, since experimental data indicate that the density of the surface contamination is influenced by the nature of the applied field. For example, the rapidity of the initial decay after the application of a negative field, as on curve 93, suggests that impurity had been collecting on the surface of the filament under the retarding positive field. Under a continuously negative field nothing but decay of the ion emission has ever been observed, while the decay phenomenon just described is characteristic of ion emission immediately after reversal of the field from retarding to accelerating. In some instances it is even possible that a relatively stable increase in the positive ion emission will result from a retarding field without changing other conditions. A comparison of curves 44 and 45, Fig. 5, will serve to illustrate this. Curve 44 was obtained after an extended period of decay. A retarding field was then applied for several hours. Characteristically rapid decay starting from values much greater than those of 44 occurred when the field was reversed. As soon as the decay had become quite gradual curve 45

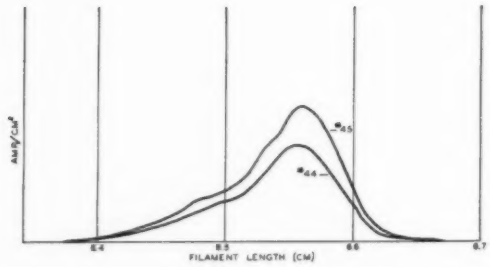

FIG. 5. Rebuilding of a surface coating of impurities in a negative applied field.

was obtained. Thus in spite of the completion of the early rapid stages of decay a sufficient change had taken place to give increased stable values of ion emission, and even though neutral atoms may evaporate from the surface at these temperatures, evaporation is not independent of applied electric fields.

ELECTRON RESULTS

On curve 82, Fig. 3, there is a component of positive ion emission near the central region of the filament which was durable at much higher temperatures than the surface coatings nearer the ends. Its durability was suggestive of an oxide coating. Curve 83, Fig. 6, taken at the same temperature shows that electron emission is measurable only where there is no emission of positive ions. Thus the surface coating in the region from 1.2 to 3.6 cm on curve 82 gave the filament a high electronic work function tending to confirm the previous suggestion in regard to its chemical nature.

At 1700°K emission of electrons takes place from regions of differing surface conditions as shown on curve 92. Areas of low work function resulting from a surface coating give rise to pronounced maxima near the ends. The central region is presumably considerably cleaner than the end regions, and has, therefore, a higher work function. The emission structure is extremely irregular as demonstrated by the numerous and pronounced irregularities in the curve. Variations of this kind could easily result from slight differences in the work function, and some of the variation could be due to changes in the actual area covered by the slit, a matter which will be discussed in greater detail later. Since the filament probably is not clean at this temperature it is reasonable to attribute the structure to patchlike distributions of the surface coating and consequent variations of the work function over the successive rings covered by the slit in making a traverse along the length of the filament.

At 2000°K an extensive portion of the filament is at very nearly constant temperature. Also, at this temperature, emissivity from the central region is high compared with the limited emission from the contaminated end regions. These two facts are sufficient to account for a considerable change in the distribution of emission from that plotted on curve 92. The structure at 2000°K, as shown on curve 99, is relatively flat with the exception of four prominences. In the end region between 0 and 1 cm a hump is superimposed upon a general background of apparent emission giving evidence again of low work function in the cooler regions. This peak is roughly three times as high as the background values and the reduction of its value to a third would result in its loss. Under these circumstances, therefore, evidence of this sort cannot be expected in every case. There is no corresponding peak, for example, at the opposite end of the same distribution curve.

Curve 100 shows further development of structure in the central region of the filament at 2300°K. The four maxima which appear on curve 99 have widened out into regions of high emission separated from each other by narrow valleys. It was suspected that the major features of curve 100 would prove to be characteristic of a clean tungsten wire, but an accident destroyed this filament and subsequent tests were made on a new sample of the same stock.

Fig. 7 shows four distributions of electron emission over the new filament under various conditions. For comparison the curves are plotted in close proximity in numeric sequence and for convenience the scales are different and the origins are shifted.

Curve 105 taken at 2150°K was believed to show the emergence of structure characteristic of the new filament. Details are entirely different from those of curve 100, proving beyond any doubt that the geometry of the tube did not determine the structure.

The same structure persisted at 2300°K and 2450°K as shown by curves 106 and 107, respectively. These later curves also show a previously undemonstrated factor, namely greater emission from one end than from the other as the result of a differential in the heating effect. At the higher temperature the electron current to the plate was 54 milliamperes, and the filament current was, therefore, 54 milliamperes greater at the negative end than at the positive. Thus emission currents in general give rise to a longitudinal temperature gradient independent of that due to end cooling by the leads.

The filament was next burned at 2900°K for six minutes to complete the aging process of the wire in accordance with the usual thermionic practice for tungsten. After reducing the temperature to 2450°K again, curve 108 was obtained. The total electron emission to the plate corresponding to curve 108 was 56 milliamperes compared with a total value of 54 milliamperes for curve 107.

After curve 108 was taken the filament was aged continuously for two hours above 2900°K, but no major changes in the filament structure occurred. A further slight increase in the total emission at 2450°K resulted, however, as the result of evaporation of tungsten from the surface.

Conclusion

The cause of irregularities in electron emission distributions is not easy to explain. One may make several postulates including (a) the influence of impurities, (b) dimensional inconsistencies in the wire, (c) differences in the value of the work function, (d) differences in the actual area covered by a slit, and (e) the related Schottky effect.

The occurrence of impurities, at least as a major consideration, may be eliminated as a consequence of the observed emissions. The shift of positive ion emission toward the end regions of the filament as shown in Fig. 3, was an indication that the central region of the filament would eventually be thoroughly cleaned. It was noted that each increase in the temperature produced a definite shift of the ion emission toward the lead connections, thus supporting the deduction that cleaning of the surface at higher temperatures can be expected.

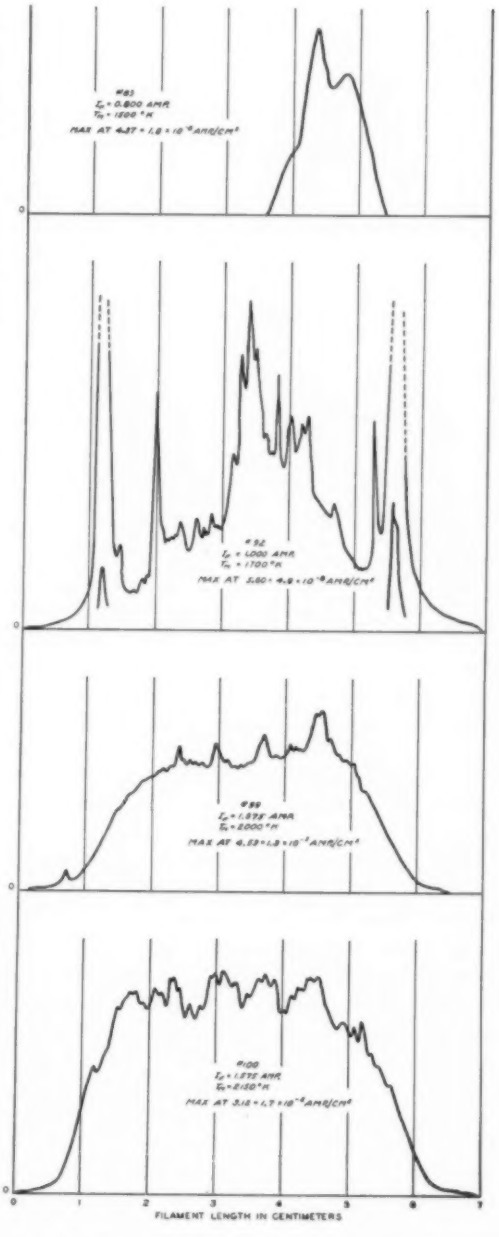

Fig. 6. Longitudinal distribution of electron emission at four stages of the aging process. The maxima of curve 92 are plotted to 1/10 the scale of other points.

Curve 92 indicates that surface impurities may give rise to abnormally high emission of electrons as shown by the peaks at the ends. The shift of

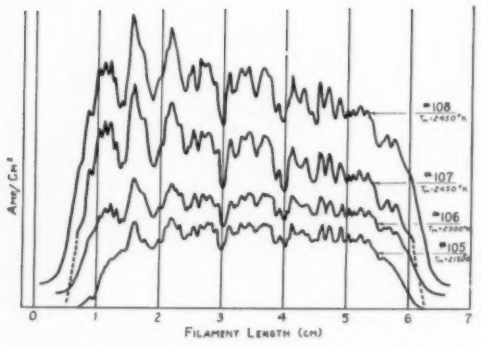

FIG. 7. Stability of characteristic electron emission distributions with various heat treatments. Curve 108 was obtained after flashing at 2900°K. Scales and origins were selected to facilitate comparison of the curves.

these maxima toward the ends with increasing temperature is evidenced by the peak occurring on curve 99 between 0 and 1 cm. The general conclusion from these data is that under usual conditions of thermionic experiments on tungsten, where data are taken from the central region of the filament only, impurities are not present in such a way as to effect the results. This conclusion is further supported by the curves of Fig. 7, which reveal the same structure after several heat treatments, yet changes would be expected if patches of impurity existed on the surface of the wire.

Dimensional irregularity can be eliminated as the cause of the observed structure by a series of simple calculations based upon curve 108. The peak at 1.6 cm on this curve is 44 percent higher than the minimum at 1.9 cm. By averaging out the structural irregularity, it is also noted that due to the 54 milliampere difference in the heating current at the two ends the general emission toward the negative end is roughly 45 percent greater than that near the positive end. The computations show that dimensional irregularities necessary to account for the emission pattern are greater than any variations actually present in the wire.

One objective of the test was to compare work function values from point to point on the filament in an effort to detect variation. Electrical difficulties with the circuit prevented a conclusive study of this quantity, although a value of 4.54 ev was indicated as the approximate value. In this connection it is important to consider the scale of the test. The apparent filament area covered by the slit and emitting electrons to the collector was 3.0×10^{-4} cm². If, as has been assumed, differences in work function are to be discovered between different crystalline faces, definite values will never be established by examination of such large areas. Etch facets on tungsten filaments are of a magnitude far inferior to 3×10^{-4} cm², and for that reason all data presented in this paper represent averages over serrated areas. It is probable in spite of this consideration, however, that with more precise technique applied to the same apparent area, a slight difference in the average work function would be detectable if one or another crystal face should predominate in making up the actual area of limited portions of the filament exterior. As indicated by Johnson and Shockley the difference might be pronounced in adjacent quarters of a filament circumference.

Differences in actual filament area covered by the slit, if independent of other factors which are possible contributors to the structure, could be used to account fully for irregularities of the observed magnitudes.[10] As shown by other investigators,[11] however, surface roughness results in the introduction of a necessary shape factor in applying the Schottky correction. Abnormally rough surfaces, at the points of which the electric fields are extremely high, make accurate revisions of the image force picture very difficult, and correction of the work function to zero field by application of the Schottky theory may be inadequate. The bearing this may have upon precise determination of work functions is obvious, even if it is granted that the difference in work function from face to face of certain crystals may be negligible.

In closing the author wishes to express appreciation of the friendly counsel of Professor Lloyd P. Smith, whose interest has contributed greatly to the progress of this work.

[10] L. Tonks, Phys. Rev. **38**, 1030 (1931).
[11] Compton and Langmuir, Rev. Mod. Phys. **2**, 149 (1930).

A Double-Focusing Mass Spectrograph and the Masses of N^{15} and O^{18}

JOSEF MATTAUCH, *University of Vienna, Austria*

(Received June 29, 1936)

After a short summary of the theory of double focusing a mass spectrograph which works as an "achromatic lens" for all masses is described in some detail. It is found to work according to the theoretical expectations. The differences of "packing fraction" (i.e., $\Delta M/M\times 10^4$) of doublets containing the rare isotopes N^{15} and O^{18} have been determined. It is found that for the doublet at mass number 15 ($C^{12}H_3^1-N^{15}$): $\Delta M/M\times 10^4=15.8_6\pm 0.05$, $\Delta M=0.02382$ and for the 18-doublet ($O^{16}H_2^1-O^{18}$): $\Delta M/M\times 10^4=6.9_8\pm 0.10$, $\Delta M=0.01257$. With Aston's masses of C^{12} and H^1 the isotopic weights referred to $O^{16}=16$ are: $N^{15}=15.0040\pm 0.0008$ and $O^{18}=18.0037\pm 0.0007$. The measurement of N^{15} gives the rare chance to compare the energy release of a nuclear reaction *viz.*: $N^{14}+H^2=N^{15}+H^1$ with its value derived entirely by mass-spectrographic determinations.

TWO years ago I published together with R. Herzog[1] the complete theory of all arrangements of a radial electric field and a homogeneous magnetic field for which direction focusing as well as velocity focusing is obtained. Allowing velocity to play the part of wave-length these combinations are truly analogous to achromatic lenses, that is, they give for each pencil of positive rays of given mass an image of the limiting slit. For the masses of course they act as spectrographs. Since that time two different double-focusing mass spectrographs have been set up by A. J. Dempster[2] and by K. T. Bainbridge and E. B. Jordan[3] which as far as can be seen from the data given are special cases of our theory. The exceedingly fine lines which Dempster was able to get are proof of the advantage of double-focusing. During the last year I succeeded with R. Herzog in constructing a mass spectrograph which corresponds to one of the special cases we had computed in our paper[1] and which could be built with the limited means of the Institute shop. It was completed at the end of last year. It differs from the two mass spectrographs mentioned in that it gives, theoretically, double focusing along the whole length of the plate. Since neither Dempster nor Bainbridge and Jordan have stated yet the conditions under which their double focusing should occur I may be permitted to give a short summary of a specialized theory here.

[1] J. Mattauch and R. Herzog, Zeits. f. Physik **89**, 786 (1934).
[2] A. J. Dempster, Proc. Am. Phil. Soc. **75**, 755 (1935).
[3] K. T. Bainbridge and E. B. Jordan, Phys. Rev. **49**, 421A (1936).

THEORY OF DOUBLE FOCUSING

After it was shown[4] that Hughes and Rojansky's case of direction focusing in a radial electric field could be generalized to a certain extent R. Herzog, upon my request, undertook a similar generalization for magnetic fields. He was able to go far beyond this task by disclosing a complete parallel to geometric optics.[5] According to this theory each radial electric or homogeneous magnetic field or any simultaneous combination of the two works like a combination of a prism and a cylindrical lens to which definite focal and principal planes and a focal length f can be ascribed. In Fig. 1 the field-free spaces I (every coordinate $'$) and II (every coordinate $''$) are the conjugate spaces of objects and images or *vice versa*. In space III a radial electric field $E=A/r$ and a homogeneous magnetic field H perpendicular to the plane of drawing is set up so that a charged particle of velocity v_0 and mass M_0 entering along x' travels along a circle of radius $r=a$ and, after being deflected through the angle ϕ, leaves along x''. A bundle of parallel rays of definite velocity $v=v_0(1+\beta)$ and mass $M=M_0(1+\gamma)$ slightly differing from v_0 and M_0 is united at the focus F with the coordinates g and y_F. A pencil of rays diverging from an object point $P'(l', b')$ is focused at the image point $P''(l'', b'')$. If we denote with h the distance

[4] W. R. Smythe, Phys. Rev. **45**, 299 (1934); R. Herzog and J. Mattauch, Ann. d. Physik **19**, 345 (1934).
[5] R. Herzog, Zeits. f. Physik **89**, 447 (1934). At the same time W. E. Stephens, Phys. Rev. **45**, 513 (1934) has published a generalization for magnetic fields with radial boundaries without however establishing the optical analogy.

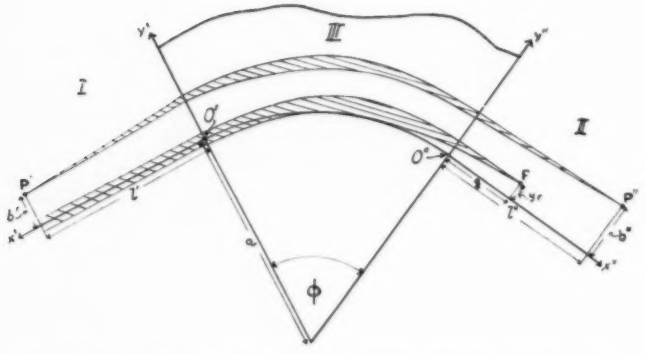

FIG. 1. A radial electric field or a homogeneous magnetic field behaves like a combination of a prism and a cylindrical lens.

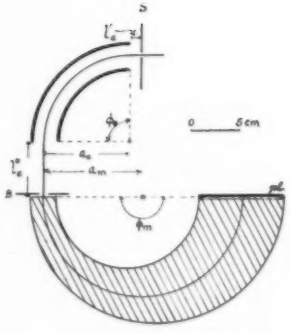

FIG. 2. Dempster's arrangement of electric and magnetic fields.

of the principal plane from O'' (or O'),[6] the results are:

$$f=g-h=(a/\kappa)(1/\sin\kappa\phi), \tag{1}$$

$$g=f\cdot\cos\kappa\phi \quad \text{and} \quad h=f(\cos\kappa\phi-1), \tag{2a, b}$$

$$y_F=a\cdot\delta, \tag{3}$$

for which as in optics the well-known equations hold:

$$(l'-g)\cdot(l''-g)=f^2$$

or

$$1/(l'-h)+1/(l''-h)=1/f. \tag{4a, b}$$

and

$$\frac{(b''-y_F)}{(b'-y_F)}=-\frac{f}{(l'-g)}=-\frac{(l''-g)}{f}. \tag{5a, b}$$

Here κ and δ are constants which depend on the fields and on β and γ. In purely electric (subscript e) or purely magnetic (subscript m) fields they become, respectively:

$$\kappa_e=\sqrt{2},\ \ \delta_e=\beta+\tfrac{1}{2}\gamma \quad \text{or} \quad \kappa_m=1,\ \ \delta_m=\beta+\gamma. \tag{6}$$

The well-known special cases where O' and O'' are conjugate are analogous to telescopic image formation where:

$$g=-f,\quad \phi=n\pi/\kappa,[7]\quad \phi_e=n\pi/\sqrt{2},[8]$$
$$\phi_m=n\pi,[9]\quad n=1, 2, 3\cdots. \tag{7}$$

We can now proceed[1] to combine a radial electric field and a homogeneous magnetic field to form an "achromatic" lens. We wish to construe the image b_m'' of a slit S of width $s(b_e'\leqq\frac{1}{2}s)$ so that b_m'' is independent of β at least for one particular mass. If the image of the first lens (subscript e) is the object of the second (subscript m) and if D denotes the distance between the end (O'') of the electric and the beginning (O') of the magnetic field, then:

$$l_e''=D-l_m' \quad \text{and} \quad b_e''=\pm b_m'. \tag{8a, b}$$

The upper sign holds when the deflections in the two fields are in the same direction and the lower sign when they are in opposite directions.[10] Introducing the abbreviations:

$$K_e=a_e(1+f_e/(l_e'-g_e))$$
$$=a_e(1-\cos\sqrt{2}\phi_e)+l_e''\cdot\sqrt{2}\sin\sqrt{2}\phi_e, \tag{9}$$

$$K_m=a_m(1+(l_m'-g_m)/f_m)$$
$$=a_m(1-\cos\phi_m)+(D-l_e'')\cdot\sin\phi_m, \tag{10}$$

and using Eqs. (8b) and (5a) we get for the ordinates of the final image b_m'' in terms of the ordinates b_e' of the points of the slit S:

$$\pm b_m''=\{(K_e/a_e-1)\cdot b_e'-\beta\cdot(K_e\mp K_m)$$
$$-\gamma\cdot(\tfrac{1}{2}K_e\mp K_m)\}\cdot\frac{1}{(K_m/a_m-1)}, \tag{11}$$

from which the condition for double focusing can

[6] Here we confine ourselves to fields with radial boundaries where $g'=g''=g$ and $h'=h''=h$.

[7] W. Bartky and A. J. Dempster, Phys. Rev. **33**, 1019 (1929); W. Henneberg, Ann. d. Physik **19**, 335 (1934).

[8] A. L. Hughes and V. Rojansky, Phys. Rev. **34**, 284 (1929).

[9] A. J. Dempster, Phys. Rev. **20**, 631 (1922) and others.

[10] In our paper we omitted the upper sign because we were interested in cases where double focusing holds for all masses.

be read off immediately:

$$K_e = \pm K_m. \tag{12}$$

The resolution of a double-focusing mass spectrograph is given by the ratio of the image width of the slit for one mass, $2b_m''$, to the coefficient of γ in Eq. (11):

$$\frac{\Delta M}{M} = \frac{2s}{a_e}\left(1 - \frac{a_e}{K_e}\right) = \frac{2s}{a_e}\left(1 \mp \frac{a_e}{K_m}\right). \tag{13}$$

The resolution therefore depends on the data of the electric field only. The energy of the rays passing a diaphragm B at l_e'' is constant, therefore:

$$M = k \cdot a_m^2, \tag{14}$$

where $k = eH^2/Ac^2$. Thence we get the difference of packing fraction of the lines of a doublet:

$$\Delta M/M = 2\Delta a_m/a_m \tag{15}$$

as well as the mass scale on the plate by computing the relation between a_m and the distance x from a fiducial point.

Design of Apparatus

Perhaps an obvious way to proceed is to use one of the well-known special cases of (7) for one of the lenses and to adjust the other lens to fit Eq. (12). This apparently was done by Dempster[9] and by Bainbridge and Jordan.[3] Since the way by which they arrived at their respective mass spectrographs was probably a different one it may be interesting to see how far their data can be derived from our equations.

Dempster (Fig. 2) chooses $\phi_m = \pi$ [i.e., $l_m' = l_m'' = 0$, $f_m = -g_m$, $D = l_e''$, $K_m = 2 \cdot a_m$], $\phi_e = \frac{1}{2}\pi$ [i.e., $f_e = a_e/(\sqrt{2} \cdot \sin \sqrt{2}(\pi/2))$, $g_e = (a_e/\sqrt{2}) \cot \sqrt{2}(\pi/2)$, $K_e = a_e(1 - \cos \sqrt{2}(\pi/2)) + l_e'' \cdot \sqrt{2} \sin \sqrt{2}(\pi/2)$] and $l_e' = 1$ cm. Other data are not given. From a photograph to scale of his apparatus however we take a_e to be equal to 8.3 cm, l_e'' to lie between 5 and 6 cm and $2a_m$ to lie between 19 and 20 cm. With this value of a_e we get from Eq. (4a) $l_e'' = 5.48$ cm and from Eq. (12) $2 \cdot a_m = 19.50$ cm in good agreement with Dempster's photograph.[11] With the comparatively wide slit width used by Dempster ($s = 0.01$ cm) we get from Eq. (13) a theoretical resolution of 1 in 700 or slightly better, which agrees quite well with Dempster's Fig. 1 in 1000.[12]

[11] Cf. A. J. Dempster, reference 9, Fig. 5. In answer to a letter Professor Dempster kindly communicated to me his data: "a_e about 7.55 cm, $l_e'' = 8.6$ cm, $a_m = 10$ cm." There must be a mistake, however, at least about the first two items. The max. value of l_e'' ($l_e' = 0$) is 0.94. $a_e \cdot l_e''$ must therefore be smaller than a_e. Besides these values of a_e and l_e'' do not fit Dempster's Fig. 5. If we take 8.6 cm to be the correct value of a_e, then we compute $l_e'' = 5.75$ and $a_m = 10.14$ cm.

[12] In his letter to the author Professor Dempster says: "As to the resolution, the figure, 1 in 1000, is only approximate, judged from the widths of the images as seen under a microscope. Actually the image should be wider than the slit, but in the photographs, due perhaps to less intensity at the edge, the images appear about the same width as the slit. But I have only approximate data at present."

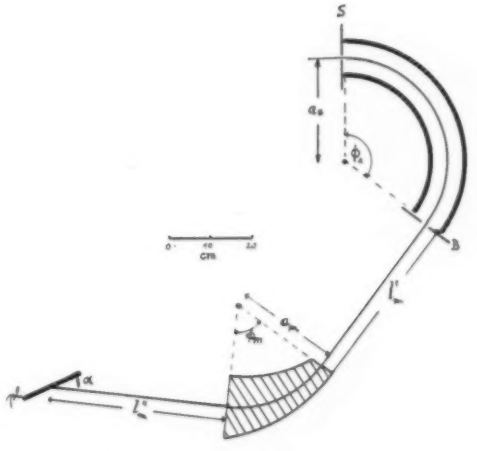

Fig. 3. Bainbridge and Jordan's arrangements of the electric and magnetic fields.

Bainbridge and Jordan choose $\phi_e = (\pi/2)\sqrt{2}$ [i.e., $l_e' = l_e'' = 0$, $f_e = -g_e$, $D = l_m'$, $K_e = 2 \cdot a_e$] and $\phi_m = (\pi/3)$ [i.e., $f_m = \frac{2}{3}\sqrt{3} \cdot a_m$, $g_m = \frac{1}{3}\sqrt{3} \cdot a_m$, $K_m = \frac{1}{2}a_m + \frac{1}{2}\sqrt{3} \cdot l_m'$]. According to Eqs. (12) and (4a) double focusing is obtained if

$$2a_e = \tfrac{1}{2}a_m + \tfrac{1}{2}\sqrt{3} \cdot l_m' \quad \text{and} \quad l_m' \cdot l_m'' - \tfrac{1}{3}\sqrt{3}a_m \cdot (l_m' + l_m'') = a_m,$$

from which l_m' and l_m'' may be computed if a_e and a_m are known. All we can gather from the short note of B. and J. is: "The mean dispersion is 5 mm for one percent mass difference, the mean radius is 25.4 cm, and a resolving power of 12,000 has been attained. Over 140 mm on the plate the maximum divergences from linearity are $\pm 1/7000$." Hence we can only make a guess at their apparatus since it is not stated whether "the mean radius" means a_e or a_m or both. However the smallest slit width ever used by Aston or Bainbridge in this kind of work is 0.002 cm and from Eq. (13) we see that one has to make a_e at least 24 cm to get the high resolving power attained by B. and J.; so we may take the figure 25.4 cm to mean a_e. If it should mean $a_e = a_m$, we get from the equations above $l_m' = l_m'' = a_m \cdot \sqrt{3} = 44.0$ cm (Fig. 3). Best approximation to linearity could be obtained if the plate is inclined by an angle α about 30° to the median ray. As it happens the same value of α also gives direction focusing as in Dempster's case. Again double focusing is obtained for one mass only. The dispersion of a mass spectrograph of so big dimensions, however, would be about three times as large as is given by B. and J. Probably a_m is much smaller than is assumed for the sketch of Fig. 3.

We wish to adjust the magnitudes which are not determined by Eqs. (12) and (13) in such a

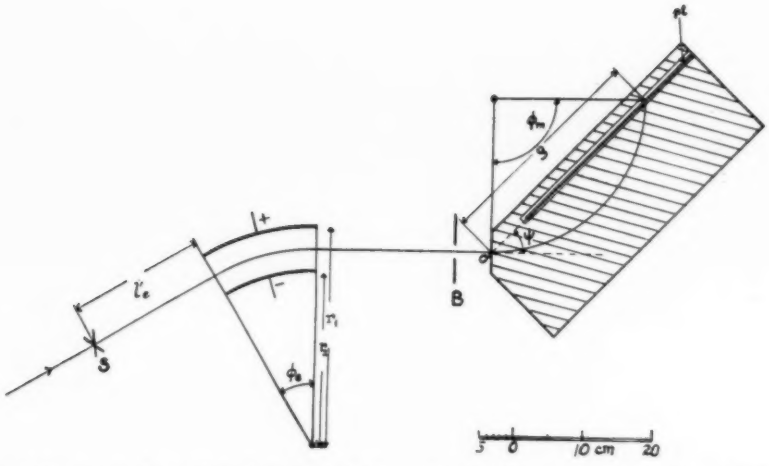

FIG. 4. Adjustment of electric and magnetic fields to give double focusing for all values of M.

way as to get double focusing for all values of M. That means, we have to look for a special case for which Eq. (12) becomes independent of a_m. This we can easily achieve by dividing Eq. (12) by l_e'' and computing the limit $l_e'' \to \infty$ (that means $l_e' = g_e$). Taking the lower sign we get:

$$\sqrt{2} \cdot \sin \sqrt{2}\phi_e = \sin \phi_m. \tag{16}$$

Since bundles of parallel rays are entering the magnetic field $l_m'' = g_m$ and D becomes indeterminate. Since ϕ_e is a constant we see from Eq. (16) that ϕ_m has to be constant too though M varies. In order not to get into contradiction with our assumption that the boundary of the field be radial we simply choose $l_m'' = 0$; then from Eqs. (2a) and (16) we get $\phi_m = \pi/2$, $\phi_e = \pi/4\sqrt{2}$ and $l_e' = a_e/\sqrt{2}$ (see Fig. 4). Introducing new polar coordinates $\rho = 2a_m \cdot \sin \psi$ and $\psi = \frac{1}{2}\phi_m$ we see that all images lie on a straight line which goes through O' and is inclined to the median ray entering the field by an angle of $\frac{1}{4}\pi$. To get the best resolution a_e was made as large as was possible in the Institute shop. The data are: $a_e = 28.0$ cm, $r_1 = 28.4$ cm, $r_2 = 27.6$ cm. The mass scale on the plate becomes:

$$M = k \cdot \rho^2, \tag{17}$$

measuring M in units of isotopic weight ($O^{16} = 16$) and denoting by F Faraday's constant corrected for the physical scale the constant of Eq. (17) becomes:

$$k = \frac{F \cdot \ln (r_1/r_2)}{c^2 \cdot 4 \sin^2 \psi} \frac{300 H^2}{X} = 1.41 \cdot 10^{-6} \cdot \frac{H^2}{X}$$

if H is measured in oersteds and X in volts. Difference of packing fraction and resolution are

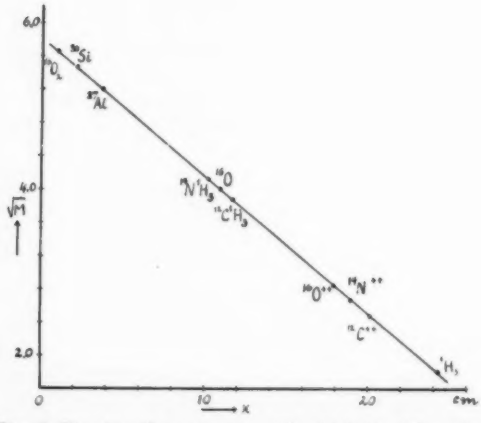

FIG. 5. Showing the accuracy with which the $M^{\frac{1}{2}} - x$ law is fulfilled.

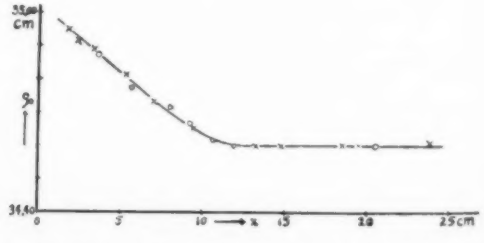

FIG. 6. Values of ρ_0 as a function of position on the plate.

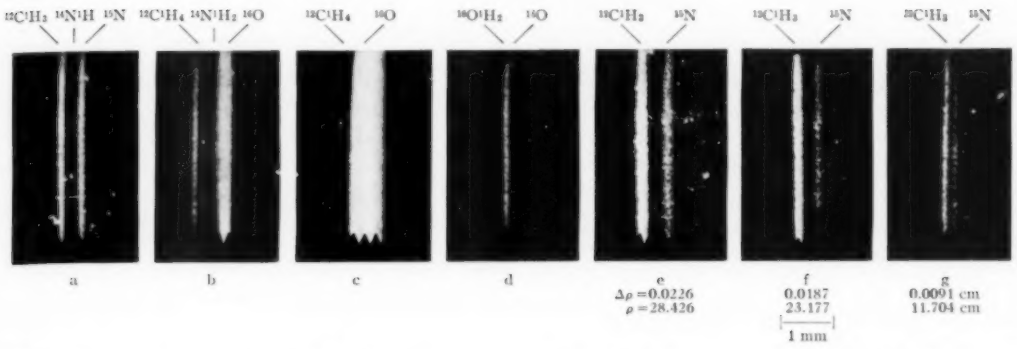

FIG. 7. Samples of the lines obtained with the present mass spectrograph as they appear in the Fraunhofer-microscope.

given by:

$$\Delta M/M = 2\Delta\rho/\rho = 2s/a_c \qquad (18)$$

with $s = 0.008$ cm in the present experiments. Therefore the resolution with the present slit should be 1 in 1750. The plate which is 298 mm long reaches from about $\rho = 6.5$ to 36.3 cm. The distances x of the lines are measured from a fiducial point about 2 cm from the farther end of the plate and $\rho = \rho_0 - x$, where ρ_0 denotes the distance of the fiducial point from O'. As far as can be seen from the design of the apparatus ρ_0 should be 34.6 cm. The distance D between the fields may be chosen arbitrarily. It was made large enough to place a diaphragm B the width of which can be set from outside the vacuum to any value between 0 and 2 mm.

EXPERIMENTAL DETAILS

Actually the plates were calibrated by means of well-known lines the masses of which were all remeasured recently by F. W. Aston.[12] Fig. 5 shows how accurately the $\sqrt{M} - x$ law is fulfilled. To comprehend the deviations ρ_0 was determined for a number of exposures with different fields from groups of two (x) or more (0) neighboring lines (in this case by means of least squares) and plotted against the mean value of x of the group used (see Fig. 6). For the first 16 cm of the plate ρ_0 proved to be constant and equal to 34.6 cm; then its value rises slowly to 35.0 cm for lines closer to the fiducial point. This can be accounted for by a slight inhomogeneity of the magnetic field, for these rays have to pass closer to the edge of the field. The values of k range from 1.32 to $1.41 \cdot 10^{-6} \cdot H^2/X$, the main error being due to the error of H and of $(r_1 - r_2)$. Fig. 7 shows samples of the lines as they show up in the Fraunhofer-microscope. Darkfield illumination is used since weak lines are seen then much better. Fig. 7a and b are triplets at mass number 15 and 16 of one and the same 4.5-min. exposure in undried room air. The same exposure shows a weak line at 17 and none at 18. That means that N is accompanied by weak lines NH, NH_2 and NH_3 in a way similar to that which is well known of C(CH, CH_2, CH_3, CH_4) or O(OH, OH_2). Fig. 7c and d are the doublets at mass number 16 and 18 of a 5-min. exposure in dried oxygen. On the original plate CH_4 is decidedly weaker than O^{18}. That means that O^{16} is at least 500 times overexposed. Nevertheless the doublet remains clearly resolved. Though doublets of such unequal intensity are unsatisfactory for precise work I measured two of them and the triplet Fig. 7b and got the values 20.5, 20.6 and 23.2 for $(\Delta M/M) \cdot 10^4$ which is to be compared with Aston's precision value 22.4_8. This comparatively close agreement means that even strong overexposure does not make the lines unsymmetrical. The closest doublet hitherto obtained in air or oxygen is that at 18. It shows that a resolution of at least 1 in 1430 has been attained. From the first part of Eq. (18) it follows that the dispersion for one percent difference of

TABLE I.

Doublet	Number of doublets measured	$(\Delta M/M) \cdot 10^4$	ΔM
$(C^{12}H_3^1 - N^{15})$	12	$15.8_6 \pm 0.05$	0.02382
$(O^{16}H_2^1 - O^{18})$	9	$6.9_5 \pm 0.10$	0.01257

[12] F. W. Aston, Nature **137**, 357, 613 (1936).

mass decreases linearly with ρ from 1.8 mm for lines near the fiducial point to 0.3_5 mm at the other end of the plate. This is demonstrated by Fig. 7e, f, g, showing the 15-doublet at different values of ρ. This comparatively small dispersion is a consequence of the small size of the magnet and the steep angle (45°) which was chosen for the incidence of the rays on the plate. The resolution however has according to the second part of Eq. (18) to remain constant which means that the lines become sharper with decreasing ρ. One therefore can safely say that in every respect the mass spectrograph is working according to theory.

Results

There were now taken (mostly in oxygen with a small trace of air) altogether 12 doublets at mass number 15 and 9 doublets at mass 18. As a rule these were on the same exposure. The value of ρ for the middle of each doublet can easily be determined to a fraction of 1 per mille, ρ being corrected according to Fig. 6. For each doublet $\Delta\rho$ was measured independently by three observers (Dr. R. Herzog, Dr. H. Hintenberger and the author). The conditions of experiment have been widely varied. The time of exposure though on the average 5-min. range from 1 min. 40 sec. to 9 min.; the width of the diaphragm B was set at 0.025 and 0.015 cm; ρ for the 15 doublet was changed from 10.465 to 30.463 cm, $\Delta\rho$ correspondingly from 0.0083 to 0.0237 cm. The values of $(\Delta M/M)\cdot 10^4$ (difference of packing fraction) lie all between 15.54 and 16.15 with a probable error of ± 0.05. The corresponding changes for the 18-doublet were much smaller. The results are given in Table I. It has to be emphasized that these results have been obtained with a slit width four times as wide as is commonly used in this kind of work. By narrowing the slit we hope to get still finer lines and an increase in accuracy. Using Aston's masses of C^{12} and H^1 the isotopic weights referred to $O^{16}=16$ are:

$$N^{15}=15.0040\pm 0.0008 \text{ and } O^{18}=18.0037\pm 0.0007.$$

These may be compared with the band-spectroscopic values: $N^{15}=15.0027\pm ?$ measured by G. Herzberg[14] and recalculated by R. T. Birge,[15] $O^{18}=17.991\pm 0.010$ (R. Mecke and K. Wurm[16]) and $O^{18}=18.0065\pm 0.00018$ (H. D. Babcock and R. T. Birge[17]) of which the last seems by far the most trustworthy.

Discussion

The mass of N^{15} is of some interest in atomic disintegration work. By bombarding nitrogen atoms with deuterons J. D. Cockcroft and W. B. Lewis[18] measured a proton group of 85.0 ± 1.0 cm corresponding to 8.53 ± 0.1 MEV.[19] If in this reaction the N^{15} nucleus is left in the ground state there should be:

$$N^{14}+H^2-N^{15}-H^1=(91.6\pm 1.1)\cdot 10^{-4} \quad (19)$$

mass units on the physical scale. If we simply insert Aston's values for N^{14}, H^2, H^1 and our value for N^{15} we get: $(98.5\pm 9.5)\cdot 10^{-4}$. The agreement might be considered as satisfactory within the rather large limits of error due to the reference of the masses to O^{16}. However, the test can be made much sharper by going back to the originally measured doublets. If we extend the left side of Eq. (19) by $+$ and $-CH_3$ we get:

$$-(C^{12}H_2^1-N^{14})+(C^{12}H_3^1-N^{15}) -(H_2^1-H^2)=(98.5\pm 1.1)\cdot 10^{-4} \quad (19^*)$$

if we use for the 14 and the 2-doublet Aston's values: $(8.89\pm 0.05)\cdot 14.01$ and $(7.54\pm 0.2)\cdot 2.015$ and for the 15-doublet the value given above. As Professor G. Stetter kindly pointed out to me neither an error in the measurement of the range of the proton group nor its reduction to MEV may be blamed for the whole discrepancy.

Of the three doublets used the one at 14 is one of the most accurately measured by Aston. $(\Delta M/M)\cdot 10^4$ of the 15-doublet would have to be 15.40 to fit Eq. (19) which is below the lowest value we measured. The 2-doublet seemed to be one of the hardest to measure since Aston needed 53 doublets to get a probable error of ± 0.2. If we take instead of this the difference between the doublets $(H_2^1-He^{4++})$ and $\frac{1}{2}(H_2^2-He^4)$

[14] G. Herzberg, Zeits. f. physik. Chemie **B9**, 43 (1930).
[15] R. T. Birge, Phys. Rev. **37**, 841 (1931).
[16] R. Mecke and K. Wurm, Zeits. f. Physik **61**, 37 (1930).
[17] H. D. Babcock and R. T. Birge, Phys. Rev. **37**, 233 (1931).
[18] J. D. Cockcroft and W. B. Lewis, Proc. Roy. Soc. **A154**, 261 (1936).
[19] This group was discovered by E. O. Lawrence, E. McMillan and M. C. Henderson, Phys. Rev. **47**, 273 (1935) who give for the kinetic energy release 8.0 MEV. The corresponding value of the proton range may presumably not be compared with that of C. and L. because Al instead of mica was used for absorption.

measured by Bainbridge[20] we get for ΔM of the $(H_2^1-H^2)$ doublet $(19.2\pm0.5)\cdot10^{-4}$ and for the mass equivalent of the energy release the value $(94.5\pm1.2)\cdot10^{-4}$, which is in better agreement with the disintegration value. This, however, would involve a slight change of all recently measured masses.

On the other hand we can use the disintegration value of Eq. (19) to compute ΔM of the 2-doublet. We get then ΔM of $(H_2^1-H^2)=(22.2\pm1.6)\cdot10^{-4}$. J. Chadwick and M. Goldhaber[21] found that $H^2=H^1+n^1-23.10^{-4}$ mass units or:

$$(n^1-H^1)=23.10^{-4}-(H_2^1-H^2).$$

With the above value of $(H_2^1-H^2)$ we find that the difference between the masses of neutron and proton is zero within the limits of error as is known of other stable isobars of adjacent elements.

In the measurements and calculations I had the valuable help of Messrs. V. Hauk and H. Lichtblau. The author desires further to thank the Rockefeller Foundation and the Akademie der Wissenschaften in Wien for grants which have made these investigations possible.

Note added in proof: There were only two other nuclear reactions observed by Cockcroft and Lewis which can be checked up entirely by the masses measured by Aston. These are the disintegrations of N^{14} and of O^{16} both by H^2 giving α-rays. The reaction energies given by C. and L. are $(13.22\pm0.1)\cdot10^6$ ev and $(2.95\pm0.04)\cdot10^6$ ev so that in units of isotopic weight:

$$N^{14}+H^2-C^{12}-He^4=(142.0\pm1.1)\cdot10^4 \qquad (20)$$

and

$$O^{16}+H^2-N^{14}-He^4=(\ 31.7\pm0.4)\cdot10^4. \qquad (21)$$

The corresponding mass-spectrographic equations with the doublets measured by Aston (see Table II) are:

$$-(C^{13}H_2^1-N^{14})+(H_2^1-H^2)+(H_2^2-He^4)=(145.7_5\pm1.1)\cdot10^4 \qquad (20^*)$$

and

$$-(C^{13}H_4^1-O^{16})+(C^{12}H_2^1-N^{14})+(H_2^1-H^2)+(H_2^2-He^4)=(34.7_5\pm2.7)\cdot10^4. \qquad (21^*)$$

The fact that the difference of the two:

$$(C^{12}H_4^1-O^{16})-2\cdot(C^{12}H_2^1-N^{14})=(111.0\pm2.5)\cdot10^4 \qquad (20^*)-(21^*)$$

agrees well with the difference (20)–(21) of the reaction energies: $(110.3\pm1.2)\cdot10^4$ was another reason for not seeking the cause of the discrepancies between the disintegration and mass-spectrographic values of the reaction energies at the 14-doublet.

Recently, however, the situation has changed since K. T. Bainbridge and E. B. Jordan[22] have remeasured the 2-, 14- and 16-doublet. With their values (19*), (20*) and (21*) become: $(92.9\pm2.2)\cdot10^4$, $(140.4\pm2.2)\cdot10^4$ and $(31.4\pm3.0)\cdot10^4$ in excellent agreement with the disintegration values. The agreement of the difference (20*) $-$(21*) giving $(109.0\pm4.5)\cdot10^4$ happens to be preserved also. That means that Aston's values for the 14- and 16-doublet must be abandoned in favor of the new ones. In addition B. and J. have measured the doublet $C^{13}H^1-C^{13}$ which together with the 2-doublet permits us to check up on the disintegration of C^{13} by H^2 giving H^1-rays. The kinetic energy release for this reaction is given by C. and L. as $(2.66\pm0.06)\cdot10^6$ ev so that:

$$C^{13}+H^2-C^{13}-H^1=(28.6\pm0.6)\cdot10^4, \qquad (22)$$

or with B. and J.'s values from Table II,

$$(C^{13}H^1-C^{13})-(H_2^1-H^2)=(29.7\pm1.1)\cdot10^4. \qquad (22^*)$$

TABLE II.

Mass-Number	Doublet	$M\cdot10^4$	Sign	Measured by:
2	H^1-H^2	$15.2\pm0.4^*$		Aston
2	H^1-H^2	$15.3\pm0.4^*$	a	Bainbridge and Jordan
4	H^2-He^4	$255.1\pm0.8^*$	b	Aston
6	$H_2^2-C^{12++}$	423.6 ± 1.8	c	Aston
13	$C^{12}H^1-C^{13}$	$45\ \pm1^*$	d	Bainbridge and Jordan
14	$C^{12}H_2^1-N^{14}$	124.5 ± 0.7		Aston
14	$C^{12}H_2^1-N^{14}$	$130\ \pm2^*$	e	Jordan and Bainbridge
15	$C^{12}H_3^1-N^{15}$	$238.2\pm0.7_5^*$	f	Mattauch
16	$C^{12}H_4^1-O^{16}$	360.1 ± 2.4		Aston
16	$C^{12}H_4^1-O^{16}$	$369\ \pm2^*$	g	Jordan and Bainbridge
18	$O^{16}H_2^1-O^{18}$	$125_7\ \pm1.8$	h	Mattauch

Of the recently measured doublets those denoted by * are therefore checked up by kinetic energy releases observed by atomic disintegration.

In order to refer the masses to $O^{16}=16$ we have to make use of Aston's keydoublet c which could not be checked up by disintegration values. All masses are influenced by this doublet, however, as well as by the doublets a and g.

$$\begin{aligned}
H^1 &= 1+\tfrac{1}{16}g+\tfrac{1}{8}c+\tfrac{3}{8}a &&= 1.00818\pm0.00003\\
H^2 &= 2+\tfrac{2}{16}g+\tfrac{2}{8}c-\tfrac{2}{8}a &&= 2.01482\pm0.00005\\
He^4 &= 4+\tfrac{4}{16}g+\tfrac{4}{8}c-\tfrac{4}{8}a-b &&= 4.0041_3\pm0.00013\\
C^{12} &= 12+\tfrac{12}{16}g-\tfrac{4}{8}c-\tfrac{12}{8}a &&= 12.0042\ \pm0.0002\\
C^{13} &= 13+\tfrac{13}{16}g-\tfrac{5}{8}c-\tfrac{9}{8}a-d &&= 13.0079\ \pm0.0002\\
N^{14} &= 14+\tfrac{14}{16}g-\tfrac{6}{8}c-\tfrac{6}{8}a-e &&= 14.0076\ \pm0.0003\\
N^{15} &= 15+\tfrac{15}{16}g-\tfrac{7}{8}c-\tfrac{3}{8}a-f &&= 15.0049\ \pm0.0002\\
O^{18} &= 18+\tfrac{2}{16}g+\tfrac{2}{8}c+\tfrac{6}{8}a-h &&= 18.0038\ \pm0.0002
\end{aligned}$$

At present these are the best mass-spectrographic determinations checked up as far as possible by nuclear reaction energies.

[20] K. T. Bainbridge, Phys. Rev. **43**, 103; **44**, 57 (1933).
[21] J. Chadwick and M. Goldhaber, Proc. Roy. Soc. **A151**, 479 (1935).
[22] K. T. Bainbridge and E. B. Jordan, Phys. Rev. **49**, 883 (1936).

Photoelectric Properties of Barium and Calcium*

N. C. JAMISON AND R. J. CASHMAN, *Northwestern University, Evanston, Illinois*

(Received July 22, 1936)

With a photoelectric cell in which Ba was fractionated and repeatedly distilled, values of φ_0 at room temperature, as obtained by Fowler's method, were found to be 2.520 and 2.510 electron volts, the difference being attributed to either differences in crystal structure or chemical purity. For both conditions of the surface, the cell showed extraordinary constancy of work function. Measurements 100°C above room temperature yielded a temperature coefficient of $(2.2\pm0.7)\times10^{-5}$ ev/°K. The absolute photoelectric yield of the surface was determined. The optical reflection coefficient was found to vary from 43 percent at 4000A to 63 percent at 7000A. The work function of a Ca surface prepared by single distillation was 2.706 ev. After repeatedly heating the surface to 100°C the data did not fit Fowler's theoretical curve. The departures were consistent with the assumption that, after heating, the surface was not homogeneous. Analysis of the data gave evidence of two emitting surfaces having work functions differing by approximately 0.2 ev.

SEVERAL writers have pointed out that the work function of a metal should show a temperature dependence.[1] The existing evidence for a temperature coefficient is based either on considerations of the constant A in Richardson's equation, contact potential measurements, or photoelectric measurements over a relatively large temperature range. The experimental evidence which gives a direct measure of the temperature dependence is meager and not conclusive.[2] The use of a large temperature range is not desirable since the gas content of the tube may be increased when the surface is heated to relatively high temperatures; also large temperature changes may cause a change in crystal structure.

If a relatively small temperature range is used, changes in work function of the order of 0.001 ev must be measured; hence, a valid determination can be made only if a surface shows extreme stability. Assuming the validity of Fowler's method,[3] work function differences of this order of magnitude can be definitely established. However, it has been found that not all photoelectric data can be fitted to Fowler's theoretical curve, even in the range near the threshold where the approximations involved in the theory are valid. An accurate fit is possible only when the surface is homogeneous. The production of such surfaces which are stable over a given temperature range has proved to be a difficult problem.

The present work was undertaken in an attempt to determine directly the temperature coefficients of the work function for the alkaline earth metals. The work is not complete at present; however, information has been obtained concerning the temperature coefficient for a Ba surface, the absolute photoelectric yield of a Ba surface, and emission from a nonhomogeneous Ca surface. It is felt that a report on this work might be of interest at the present time.

Accuracy of Measurements

There are four quantities which must be measured in order to fit photoelectric data to Fowler's theoretical curve; namely, temperature, wave-length, photoelectric current, and radiation energy. Of these, the temperature measurement is by far the least critical. An error of even a few degrees at room temperature would cause a negligible error in the work function, since the horizontal shift depends upon $1/T$ and the computation of the work function from the shift depends upon T. A large error in temperature measurement, however, would result in a poor fit to Fowler's theoretical curve.

* Presented in part at the Baltimore and Washington meetings of the Am. Phys. Soc. Nov. 29–30, 1935 and Apr. 30–May 2, 1936, respectively. See Phys. Rev. **49**, 195 (1936); **49**, 201 (1936); **49**, 877 (1936).

[1] P. W. Bridgman, Phys. Rev. **31**, 90 (1928); K. F. Herzfeld, Phys. Rev. **35**, 248 (1930); J. A. Becker and W. H. Brattain, Phys. Rev. **45**, 694 (1934); L. A. DuBridge, *Actualités Scientifiques et Industrielles*, No. 268, Paris, 1935; W. B. Nottingham, Phys. Rev. **49**, 646A, 649A (1936); E. Wigner, Phys. Rev. **49**, 696 (1936).

[2] Cf. Becker and Brattain, and DuBridge, reference 1; also R. Suhrmann and A. Schallamach, Zeits. f. Physik **91**, 775 (1934); W. B. Nottingham, Phys. Rev. **49**, 78 (1936); D. B. Langmuir, Phys. Rev. **49**, 428 (1936).

[3] R. H. Fowler, Phys. Rev. **38**, 45 (1931); E. Rudberg, Phys. Rev. **48**, 811 (1935).

Before the wave-length measurements are discussed attention should be called to the fact that the radiation used must be free from scattered light; also, if a source of continuous spectrum is used the dispersion should be adequate. Since line sources are subject to fluctuations, a continuous source is desirable for work in the visible range. Two sirgle prism instruments were found entirely unsatisfactory due to scattered light; in the work here reported a double Van Cittert glass monochromator was used. Direct wave-length measurements of the resolved light were made with a Hilger spectrometer. The wave-length spread for the slit width used was approximately 8 angstrom units at 4000A and increased to about 37 units at 5000A. The effect of this finite range of wave-lengths was analyzed and it was found that the use of the mean wave-length introduced a negligible error in the determinations of work functions to 0.001 ev. The accurate determination of small changes in work function is not affected by this approximation.

Current measurements were made using an FP–54 Pliotron tube and the circuit of DuBridge and Brown,[4] all measurements being made in a shielded room. For each setting of the monochromator a series of deflections was taken, the probable error for all except the two smallest deflections being less than one percent for the room temperature data and less than two percent for the high temperature data.

An improved form of Nichol's radiometer[5] was used to obtain the energy calibration. The interception of light by the radiometer vane was checked by a microscope mounted behind the vane. The amount of light not striking the vane was small and very nearly a constant fraction of the total. This was established by simultaneously measuring radiometer deflections and the photo-current of a cell illuminated by light that failed to strike the vane. The accuracy of the energy measurements was estimated at better than one percent. The radiometer was calibrated for absolute energy by comparison with a lamp checked at the Bureau of Standards.

The quantities thus far discussed relate to the accuracy of plotted points. The determination of the work function (or temperature coefficient of the work function) depends upon the horizontal shift necessary to superimpose the experimental data upon Fowler's theoretical curve. In order that the accuracy of the curve fitting be consistent with the accuracy of the experimental data it was necessary to obtain data over a sufficiently wide frequency range, and to plot to a large scale. The plots such as Fig. 3 were approximately 40×50 cm. The frequency range used corresponded to approximately 0.6 ev.

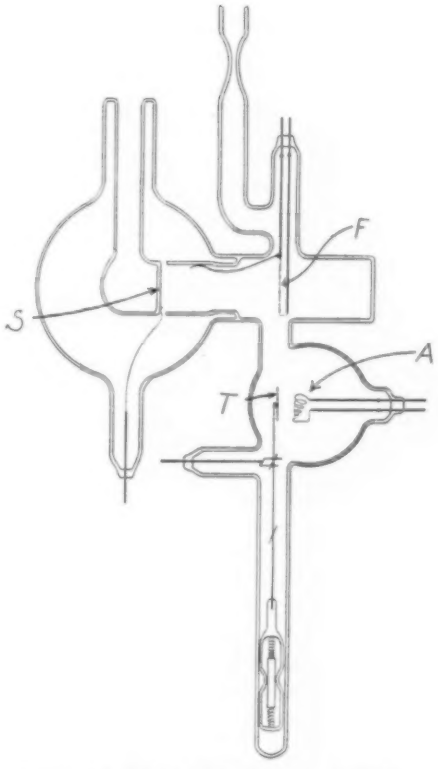

FIG. 1. Photoelectric cell used in work on Ba.

EXPERIMENTAL PHOTO-CELLS; OUTGASSING

Barium

The construction of the cell used in the work on barium is shown in Fig. 1. The great efficiency of Ba as a "getter" metal might at first seem disadvantageous if "clean" Ba surfaces are to be investigated. That this characteristic permits

[4] L. A. DuBridge and H. Brown, Rev. Sci. Inst. **4**, 532 (1933).
[5] B. J. Spence, J. Opt. Soc. Am. **6**, 625 (1922).

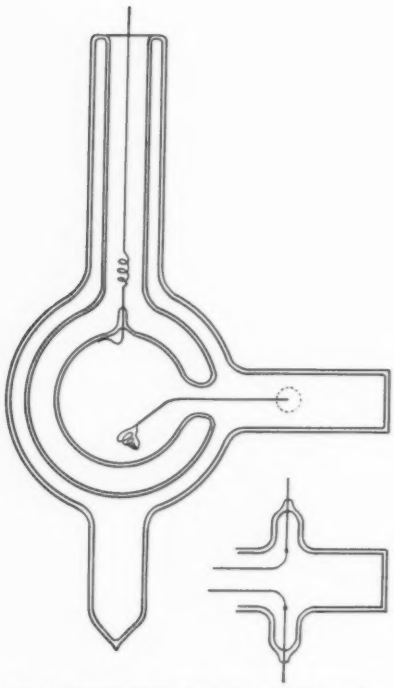

FIG. 2. Photoelectric cell used in work on Ca.

the design of a cell which possesses distinct advantages will be evident from what follows. Before the introduction of the Ba, the tube was baked at temperatures up to 550°C for about one week and the metal parts were accorded a severe heat treatment. Dry nitrogen was then admitted to the system and a freshly turned slug of Ba was placed in the spiral filament *A*. A week of pumping and baking followed at a lower temperature (350°C) during which time all metal parts were frequently heated as before. The Ba was progressively heated to higher and higher temperatures until it finally melted and formed a large drop around the lower turns of the filament. After a considerable quantity of Ba had condensed on the lower bulb wall the tube was sealed off. The work function of this surface was approximately 0.15 ev lower than that finally obtained, due no doubt to the clean-up of gas released in the sealing-off process.[6] More Ba was vaporized until approximately one-third had condensed on the lower bulb wall.

A magnetic control served to bring the tantalum plate, *T*, down to the lower chamber where it received a coating of Ba. After being raised and turned the plate was heated by radiation from the filament, *F*, so the resulting vaporization formed a deposit on the plate, *S*. Several deposits were made in this way until an opaque coating was formed. The deposit of Ba on the

[6] R. J. Cashman and W. S. Huxford, Phys. Rev. **48**, 734 (1935).

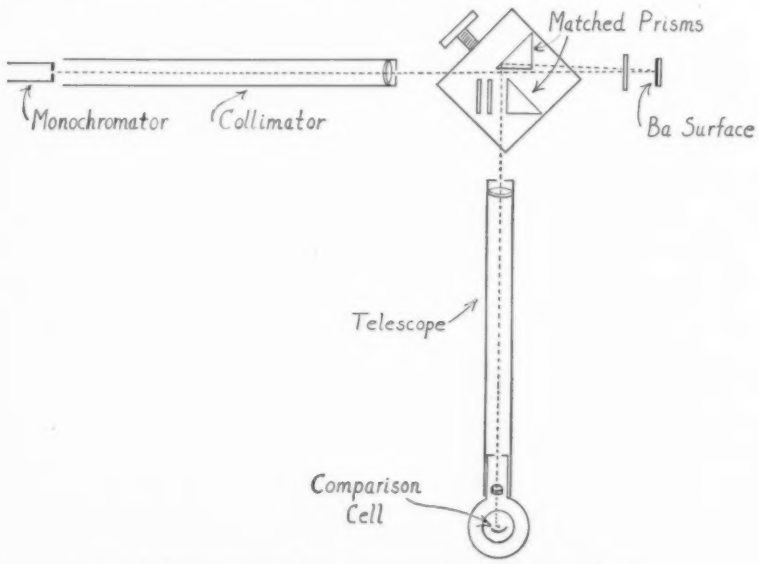

FIG. 3. Apparatus used for the measurement of optical reflection.

walls of the horizontal tube served as anode, contact being made by a wire supported by the filament leads.

Such a method of fractional distillation plus repeated distillation should yield effectively gas free layers of higher chemical purity. Since the work function did not change measurably with time after deposit, the vacuum conditions were considered adequate.[6]

Calcium

The work done with Ca has been confined so far to a cell using a single distillation. The type of cell used is shown in Fig. 2. The outgassing procedure was essentially the same as that just described. A single distillation cell, however, is not suited to the determination of the temperature coefficient, particularly for elevated temperature measurements, since residual gas trapped in the first condensed layers very likely diffuses to the surface. Also unless the optical reflection coefficient varies but little over the frequency range used, a multiple reflection cell may not be desirable.

TABLE I. *Reflection coefficient of barium.*

Wave-length in angstroms	4000	4500	5000	5500	6000	6500	7000
Reflection Coefficient (%)	43.	45.	48.	52.	55.	59.	63.

TABLE II. *Data from which the Fowler plots of Fig. 5 and Fig. 6 were made. Wa was computed on the basis of two free electrons per atom.*

λ(A)	Current/unit intensity $T=295.4°K$	$T=397.2°K$
4189	124	111
4248	101	91.9
4310	81.1	74.5
4379	62.2	56.8
4452	46.6	42.5
4524	33.0	30.0
4572	25.7	24.0
4614	19.7	18.8
4641	16.7	15.9
4666	13.4	13.1
4698	10.9	10.7
4726	8.42	8.46
4756	6.55	6.60
4776	5.28	5.61
4808	3.63	4.06
4841	2.45	2.78
4874	1.44	1.95
4908	.88	1.36
4942	.52	.83
4976		.55

TABLE III. *Values of the work function for a barium surface as obtained from five room temperature and three high temperature determinations.*

$T=295.4°K$ Horizontal Shift	$T=397.2°K$ Horizontal Shift
98.64	73.43
98.69	73.48
98.72	73.44
98.67	
98.69	Mean 73.45
Mean 98.68	(Mean) $\varphi_0=2.5128$ ev.
(Mean) $\varphi_0=2.5106$ ev.	

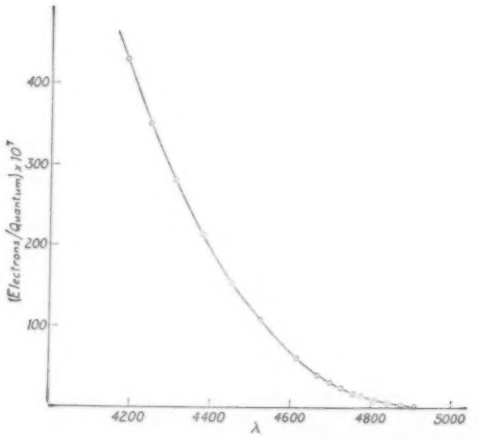

FIG. 4. The absolute photoelectric yield of a Ba surface as a function of wave-length.

Optical Reflection Coefficient Apparatus

In order to discover any possible correlation between photoelectric and optical properties. the reflectivity was measured as a function of wave-length and temperature using a photometer arrangement shown in Fig. 3. This device permits alternate readings of incident and reflected light to be made by a simple translation of matched prisms, with the assurance that the two beams will strike the same spot on the comparison cell. Since many commercial photo-cells respond differently over their surfaces such a method seems necessary. Measurements were limited to the range over which the lenses were achromatic; the window and reflecting surface must be approximately plane.

Results

Optical reflectivity of barium

Table I shows the results of the reflection coefficient determinations. No correlation be-

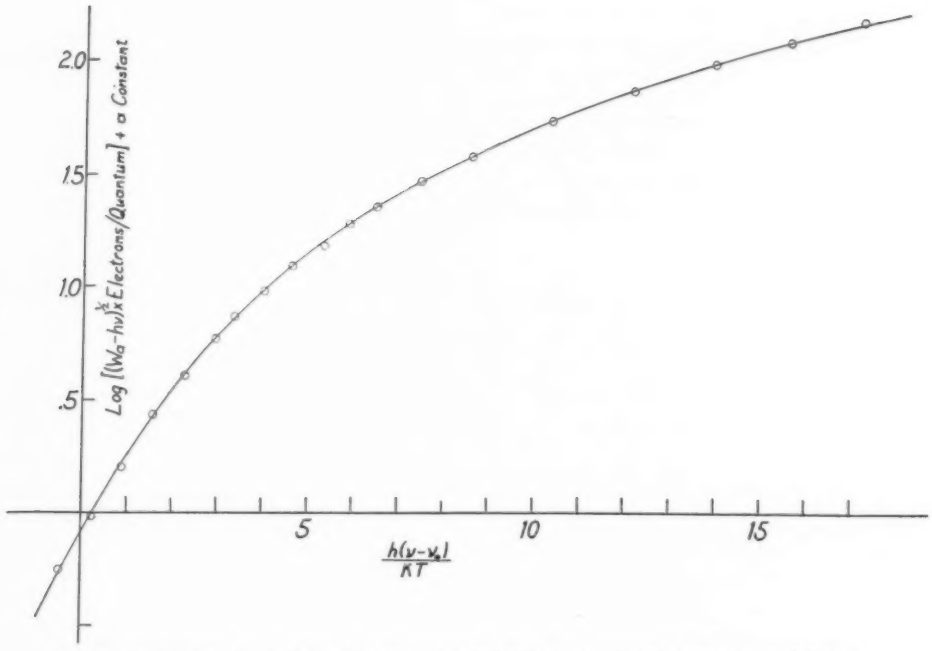

FIG. 5. Typical Fowler plot for a Ba surface at 295.4°K. Horizontal shift 98.65; $\varphi_0 = 2.510$ ev.

tween photoelectric emission and reflection coefficient was observed; also the value of reflection coefficient at dry ice temperature was no different than at room temperature, as the theory of Kronig[7] predicts. The values are considerably higher than those obtained by O'Bryan[8] using a polarized light method.

Room temperature work function of Ba

By using Fowler's method, the work function obtained for the initial series of deposits was 2.520 ev[9] as found from measurements made from two hours to three months after laying down deposits. During this period the surface experienced no large temperature changes with the exception of being lowered to −77°C. The variation of photoelectric efficiency of this surface as a function of wave-length is shown in Fig. 4. The low efficiency obtained is characteristic of gas free metals.

No change in the room temperature work function was found after lowering the temperature of the surface to −77°C. Lowering the temperature of the surface to liquid-air temperature so changed the surface that subsequent room temperature data failed to fit Fowler's curve accurately. The experimental curve gave evidence of a nonhomogeneous surface (an analysis of photoemission from such surfaces will be given later using data obtained with calcium). A tentative explanation of this failure to fit Fowler's curve is based on the hypothesis that the extremely low temperature produced such stresses between the barium layer and the glass base that the surface was permanently strained. Such a condition might presumably disturb the original microcrystalline character of the surface and thus produce areas having different emission characteristics.

A new deposit of barium failed to give data in good accord with theory, but a series of heat treatments totaling about 6 hours at 120°C

[7] Kronig, Proc. Roy. Soc. **A124**, 409 (1929); **A133**, 255 (1931); Mott and Zener, Proc. Camb. Phil. Soc. **30**, Part 2 (1934).

[8] H. M. O'Bryan, J. Opt. Soc. Am. **26**, 122 (1936).

[9] Work function values given here will be found to differ slightly from those given by us in previous reports. Those given here were obtained by plotting electrons $\times (Wa - h\nu)^{\frac{1}{2}}$/quantum as ordinate, while those previously reported were obtained from current/unit intensity plots. For a discussion of different methods of plotting see, R. J. Cashman and N. C. Jamison, Phys. Rev. **50**, 568 (1936).

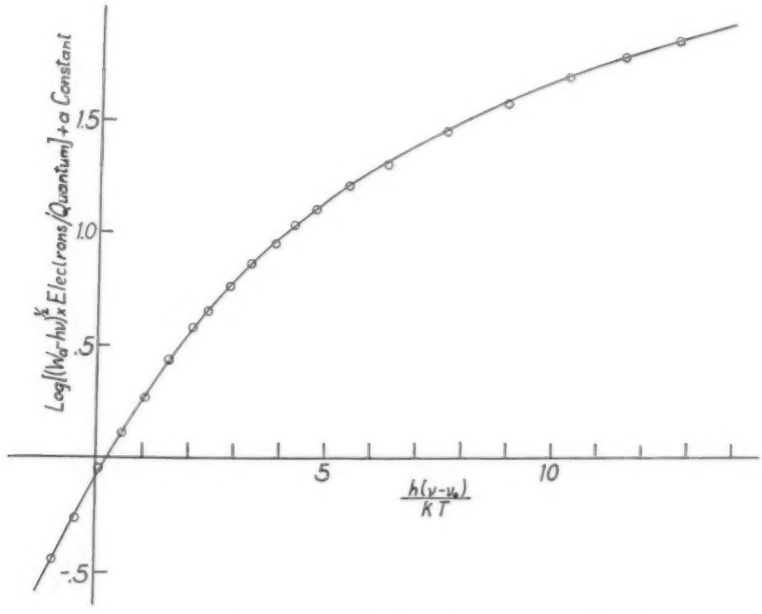

FIG. 6. Typical Fowler plot for a Ba surface at 397.2°K. Horizontal shift 73.43; $\varphi_0 = 2.512$ ev.

brought about a surface condition furnishing data in excellent agreement. A typical room temperature Fowler plot is shown in Fig. 5 with the data given in Table II. The results of five room temperature determinations are shown in Table III, the mean value being 2.5106 ev. We do not maintain that these work functions are accurate to 0.0001 ev; the fifth significant figure has been retained only for purposes of comparison with values obtained at a higher temperature. Between these runs the surface was heated to temperatures of 100° to 140°C for a total time of about 150 hours, indicating the existence of an extremely stable surface over this temperature range.

It will be observed that there is a difference of 0.01 ev between this mean value and that obtained for the initial series of deposits. We do not believe that the change is due to gas contamination, but rather that it is to be attributed either to a change in crystal structure or to a change in chemical purity.

These values of the work function of Ba are higher than any previously reported. Early determinations of the work functions of the alkaline earths were generally too low due to gas contamination.[6] It is of interest to compare our results with those of Anderson[10] who obtained 2.39 ev for Ba using contact difference in potential measurements with reference to tungsten. These measurements were carried out on surfaces prepared by fractional distillation in a gettered vacuum. The discrepancy can hardly be explained on the basis of gas contamination; the possibility of a slight difference in chemical purity exists. There might also be an effect on the crystal structure due to the influence of the backing materials and the temperature at which the deposits were made. A tentative explanation which seems reasonable is based on the work function of tungsten, 4.52 ev, used by Anderson. This value is the heat function and has not been corrected for a possible temperature dependence (Anderson's measurements were made at liquid-air temperature).

Temperature coefficient of the work function

The horizontal shifts and the mean value of the work function for 397.2°K are given in Table III. A typical set of data at this tempera-

[10] P. A. Anderson, Phys. Rev. **47**, 958 (1935); **49**, 320 (1936).

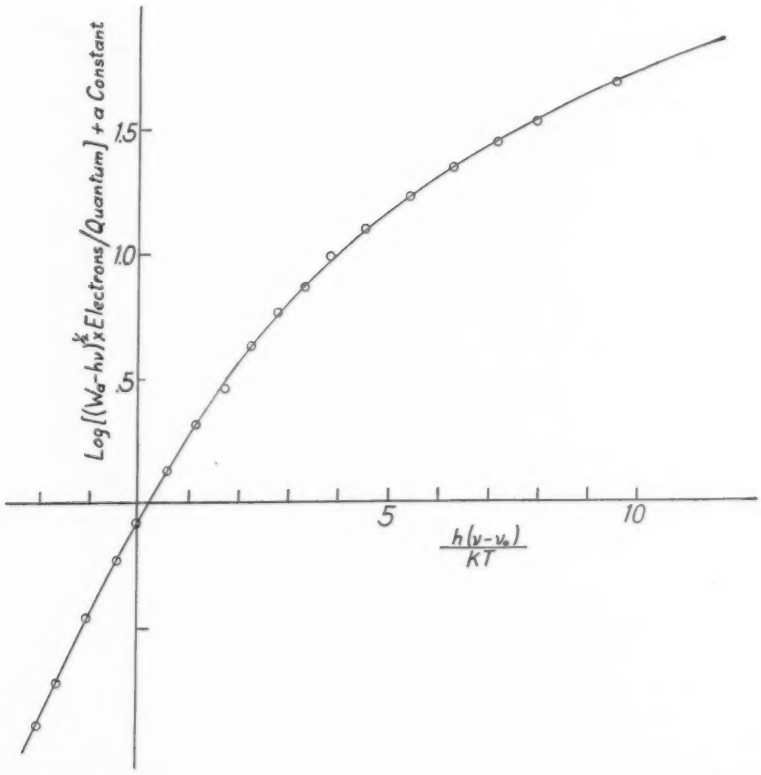

FIG. 7. Typical Fowler plot for a Ca surface at 298.4°K. Horizontal shift 105.28; $\varphi_0 = 2.706$ ev.

ture is shown in Fig. 6, the numerical data being given in Table II. A comparison of these values with the room temperature values shows a positive temperature coefficient of $(2.2 \pm 0.7) \times 10^{-5}$ ev/°K. It appears that this change in work function is due explicitly to temperature and not to other causes. It is well known that surfaces which are slightly contaminated with gas are erratic in their behavior. As will be cited in the discussion of the work on Ca, minute amounts of gas may be expected to give data not in agreement with Fowler's theory, and in this case also the surfaces do not exhibit the stability shown by the Ba specimens.

We do not maintain that the value given is more than an estimate for the particular surface studied for the given temperature range. The temperature coefficient would be expected to depend upon the crystal state of the surface and may well be a function of temperature. The influence of the backing material on the expansion of the metallic layers may be important.

Data taken at dry ice temperature were not so accurate as those taken at higher temperature; however an estimation of the work function at the low temperature showed it to be slightly lower than the room temperature value.

Data obtained at 224°C failed to fit Fowler's curve accurately as did also subsequent room temperature data. A situation had apparently arisen similar to that which occurred when liquid-air temperature measurements were attempted.

Value of A in Richardson's equation

If one assumes that the departure of the value of A from the theoretical value of 120 amp./cm² °K² is due entirely to a temperature coefficient of the work function, that is, that the transmission coefficient for electrons is unity and that

field effects and surface irregularities are negligible, one can compute the value of A for a Ba surface emitting thermionically.[11] Assuming a constant temperature coefficient of 2.2×10^{-5} ev/°K, A becomes approximately 93 amp./cm² °K². It is well known that most metals have an experimental value of A less than 120; this is also predicted by the theory of Wigner.[1]

Photoelectric Properties of Ca and Photo-Emission from Nonhomogeneous Surfaces

With a single distillation cell the mean value of the work function for a Ca surface, as determined by Fowler's method, was 2.706 ev with the greatest deviation from the mean for seven determinations being 0.004 ev. A typical plot is shown in Fig. 7. The work on calcium was preliminary to that on Ba and the measurements were not as accurate. After repeatedly heating the surface to 100°C the results obtained were somewhat erratic; surface conditions obviously had been altered (in this case very likely due to gas) and the data did not in general fit Fowler's curve accurately. The departures from the curve were consistent with the assumption that, after heating, the surface was not homogeneous. Such a set of data is shown in Fig. 8. That this distribution of points can be fitted to a theoretical curve is demonstrated by the close fit to the full line curve which represents the computed emission from two surfaces, according to Fowler's theory, one surface having a work function of 2.728 ev and the second with $\varphi_0 = 2.537$ ev, the first surface having a greater effective area by a factor of 69. The term "effective area" is used to include such factors as optical absorption, electron reflection, emission efficiency, etc. The two dashed curves are Fowler plots for the two surfaces whose existence is assumed.

In the discussion of the work on Ba it was stated that some plots suggested the existence of a nonhomogeneous surface. These plots showed small departures from Fowler's theoretical curve. The departures were not great enough, however, to warrant the analysis of the curves as done for the nonhomogeneous Ca surface discussed above.

[11] J. A. Becker, Rev. Mod. Phys. **7**, 95 (1935).

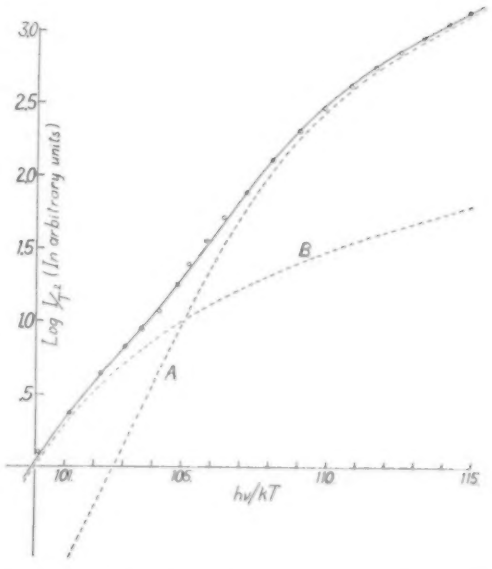

FIG. 8. The full line curve represents the computed emission from two surfaces according to Fowler's theory. The Fowler plots for the two surfaces assumed are shown by the dotted line curves. For curve A, $\varphi_0 = 2.728$; for curve B, $\varphi_0 = 2.537$.

The suggested nonhomogeneous character of the Ba surfaces was attributed to areas showing slightly different crystal structure or orientation.

In view of the experimental evidence that patches do exist in the case of thorium on tungsten,[11] the above explanation of the data seems reasonable. The design of the tube was not suited to the investigation of possible field effects.

Fig. 8 not only serves to demonstrate the possibility of investigation of nonhomogeneous surfaces but also emphasizes the value of taking data over a sufficiently wide range. Had experimental points been taken over but a short range of wave-lengths, a fair fit to Fowler's theoretical curve might have been obtained and a false value of work function determined. An accurate fit to Fowler's curve over the long wave-length range denies the existence of a second surface having a slightly lower work function; also an accurate fit to Fowler's curve over the short wave-length range denies the presence of a second surface having a slightly higher work function.

The Lower Ionosphere

R. C. COLWELL AND A. W. FRIEND, *West Virginia University, Morgantown, West Virginia*
(Received July 24, 1936)

There are two well-defined regions in the lower part of the ionosphere. One of these (the *D* region) extends from 35–65 km, the other (the *C* region) lies between 2–30 km. They have been detected by the use of a very short pulse of the order of 3 microseconds and a receiving set with a small time lag. The ground and reflected pulses are separated by using a rapid sweep on a cathode-ray oscilloscope. Similar results have been obtained by Watson-Watt, Mitra and their co-workers.

FOR many years, it has been observed that there is a close connection between weather phenomena and radio wave propagation.[1–6] The changes in signal strength depend upon the location of the sending and receiving stations. For instance, the broadcast station KDKA, 150 km north of Morgantown, W. Va., sends out a signal which is steadier and of lower amplitude at night whenever a region of high barometric pressure is establishing itself over the signal path. When a low pressure area is approaching from the northwest, the night signals fade severely and increase their maximum amplitude to many times the day level. Wide fluctuations in day to day signal strength have also been measured.[4]

It was thought that the reasons for these fluctuations in intensity could be determined by exploring the ionosphere by the method of Breit and Tuve.[7] A transmitter was designed which sends out sixty pulses per second, each pulse lasting for 3 microseconds or less (Fig. 1). The operation of this pulse generator is as follows: the condenser C_p is charged on the positive alternation of the 60-cycle power line by the transformer X_p acting through the diode valve D_p; on the negative alternation, the grid of the mercury vapor triode T_p, operating 180° out of phase with the condenser charging potential, causes the condenser C_p to discharge through T_p and R_p. The current through R_p produces a potential drop which opposes the grid bias of the radiofrequency amplifier $T_{R.F.}$ and, therefore, causes the emission of a pulse of radiofrequency power from the transmitter.

The transmitter circuit is a pentode crystal-controlled oscillator driving the pulse modulated 200-watt pentode power amplifier which supplies energy to a horizontal quarter wave Marconi antenna suspended 70 feet above the ground.

The receiving equipment is located 200 meters from the transmitter. The strong ground wave prevents the use of any type of antenna except a loop universally mounted so that it is rotatable about both the horizontal and vertical axes. A good commercial receiver gives satisfactory results for reflections from regions 10 km or more above the ground but for lower elevations, a special receiver was designed to eliminate long time constants and spurious damped oscillations in the various circuits. This receiver consists of three stages of screen grid tuned radiofrequency amplification and a screen grid detector. The complete circuit is shown in Fig. 2. Each stage is battery operated and completely shielded in a galvanized steel box which contains the amplifier and all the necessary batteries. The detector may be modified for use as a fourth radiofrequency amplifier for making oscilloscopic observations of the radiofrequency wave.

The pattern produced by the incoming ground and sky waves is viewed on the five-inch screen of a cathode-ray oscilloscope. The middle part of a 2000 volt (peak) swing produced by a 60-cycle a.c. sine wave sweeps the spot rapidly across the screen. Synchronization of the sweep circuit is obtained automatically by the use of the 60-cycle line voltage. Linearity is assured by the use of only one-twentieth of the total voltage swing for the base line on the cathode-ray tube screen. The scale is calibrated with a device which generates a high harmonic of the 60-cycle

[1] C. T. R. Wilson, Proc. Phys. Soc. **37**, 32D (1925).
[2] R. C. Colwell, Proc. I.R.E. **16**, 1570 (1928).
[3] I. Ranzi, Nature **130**, 369 (1932).
[4] R. C. Colwell, Proc. I.R.E. **21**, 721 (1933).
[5] R. C. Colwell and A. W. Friend, Nature **137**, 782 (1936).
[6] Cherry and Martyn, Comm. Australia, Bull. **63**, 33 (1932).
[7] Breit and Tuve, Phys. Rev. **28**, 554 (1926).

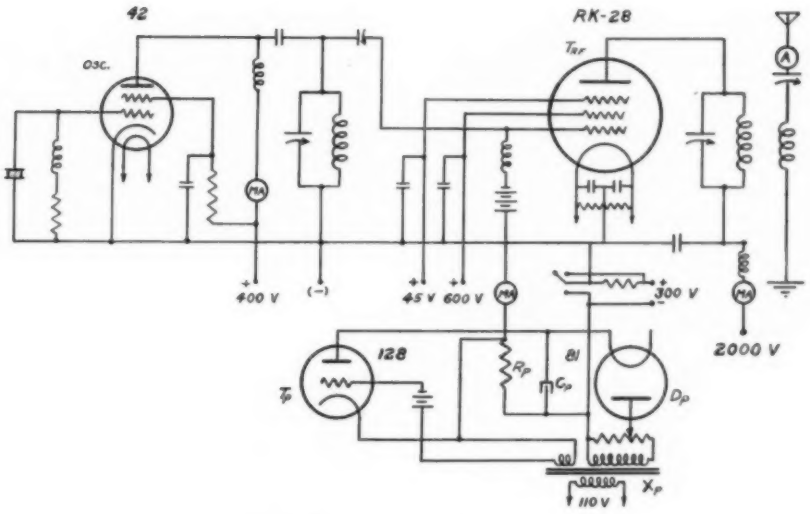

FIG. 1. Circuit diagram of transmitter.

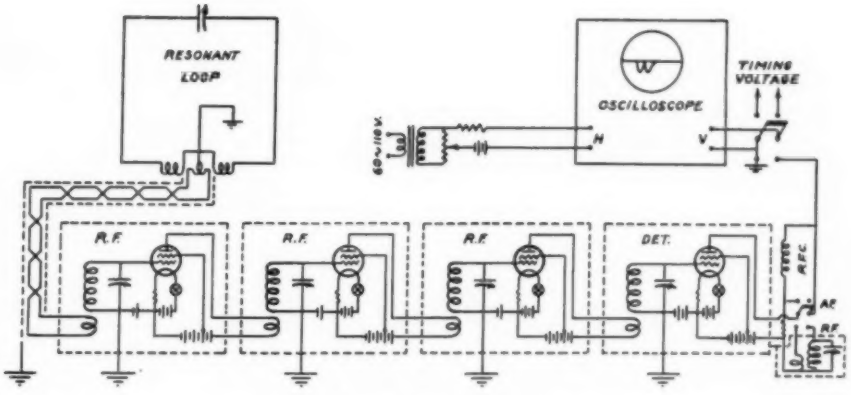

FIG. 2. Circuit diagram of receiver.

current. This harmonic sweeping vertically is used to measure the time intervals on the scale.

In operation, all radiofrequency circuits are tuned for maximum signal output. This exact condition eliminates beat phenomena produced by shock excitation. In Fig. 3, apparent peaks are shown which come from the receiver and not from the ionosphere. These do not appear when the receiver is properly tuned.

When the loop antenna, which is rotatable about the vertical and horizontal axes, is turned so as to pick up a strong direct (ground) signal, the ground and sky wave impulses merge on the screen; but when the loop is properly oriented so as to weaken the reception of the ground wave and increase that of the sky wave or *vice versa*, either wave may be made to appear on the screen without the other.

In measuring the height of the lowest reflecting layer, the loop is adjusted so as to pick up a small signal from both the ground and sky waves (Fig. 4). When this adjustment is obtained the horizontal and vertical angles of the loop are recorded, along with the virtual height of the reflecting region. When the loop antenna is turned for maximum pickup of the combined

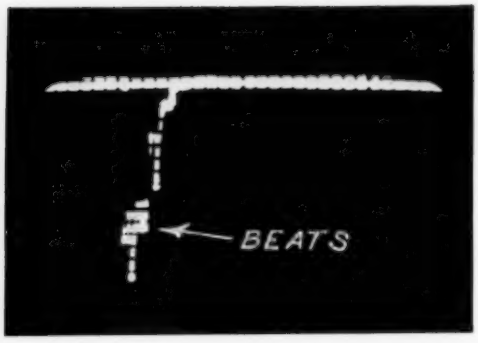

FIG. 3. Oscilloscope pattern which shows apparent peaks coming from the receiver when it is not properly tuned.

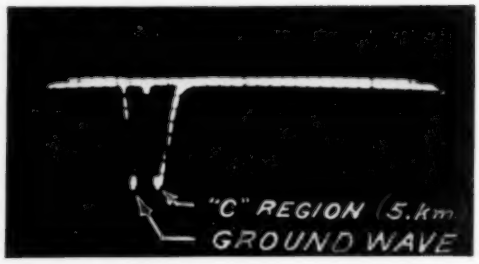

FIG. 4. Form of oscilloscope pattern when the receiving loop is adjusted to pick up a small signal from both the ground and sky waves.

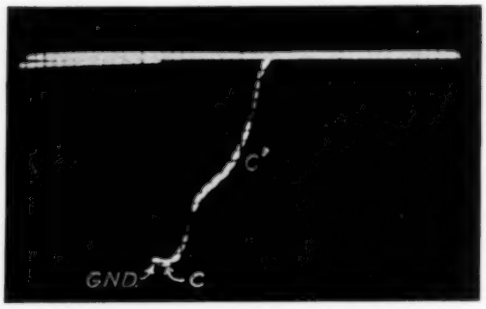

FIG. 5. Form of oscilloscope pattern when the loop antenna is turned for maximum pickup. $C = 4.8$ km; $C' = 26$ km (approximately).

signals, the received signal takes the form shown in Fig. 5. The ground wave in the photograph is marked *"GND,"* the signal from the low side of the reflecting medium is marked *C* and that from the top of this particular region is marked *C'*. The *"GND"* and *"C"* signals were run together by overloading the amplifier.

It has been repeatedly observed that, at this short distance (200 meters), strong reflections from the *C* region (2–30 km) or the *D* region (35–65 km) coincide with weak reflections from the *E* and *F* regions. Neither the *E* or *F* reflections are shown in these photographs since they fall off the edge of the screen because their height is very great compared to that of the *C* region.

These measurements have been made on frequencies of 1614 kc, 2398 kc and 3492.5 kc. The heights and penetrations on these frequencies do not differ greatly. The highest frequency 3492.5 kc gives much more erratic performance than the other two. It shows wider deviations in the angles of polarization. The wave

TABLE I. *Fluctuations both in height and intensity of the C and C' layers.*

Date	Time	Height C	Strength C	Height C'	Strength C'	Height D	Strength D
3– 5–36	5:00 P.M.	5 km	strong	17 km	medium		
3– 9–36	6:30 P.M.	3–12 km	"	33 km	strong	60 km	medium
3–11–36	8:30 P.M.	11 km	"	35 km	"	none	
3–12–36	2:56 P.M.	8–12 km	"			50 km	strong
3–31–36	2:57 P.M.	7.5 km	"	18 km	weak		
4– 6–36	9:20 P.M.	10.5 km	"	18 km	very weak	none	
4–28–36	11:15 A.M.	2–4 km	very strong	12–14 km	strong		
5–10–36	12:03 P.M.	4.3 km	strong	12 km	fairly strong		
5–24–36	1:05 P.M.	5.1 km	very strong	12 km	medium		
5–30–36	11:40 A.M.	3.6 km	" "	10 km	strong		
6– 6–36	11:10 A.M.	3.7–4.6 km	" "	18 km	medium		
6– 6–36	11:29 P.M.	7.5 km	strong	20 km	strong		
6– 7–36	2:55 A.M.	8.6 km	"	22 km	medium		
6– 7–36	12:35 P.M.	4.3 km	very strong	16 km	strong		
6– 7–36	11:03 P.M.	8 km	strong	18 km	"		
6– 8–36	11:30 A.M.	4.3 km	"	14.5 km	"		
6–11–36	5:15 P.M.	0–2 km	extra strong	16 km	"		
6–29–36	12:30 P.M.	3.5 km	very strong	21 km	medium		
7– 5–36	3:34 P.M.	1.5 km	strong	23 km	"		

seems to be more penetrating and permits more frequent observations on the E region.

The readings given in Table I show the great fluctuation of the C and C' layers in both height and intensity. It is much more difficult to detect the D region in summer than in winter.

Similar observations have been made in England on frequencies from 6–12 megacycles and also in India.[5] Extreme care must be exercised so as not to interpret beats caused by circuit oscillations for multiple layers or reflections. The peaks caused by circuit oscillations are always fixed in position and intensity; the peaks caused by the sky wave vary rapidly in intensity and shift their position from minute to minute as the reflecting layer rises or falls. The sky wave from the C region may be described as fluctuating or scintillating. In the summer months it is so strong that it prevents observations on the D region.

Messrs. N. I. Hall and L. R. Hill collaborated with us in the development and construction of the apparatus.

[5] R. A. Watson-Watt, L. H. Bainbridge-Bell, A. F. Wilkins and E. G. Bowen, Nature **137**, 866 (1936); Mitra and Syam, Nature **135**, 953 (1935); Syam, Ind. J. Phys. **10**, 13 (1936); S. K. Mitra, Nature **137**, 896 (1936).

OCTOBER 1, 1936 PHYSICAL REVIEW VOLUME 50

Must Neutron-Neutron Forces Exist in the H^3 Nucleus?*

R. D. PRESENT, *Purdue University, Lafayette, Indiana*

(Received July 13, 1936)

A wave function in the form of a series in the three interparticle distances with coefficients to be determined by the variational method is used to solve the H^3 problem for a Wigner neutron-proton interaction of the form $B\ e^{-2r/b}$. For interaction radii b of 1.0 and 2.0×10^{-13} cm the best energies obtained are -11.0 and $-9.5\ mc^2$, respectively, and the convergence of the energies obtained from successive improvements in the wave function is so rapid that the eigenvalues may be estimated to occur at -11.5 ± 0.3 and $-9.6\pm0.1\ mc^2$. Both pure and mixed exchange operators must give a higher total energy. It is shown that the narrower interaction radius is too small to be compatible with the known mass defects of H^2 and He^4 and that, accordingly, the value of $11.5\ mc^2$ is a very safe upper limit for the binding energy. From this we can conclude the existence of direct like-particle forces in the nucleus. Possible modification of the experimental data is considered and a comparison is made with the results of the equivalent two-body method.

LIKE-PARTICLE FORCES

THE evidence for explicit like-particle forces in the nucleus falls under four categories. The most recent, direct and incontrovertible evidence is furnished by the anomalous scattering of high energy protons in hydrogen. The experiments of White[1] indicated a departure from the Coulomb law at small distances; the more precise measurements of Tuve, Heydenburg and Hafstad[2] remove certain difficulties that were present in the earlier experiments and offer accumulating evidence for a short range attractive interaction between two protons with antiparallel spins.[3] Probably second in order of reliability is the evidence derived from explicit computations of the binding energies of the hydrogen and helium isotopes. This will be discussed below in detail. Thirdly, there are certain well-known properties of heavier nuclei (e.g., the existence of pairs of stable isobars of even weight and charge, differing by two charge units, with intermediate odd-charged isobar unstable) which seem to require an attractive interaction between like-particles.[4, 5] Weizsäcker[6] has shown that such an interaction might be partially, if not wholly, explained by second-order effects in the binding of a second neutron (or proton) due to a distortion of the nuclear field by the introduction of the first. Since it is not known to what extent the interaction must be attributed to *explicit* attractive forces, this

* Presented at the New York Meeting of the American Physical Society.

[1] M. G. White, Phys. Rev. **49**, 309 (1936).

[2] Tuve, Heydenburg and Hafstad, Phys. Rev. **49**, 402 (1936).

[3] Breit, Condon and Present, in a forthcoming article in this journal.

[4] Bethe and Bacher, Rev. Mod. Phys. **8**, 82 (1936).

[5] L. A. Young, Phys. Rev. **48**, 913 (1935).

[6] C. F. v. Weizsäcker, Zeits. f. Physik **96**, 431 (1935).

evidence is corroborative but in itself inconclusive. Lastly, it has been pointed out by Bethe and Bacher[4] that if the neutron-proton forces are to be explained by a Fermi field, then the order of magnitude of the like-particle forces, which appear in second approximation, is entirely comparable.

Evidence from H^2, H^3, He^4

Several authors have made explicit calculations on the hydrogen and helium isotopes in order to fix the constants in a simple two-parameter neutron-proton potential function and to test the compatibility of the function so obtained with the known mass defects. The pioneering work of Wigner[7] showed that the binding energies of H^2 and He^4 could be explained by a narrow and deep potential well and predicted that the binding energy of H^3 must exceed twice that of the deuteron. The most extensive calculations of this nature have been made by Feenberg,[8] who first applied a simple variational method, employing Gaussian wave functions, to the H^3 and He^4 nuclei. The limitations of this method proved so severe, particularly in the case of H^3 where no binding could be obtained for reasonably narrow radii, that Feenberg was led to the use of a plausible pseudo-variational procedure, the method of the equivalent two-body problem, which was found to give very consistent results in spite of the absence of a rigorous justification.[8a] When the experimental binding energies for the H^2 and He^4 nuclei were used to fix the parameters in Gaussian potentials of the Wigner and Majorana type, it was found that the neutron-proton potential so determined gave a computed binding energy for H^3 somewhat smaller than the experimental 16 mc^2, the results for Wigner and Majorana operators being sensibly the same.

A more refined variational calculation on H^3 has been made by Massey and Mohr,[9] using ordinary potentials of the rectangular well and simple exponential types. Their trial wave function, especially for the simple exponential potential, becomes rapidly worse for radii of interaction smaller than 10^{-13} cm, in agreement with the experience of Feenberg. Also their conclusion as to the necessity of like-particle forces, without reference to the alpha-particle, appears to be not quite justified. Finally Dolch[10] has performed variational calculations on H^2, H^3 and He^4, but his conclusions are vitiated by an especially poor approximation to the solution of the two-body problem. We may conclude that the theoretical uncertainties involved in the three treatments mentioned above, would render dubious any definite conclusion as to the need for explicit neutron-neutron interaction. In fact Massey and Mohr and Dolch have drawn precisely opposite conclusions on this point from their respective calculations.

Choice of Method

It is evident from the above that a rigorous solution of the H^3 problem would provide a crucial test for the hypothesis that specific nuclear forces occur only between unlike particles. The very deep, short range forces impose exacting conditions on a variational wave function, for the binding energy appears as a small difference between large potential and kinetic energy terms. Now the wave function must have a dual character, since it varies rapidly within the potential well but comparatively slowly outside. The intermediate region must then be difficult to represent, even if one possessed a suitable approximation for both exterior and interior regions. But it is precisely this intermediate region which makes a large contribution to the kinetic energy, since the slope of the wave function undergoes a rapid change. It is therefore apparent that the trial wave functions must possess great flexibility, i.e., a large number of adjustable parameters. This at once suggests the powerful and systematic variational procedure developed by Hylleraas[11] in his treatment of the lowest states of the helium atom. This method has been extended to the normal and excited states of the hydrogen molecule,[12] where

[7] E. Wigner, Phys. Rev. **43**, 252 (1933).
[8] E. Feenberg, Phys. Rev. **47**, 850 (1935).
[8a] In a paper to be published shortly, Feenberg and Share have shown that the equivalent two-body method, when used with the Gaussian potential, must give slightly too great a binding energy for H^3 and He^4. Added in proof: Feenberg and Share, Phys. Rev. **50**, 253 (1936).
[9] Massey and Mohr, Proc. Roy. Soc. **A152**, 693 (1935).
[10] H. Dolch, Zeits. f. Physik **100**, 401 (1936).
[11] E. Hylleraas, Zeits. f. Physik **54**, 347 (1929).
[12] James and Coolidge, J. Chem. Phys. **1**, 825 (1933); R. D. Present, J. Chem. Phys. **3**, 122 (1935); James, Coolidge and Present, J. Chem. Phys. **4**, 187 (1936).

it has led to results of great precision (lying within the range of band spectroscopic experimental error). In this paper we propose to carry out an analogous extension to the H^3 nuclear problem.

Choice of Potential

It is first necessary to specify the nature of the interaction operator, the special form of the potential function and a suitable range for the forces. This must be done in such a fashion that we are certain to obtain an upper limit for the H^3 binding energy consistent with our initial assumption of neutron-proton interaction only. It has been shown by Eckart[13] that, for the same potential function, an exchange operator must give a higher total energy than an ordinary or Wigner potential. It is readily shown[14] that the mixed Majorana-Heisenberg operator, suggested by Wigner to explain slow neutron-proton scattering, must give a higher energy than a pure Majorana operator with the same potential function. We shall then obtain a lower bound for the total energy (i.e., an upper bound for the binding energy) if we make our calculation with ordinary forces. This choice will simplify the calculation very considerably and afford us a worth-while gain in generality.

This gain in generality is justified principally by the fact that there exists an alternative explanation for the scattering of slow neutrons in hydrogen, which does not make use of the spin-dependent mixed operator hypothesis. Mamasachlisov[15] has shown that these experiments, together with the experiments on recombination of neutron and proton, may be explained by a pure Majorana potential if one assumes the existence of additional shallow long range repulsive forces. Since the long range forces can have but little effect on the binding calculation, this explanation would justify a treatment of H^3 with a pure Majorana or ordinary potential.

Evidence against the long range force explanation is furnished by the experiments on proton-proton scattering in conjunction with the binding calculations of Feenberg and Knipp.[16] The latter calculations, which take into account explicit like-particle forces, give very different results for the depth of the like-particle well depending on whether a pure or mixed Majorana operator is used for the neutron-proton interaction. On the other hand the proton-proton scattering is extremely sensitive to small variations in the depth of the like-particle well for a given radius, and, regardless of the experimental accuracy, must, if the potential well concept be applicable, agree closely with the Feenberg-Knipp estimate of its depth when the mixed neutron-proton operator is used and disagree with the estimate obtained with a pure Majorana operator.[17] Since the long range forces have little effect on binding, this would seem to rule out the Mamasachlisov hypothesis.

The simple exponential function $Be^{-2r/b}$ has been chosen to represent the neutron-proton potential. Unpublished calculations of Feenberg by the equivalent two-body method show that the two potentials $Be^{-2r/b}$ and $Ae^{-(r/a)^2}$ give almost identical results for the H^3 and He^4 problems over a large range of the parameters, if the interaction radius b of the exponential function is identified with the interaction radius a of the Gaussian potential. Massey and Mohr's calculations (reference 9, Fig. 3) show a similar correspondence between the simple exponential function and the rectangular well (which holds down to $b=10^{-13}$ cm after which their variational method grows rapidly poorer) and in this case the radius b is to be identified directly with the width of the well. These approximate relations for translating between the three potentials make it possible to assign more definite meaning to the rather loose expressions: "radius of interaction" and "range" of the forces. The binding energies of the light nuclei appear, then, to be very insensitive to the analytic form of the potential, and we are justified in making an arbitrary choice of the simple exponential function, which gives an exactly soluble equation for the deuteron and is somewhat simpler to handle in the H^3 problem as here treated.

It remains to select a suitable radius of interaction for the forces; the known binding energy of the deuteron will then determine the depth of the potential, which will be the same for all types of interaction operator. Thomas[18] and Feenberg[8] have pointed out that the binding energy of H^3 must increase as the range of the forces is decreased; then an upper limit will be obtained from too narrow a potential hole. In order to select a sufficiently narrow interaction radius, reference must be made to other calculations that are consistent with the initial assump-

[13] C. Eckart, Phys. Rev. **44**, 109 (1933).
[14] Cf., e.g., reference 16, Eqs. (18)–(22).
[15] V. I. Mamasachlisov, Physik. Zeits. Sowjetunion **9**, 198 (1936).
[16] Feenberg and Knipp, Phys. Rev. **48**, 906 (1935).
[17] R. D. Present, Phys. Rev. **48**, 919 (1935).
[18] L. H. Thomas, Phys. Rev. **47**, 903 (1935).

tion of neutron-proton forces only. In particular Feenberg's variational calculations on He^4 with a Wigner potential show that 4/5 of the binding energy can be accounted for when the radius of interaction is 10^{-13} cm. The extreme simplicity of the two-parameter Gaussian wave function used in this calculation together with the inadequacy of the variational method for such a narrow interaction distance, make it plausible that a rigorous wave function would give at least the true binding energy. The interaction radius for a Wigner potential must then exceed 10^{-13} cm. The equivalent two-body method when applied to both Gaussian and simple exponential potentials, shows that the true value must be in the neighborhood of 1.4×10^{-13} cm. Nearly the same result holds for a pure Majorana potential. For the mixed operator, however, one requires a narrower hole[19] to compensate for the weaker attraction caused by the small Heisenberg term. If the mixed operator hole is made narrower than the pure Majorana hole by the amount necessary to compensate for the Heisenberg term in the alpha-particle, there seems to be no assurance that an equal compensation will then occur in the H^3 nucleus, i.e., the mixed operator potential determined from H^2 and He^4 need not give a smaller binding energy for H^3 than a similarly determined pure Majorana potential (or Wigner potential). Therefore, in order to obtain an upper limit for the binding energy of H^3 which will be valid regardless of whether the interaction is of the Wigner, Majorana or mixed operator type, one should use the radius of interaction appropriate to the mixed operator even though the calculation is carried out with Wigner forces. In this way one would obtain a very conservative upper limit. A calculation with mixed operator forces by the equivalent two-body method using both Gaussian and exponential potentials, shows that the H^2 and He^4 problems determine a radius of interaction of 1.0×10^{-13} cm.*

The following calculations have been made with a Wigner potential of the simple exponential type, employing this radius of interaction. Since for each new radius chosen, the matrix elements of potential energy and the secular equations must be all recalculated, considerations of time and labor have restricted us to a calculation at only one additional radius: 2×10^{-13} cm. A linear interpolation in this range would seem to be justified by the almost linear increase of binding energy, plotted against the reciprocal square of the interaction radius, obtained by Feenberg with the equivalent two-body method.

Mathematical Details

The solution for the two-body problem with a simple exponential potential has been discussed by several authors and will not be repeated here.[20] The procedure for the three-body problem follows closely that described by Hylleraas[11] in his precise calculation of the ground state of parahelium, with the exception that the potential energy terms must be given a special and more extended treatment here.

The wave equation, with center of gravity terms separated out, is expressed in terms of the three interparticle distances r_{12}, r_{13}, r_{23} where the subscript 1 refers to the proton. The resulting equation may be written as an Euler equation for the following variational integral

$$\kappa E=\int_0^\infty dr_{12}\int_0^\infty dr_{13}\int_{|r_{13}-r_{12}|}^{|r_{13}+r_{12}|} dr_{23}F,$$

$$F=r_{12}r_{13}r_{23}\left[\left(\frac{\partial\varphi}{\partial r_{12}}\right)^2+\left(\frac{\partial\varphi}{\partial r_{13}}\right)^2+\left(\frac{\partial\varphi}{\partial r_{23}}\right)^2\right]+r_{23}\frac{r_{12}^2+r_{13}^2-r_{23}^2}{2}\frac{\partial\varphi}{\partial r_{12}}\frac{\partial\varphi}{\partial r_{13}}+r_{13}\frac{r_{12}^2+r_{23}^2-r_{13}^2}{2}\frac{\partial\varphi}{\partial r_{12}}\frac{\partial\varphi}{\partial r_{23}}$$
$$+r_{12}\frac{r_{13}^2+r_{23}^2-r_{12}^2}{2}\frac{\partial\varphi}{\partial r_{13}}\frac{\partial\varphi}{\partial r_{23}}+\kappa V\varphi^2 r_{12}r_{13}r_{23}$$

[19] This will no longer be true if like-particle forces are included.

* Cf. Bethe and Bacher, reference 4, p. 144.

[20] Cf. e.g., reference 4, p. 110.

subject to the condition that:

$$\int_0^\infty dr_{12}\int_0^\infty dr_{13}\int_{|r_{13}-r_{12}|}^{r_{13}+r_{12}} dr_{23}r_{12}r_{13}r_{23}\varphi^2=1.$$

Here $\kappa=4\pi^2M/h^2$ where M is the mass of neutron or proton. In the units we have chosen ($(h^2/4\pi^2c^2mM)^{1/2}=8.97\times10^{-13}$ cm for length and mc^2 for energy) $\kappa=1$, and will be omitted from all remaining equations. We transform to elliptical coordinates defined by the relations: $s=r_{12}+r_{13}$, $t=r_{12}-r_{13}$, $\rho=r_{23}$ in terms of which the variational integral takes on the form: $E=\frac{1}{8}\{M+L\}$,

$$M=\int_0^\infty ds\int_0^s d\rho\int_0^\rho dt\left\{\left(\frac{\partial\varphi}{\partial s}\right)^2[3\rho s^2-\rho t^2-2\rho^3]+\left(\frac{\partial\varphi}{\partial t}\right)^2[\rho s^2-3\rho t^2+2\rho^3]+\left(\frac{\partial\varphi}{\partial\rho}\right)^2\rho(s^2-t^2)\right.$$

$$\left.+\frac{\partial\varphi}{\partial\rho}\frac{\partial\varphi}{\partial s}[2s\rho^2-2st^2]+\frac{\partial\varphi}{\partial\rho}\frac{\partial\varphi}{\partial t}[2ts^2-2t\rho^2]\right\},\quad L=\int_0^\infty ds\int_0^s d\rho\int_0^\rho dt\rho(s^2-t^2)V\varphi^2,$$

subject to the condition that $\frac{1}{8}N=1$

$$N=\int_0^\infty ds\int_0^s d\rho\int_0^\rho dt\rho(s^2-t^2)\varphi^2.$$

The wave function φ takes the simple form:

$$\varphi=e^{-k(s/2)}\sum_{pqr}c_{pqr}s^pt^q\rho^r,$$

where the summation is to be extended over all positive values of the indices with the exception that q can assume only even values because of the antisymmetry in neutron spins.[21] As many terms will then be taken as result in an appreciable lowering of the total energy. If we make the transformation: $s'=ks$, $t'=kt$, $\rho'=k\rho$ (and drop the primes), the "shielding" parameter k disappears from φ and the energy eigenvalue is given by:

$$E=(k^2M+L(k))/N.$$

The matrix elements of energy (H_{mn}) and of unity (N_{mn}) between the mth and nth terms of the series wave function are given by the formulae:

$$H_{mn}=k^2(P_{mn}+Q_{mn})+L_{mn}(k),$$

$$P_{mn}=\tfrac{1}{4}[3J(201)-J(021)-2J(003)]-\frac{p_m+p_n}{2}[3J(101)-J(-121)-2J(-103)]+p_mp_n[3J(001)$$

$$-J(-221)-2J(-203)]+q_mq_n[J(2-21)-3J(001)+2J(0-23)]+r_mr_n[J(20-1)-J(02-1)],$$

$$Q_{mn}=(r_mp_n+r_np_m)[J(001)-J(02-1)]-\frac{r_m+r_n}{2}[J(101)-J(12-1)]$$

$$+(q_mr_n+q_nr_m)[J(20-1)-J(001)],$$

$$L_{mn}=K(201)-K(021),\quad N_{mn}=J(201)-J(021),$$

$$J(abc)=\int_0^\infty dse^{-s}s^{p_m+p_n+a}\int_0^s d\rho\rho^{r_m+r_n+c}\int_0^\rho dtt^{q_m+q_n+b},$$

$$K(abc)=\int_0^\infty dse^{-s}s^{p_m+p_n+a}\int_0^s d\rho\rho^{r_m+r_n+c}\int_0^\rho dtt^{q_m+q_n+b}V'(k).$$

[21] The spin-dependent mixed operator would "mix-in" terms of odd q, corresponding to parallel neutron spins.

For the remainder of the discussion J and K will be redefined as follows:

$$J(abc)=\int_0^\infty ds e^{-s}s^a\int_0^s d\rho\rho^c\int_0^\rho dtt^b,\quad K(abc)=\int_0^\infty ds e^{-s}s^a\int_0^s d\rho\rho^c\int_0^\rho dtt^bV'(k).$$

From our choice of potential $V=Be^{-2r_{12}/b}+Be^{-2r_{13}/b}=B[e^{-(s+t)/b}+e^{-(s-t)/b}]$ and $V'(k)=B[e^{-\alpha(s+t)}+e^{-\alpha(s-t)}]$, where $\alpha=1/bk$;

$$\therefore\quad K(abc)=B\int_0^\infty ds e^{-(\alpha+1)s}s^a\int_0^s d\rho\rho^c\int_0^\rho dtt^b(e^{\alpha t}+e^{-\alpha t}).$$

The evaluation of the kinetic energy terms is extremely simple and will hold for all radii of interaction since the integrals are independent of k. We have:

$$J(abc)=(a+b+c+2)!/(b+1)(b+c+2).$$

The potential energy terms are more difficult to evaluate, but much lengthy integration can be avoided by calculating tables of auxiliary integrals in accordance with the following recursion formulae:

$$K(abc)=B\{K_+(abc)+K_-(abc)\},$$

$$K_\pm(abc)=\int_0^\infty ds e^{-(\alpha+1)s}s^a\int_0^s d\rho\rho^c\int_0^\rho dtt^be^{\pm\alpha t},$$

$$K_\pm(abc)=\frac{1}{\pm\alpha}\{R_\pm(a,b+c)-bK_\pm(a,b-1,c)\},$$

$$R_\pm(a,b)=\int_0^\infty ds e^{-(\alpha+1)s}s^a\int_0^s\rho^be^{\pm\alpha\rho}d\rho,$$

$$R_\pm(a,b)=\frac{1}{\pm\alpha}\{S_\pm(a+b)-bR_\pm(a,b-1)\},$$

$$S_\pm(n)=\int_0^\infty ds e^{-(\alpha\mp\alpha+1)s}s^n=\frac{n!}{(\alpha\mp\alpha+1)^{n+1}},$$

$$K_\pm(a0c)=\frac{1}{\pm\alpha}\left\{R_\pm(ac)-\frac{1}{c+1}T(a+c+1)\right\},$$

$$R_\pm(a0)=\frac{1}{\pm\alpha}\{S_\pm(a)-T(a)\},$$

$$T(n)=\int_0^\infty ds e^{-(\alpha+1)s}s^n=\frac{n!}{(\alpha+1)^{n+1}}.$$

The energy is calculated from the usual secular equations obtained by varying the parameters c_{pqr} in the wave function. This procedure gives the familiar condition that the determinant $||H_{ij}-\lambda N_{ij}||$ must vanish when λ is the minimum energy obtainable from the best linear combination of the terms considered. The proper value of λ was found by evaluating symmetric determinants and interpolating for the root.[12]

Results

The calculations were carried out for interaction radii of 2.0 and 1.0×10^{-13} cm. Because a better convergence of the energy contributions due to successive additional terms in the eigenfunction was to be expected for the wider radius, this was the first to be investigated. An exact solution of H^2 in terms of Bessel functions gives for the potential in the units chosen: $Be^{-2r/b}=-189e^{-8.97r}$. This value corresponds to a binding energy for the deuteron of 4.0 mc^2; the effect of a slightly larger value upon the subsequent calculations will be considered later. A suitable value for the "shielding" parameter k in the H^3 wave function must be selected at the outset of the calculation. This was done by minimizing with respect to k the energy obtained from the first term in the series, i.e., the function $e^{-ks/2}$, which proved subsequently to be the most important single term. This term alone gives a binding energy of 7.62 mc^2 and the corresponding value of k is 7.83. The optimum value of k will of course be modified by the presence of the remaining terms in the series, but it is to be expected that such modification will be slight and that it will be automatically compensated for by slight alterations in the coefficients of low power terms in s.

The four-term function $e^{-ks/2}\{c_1+c_2s+c_3\rho+c_4t^2\}$ gives a binding of 9.39 mc^2. This repre-

sents the basic function and it is found that additional terms give an almost negligible improvement to the energy. The nine-term function $e^{-ks/2}\{c_1+c_2s+c_3\rho+c_4t^2+c_5s^2+c_6\rho^2+c_7\rho^3+c_8\rho s+c_9\rho t^2\}$ brings the binding energy up to 9.51 mc^2. Now it is reasonable to expect and, in similar calculations[11] invariably observed that the terms of higher index go down very rapidly in importance when combined with terms of lower power, if a suitable "shielding" parameter has been selected. Since the wave function chosen represents a complete function system for the problem, there is then little likelihood that an essential dependence of the wave function has been overlooked. It is possible to make an estimate of the probable contribution of remaining terms in the series from the observed rate of convergence of the energies obtained from the terms investigated. We may then say that for a radius of interaction of 2×10^{-13} cm, the true binding energy of the H^3 problem without explicit like-particle forces is 9.60 ± 0.10 mc^2. This may be compared with the value of 9.2 mc^2 obtained by Massey and Mohr[8] with their best trial wave function for the same radius.

By a simple generalization of Eckart's criterion relating the errors in wave function and calculated energy, we can obtain an approximate relation between the mean-square relative deviation of two fairly good trial wave functions and the errors in their respective energies. A detailed comparison of Massey and Mohr's best wave function with our basic four-term function, similarly normalized, over a representative set of points in configuration space, shows a mean square relative deviation of 6 percent. This would correspond to an eigenvalue in the neighborhood of -9.6 mc^2, thus giving a rough but independent check on the previous estimate.

For the interaction radius of 1×10^{-13} cm the potential determined from the deuteron is: $-602e^{-17.93r}$. Although the potential hole is now half as wide, the best binding energy that can be obtained from the single term $e^{-ks/2}$ is 5.93 mc^2 or less than before. The corresponding value of k is 11.40. The basic five-term function $e^{-ks/2}\{c_1+c_2s+c_3\rho+c_4t^2+c_5s^2\}$ gives a binding of 10.5 mc^2. Eight other low power terms have been investigated in combination with this function; none was found to contribute more than 0.2 mc^2 and most gave considerably less. A wave function comprising all thirteen terms gave a binding energy of 11.0 mc^2. Again it is possible to estimate a convergence limit for the binding energy; this appears to be 11.50 ± 0.30 mc^2. For the same radius Massey and Mohr obtain 9.2 mc^2 again.

Since no direct check on the equivalent two-body method has yet been obtained, it is of interest to compare the results of Feenberg with those obtained here. The equivalent two-body method can be applied to the simple exponential function in the same way as to the Gaussian potential. If $Be^{-2r/b}$ represents the true potential and $Ce^{-2r/c}$ the fictitious two-body potential and if σ is a parameter, then the energies of the two and three-body problems are given by:

$$E_{H^3}=\frac{3}{2}\left(\frac{\sigma}{c}\right)^2-C\frac{4}{\pi^{\frac{1}{2}}}\int_0^\infty e^{-r^2}e^{-2r/\sigma}r^2dr,$$

$$E_{H^3}=2.7991\left(\frac{\sigma}{b}\right)^2-2B\frac{4}{\pi^{\frac{1}{2}}}\int_0^\infty e^{-r^2}e^{-2r/\sigma}r^2dr,$$

whence $c^2=0.5359b^2$, $C=2B$. This determines the potential in the equivalent two-body equation, which may then be solved exactly. For an interaction radius of 2×10^{-13} cm one obtains a binding energy of 10.26 mc^2 and for a radius of 1×10^{-13} cm a value of 12.48 mc^2. A comparison with the results of the present calculation (9.6 and 11.5 mc^2) shows close agreement, but indicates that the equivalent two-body problem cannot be trusted to be wrong in the sense of a variational calculation.[8a]

Conclusion

In view of the fact that evidence strongly favors the mixed-operator hypothesis, it must be concluded that 11.5 mc^2 represents a very conservative upper limit for the H^3 binding energy. The choice of a proper interaction radius would be very little affected by slight modifications in the mass defects of H^2 and He^4; however a greater binding energy would be obtained for H^3 if the H^2 binding energy should prove to be larger than 4.0 mc^2. If the rather large value of 4.5 mc^2 is used, the increase in the H^3 binding energy may be easily estimated by the equivalent two-body method and is found to be 1.3 mc^2 for

the radii considered. There also exists the possibility that the theory may have to be modified in some way in order to take into account the relativistic effects that are found to be quite appreciable in the deuteron for interaction radii less than 10^{-13} cm.[22] Using a simple second-order "relativistic" equation, Blochinzew has estimated that the Schrödinger equation for H^2 gives a potential hole which is over ten percent too deep at a radius of 10^{-13} cm and for a binding energy of 4 mc^2. A relativistic treatment of the deuteron without a corresponding treatment of the H^3 problem would then give a smaller binding energy than the one we have calculated. However it seems reasonable to expect a near compensation of relativistic effects in the two problems, because of the relatively small binding energies in both.

Since these calculations were carried out the accepted binding energies of H^2 and H^3 have undergone slight modification. According to Bethe[23] the correct value for H^2 is 4.35 ± 0.1 mc^2, which would lead to a value for H^3 of 16.55 ± 0.25 mc^2 if one uses the reaction: $H^2+H^2 \rightarrow H^3+H^1$. Since the energies involved in this reaction have been very precisely measured (within 0.03 mc^2), the largest uncertainty enters through the value of the H^2 binding energy. When the value of 4.35 mc^2 is used in our calculations, an upper limit of 12.5 mc^2 is found for the H^3 binding energy, which differs from the experimental value by 4 mc^2. If the accepted binding energy of H^2 should undergo a further increase of ϵ mc^2, the experimental value for H^3 would obviously increase by 2ϵ and the theoretical value by approximately 2.6ϵ. The difference of 4 mc^2 can then be reduced by only 0.6ϵ mc^2. We are forced to conclude that the hypothesis which states that the only specific nuclear forces are those between unlike particles, is incompatible with the experimental evidence. Thus the binding energy calculations for the hydrogen and helium isotopes give strong, independent support to the conclusion that direct like-particle forces must exist in the nucleus.

In conclusion the writer wishes to acknowledge valuable information, received from Dr. Eugene Feenberg, concerning the application of the equivalent two-body method to the H^3 problem.

---

[22] Blochinzew, Physik. Zeits. Sowjetunion **8**, 270 (1935); Margenau, Phys. Rev. **49**, 873 (1936).

[23] I am much obliged to Professor Bethe for a discussion of the most recent experimental material. Cf. M. L. Oliphant, Nature **137**, 396 (1936).

The Dependence of Nuclear Forces on Velocity

JOHN ARCHIBALD WHEELER, *University of North Carolina, Chapel Hill, North Carolina*

(Received July 2, 1936)

It is shown that the Majorana force may be considered as a special case of a neutron-proton interaction dependent on velocity and angular momentum. Any interaction of this more general form, which is non-Wignerian, and represents attraction, accounts for the saturation properties of nuclear binding in the same way as do the Heisenberg and Majorana potentials. An analysis of the binding in heavy nuclei in terms of angular momentum is given on the basis of the Fermi-Thomas statistical model. An illustration is given showing that the assumption of velocity dependent forces is also consistent with the properties of light nuclei: a particular form of interaction, containing two parameters, is found to give results much the same as those of the ordinary Majorana theory. Finally, the most general dependence of two-particle forces on spin, separation, and velocity, consistent with the conservation laws, is determined, and it is pointed out that experiments on the scattering of fast neutrons in hydrogen are capable of deciding between Majorana forces and a more general form of velocity dependence.

WITH forces of an exchange nature acting between neutrons and protons, Heisenberg was able to account for the dominating feature of nuclear stability—the fact that for heavy nuclei the binding energy per particle is nearly a constant. Majorana's modification of the interaction to account for the closed shell nature of the alpha-particle gave support for a neutron-proton force which corresponds to an exchange of the coordinates but not the spins of the two particles. In contrast with Heisenberg's potential, however, just this last feature of the Majorana force takes away the possibility of a simple picture of the neutron-proton interaction in terms of the kind of exchange familiar in the theory of molecular structure.

It is therefore interesting to notice that Majorana's interaction may be described as an ordinary potential without exchange but with dependence on both the separation and the relative velocity of the neutron and proton. To bring this fact into evidence let us describe the motion of the two particles by a wave function ψ depending on the position of their center of gravity $\mathbf{A}=(A_1, A_2, A_3)$ and on their separation $\mathbf{X}=(X_1, X_2, X_3)$. Then, when we multiply the Majorana potential $V_{12}\cdot$ into $\psi(\mathbf{A}, \mathbf{X})$, we obtain a new function of $\mathbf{A}$ and $\mathbf{X}$, given by

$$V_{12}\cdot\psi = V(\mathbf{X})\psi(\mathbf{A}, -\mathbf{X}),$$

the change from $\mathbf{X}$ to $-\mathbf{X}$ bringing about the exchange of the neutron and proton. Taylor's theorem assures us now that the operator

$$V(\mathbf{X}) \sum_{n_1, n_2, n_3} \frac{(-2X_1)^{n_1}(-2X_2)^{n_2}(-2X_3)^{n_3}}{n_1!n_2!n_3!}\left(\frac{\partial}{\partial X_1}\right)^{n_1}\left(\frac{\partial}{\partial X_2}\right)^{n_2}\left(\frac{\partial}{\partial X_3}\right)^{n_3}$$

has all the properties of $V_{12}\cdot$, provided that ψ and its derivatives are continuous. But the operator $\partial/\partial\mathbf{X}$ represents just $i/\hbar$ times the relative momentum, $\mathbf{P}$, of the two particles. Consequently, we have in

$$V_{12}\cdot = V(\mathbf{X}) \sum_{n_1, n_2, n_3} (-2iX_1/\hbar)^{n_1}(-2iX_2/\hbar)^{n_2}(-2iX_3/\hbar)^{n_3}P_1^{n_1}P_2^{n_2}P_3^{n_3}/n_1!n_2!n_3! \qquad (1)$$

the representation of the Majorana interaction in terms of relative momentum and separation of the neutron and proton.

The expression (1) shows the very special dependence on momentum of Majorana's force, and at the same time suggests the question: What are the consequences for nuclear structure of assuming between neutrons and protons a more general interaction. In the following we attempt partially to answer this question.

If we assume an interaction, $V_{12}\cdot$, depending on momentum and separation in a general way, $V(\mathbf{X}, \mathbf{P})$, we will find it convenient to represent it not as a differential operator by replacing

$\mathbf{P}$ by $-ih\partial/\partial\mathbf{X}$, but as an integral operator,[1] according to the equation

$$V_{12}\cdot\psi(x)=\int J(\mathbf{X},\xi)\psi(\xi)d\xi, \tag{2}$$

where

$$J(\mathbf{X},\xi)=h^{-3}\int V(\mathbf{X},\mathbf{P})\exp\{i\mathbf{P}(\mathbf{X}-\xi)/\hbar\}d\mathbf{P}. \tag{3}$$

As is well known, the Majorana force in this representation is simply $J(\mathbf{X},\xi)=V(\mathbf{X})\delta(\mathbf{X}+\xi)$, and the Wigner force $V(\mathbf{X})\delta(\mathbf{X}-\xi)$.

The general interaction "kernel,"[2] $J(\mathbf{X},\xi)$, may be viewed as a matrix of (continuously) many rows and columns. The matrix element at the point $\mathbf{X},\xi$ determines that part of the time rate of change at ψ at $\mathbf{X}$ which is proportional to the probability amplitude for the two particles being at some other separation ξ. To be in accord with the law of conservation of energy, $J(\mathbf{X},\xi)$ must be self-adjoint: $J(\xi,\mathbf{X})=J^*(\mathbf{X},\xi)$. Because of the fact that J is independent of the position of the center of gravity, conservation of total linear momentum is automatically maintained. The requirement of constancy of angular momentum is equivalent to saying J must be independent of the orientation of the reference system in space; i.e., J depends on the magnitudes r and ρ of the vectors $\mathbf{X}$ and ξ and the angle θ_{12} between them, but not on the orientation of these vectors in space.

What conclusions of a general nature can we draw from the binding energies of heavy nuclei as to the interaction $J(\mathbf{X},\xi)$ between neutrons and protons? Following Majorana, let us apply to a heavy nucleus the Fermi-Thomas statistical method, in the form given it by Dirac.[3] In the first approximation, the wave function for a nucleus composed of P protons and N neutrons is given by

$$(P!)^{-\frac{1}{2}}(N!)^{-\frac{1}{2}}\begin{vmatrix}\Phi_1(1) & \cdots & \Phi_1(P)\\ \cdot & \cdots & \cdot\\ \Phi_P(1) & \cdots & \Phi_P(P)\end{vmatrix}\cdot\begin{vmatrix}\Psi_1(1) & \cdots & \Psi_1(N)\\ \cdot & \cdots & \cdot\\ \Psi_N(1) & \cdots & \Psi_N(N)\end{vmatrix}.$$

For the potential energy due to the neutron-proton interaction we obtain

$$V_{np}=\sum_{i,k}\int\Phi_i^*(p)\Psi_k^*(n)\,V_{ik}\cdot\Phi_i(p)\Psi_k(n)d\tau_p d\tau_n.$$

If we may neglect spin forces, we have $\Phi_i(p)=f_i(\sigma_p)\varphi(x_p)$, etc. On expressing the integral in terms of the position, $\mathbf{R}$, of the center of gravity of the typical neutron and proton, and the separation $\mathbf{X}$ of the two particles, we then have

$$V_{np}=\int\left\{\sum_{i=1}^{P}\varphi_i^*\left(\mathbf{R}+\frac{\mathbf{X}}{2}\right)\varphi_i\left(\mathbf{R}+\frac{\xi}{2}\right)\right\}J(\mathbf{X},\xi)\left\{\sum_{k=1}^{N}\psi_k^*\left(\mathbf{R}-\frac{\mathbf{X}}{2}\right)\psi_k\left(\mathbf{R}-\frac{\xi}{2}\right)\right\}d\mathbf{X}d\xi d\mathbf{R}. \tag{4}$$

Applying the Fermi-Thomas statistical treatment, we express the density of particles at any point in terms of the maximum momentum of the particles there through the relations

$$\rho_p(\mathbf{x}_p)=2h^{-3}\int_0^{\mathbf{P}_p(\mathbf{x}_p)}d\mathbf{P}\quad\text{and}\quad\rho_n(\mathbf{x}_n)=2h^{-3}\int_0^{\mathbf{P}_n(\mathbf{x}_n)}d\mathbf{P}'.$$

Analogously, following Dirac, we express the mixed proton and neutron densities in the brackets in (4) by

[1] The well-known equivalence of the two representations may be demonstrated by partial integrations, as shown for example by Dirac. (In the expansion of $V(\mathbf{X},\mathbf{P})$, the order of factors is taken to be $\mathbf{X}^m\mathbf{P}^n$.)

[2] Following the language of integral equations.

[3] P. A. M. Dirac, Proc. Camb. Phil. Soc. **26**, 376 (1930). See also W. Heisenberg, *Report of 1933 Solvay Congress* (Paris, 1934).

$$2h^{-3}\int_0^{\mathbf{P}_p(\mathbf{R}+(\mathbf{X}+\xi)/4)} \exp\{i\mathbf{P}(\xi-\mathbf{X})/2h\}d\mathbf{P} \qquad \text{(a)}$$

and

$$2h^{-3}\int_0^{\mathbf{P}_n(\mathbf{R}-(\mathbf{X}+\xi)/4)} \exp\{i\mathbf{P}'(\mathbf{X}-\xi)/2h\}d\mathbf{P}', \qquad \text{(b)}$$

respectively. Now if the density of particles in the nucleus is very great, and if further $\rho_n > \rho_p$, as is in general the case, then the mixed densities (a) and (b) behave with respect to $\mathbf{X}-\xi$ very nearly as δ-functions, but (b) dominates, having a narrower width and higher peak. Thus the integral giving the potential energy of the nucleus,

$$V_{np}=\int d\mathbf{R}\int\int d\mathbf{X}d\xi J(\mathbf{X},\xi)\int_0^{\mathbf{P}_p(\mathbf{R}+(\mathbf{X}+\xi)/4)} 2h^{-3}d\mathbf{P}\int_0^{\mathbf{P}_n(\mathbf{R}-(\mathbf{X}+\xi)/4)} 2h^{-3}d\mathbf{P}' \exp\{i(\mathbf{P}'-\mathbf{P})(\mathbf{X}-\xi)/2h\},$$

only depends on the value of $J(\mathbf{X}, \xi)$, in the neighborhood of $\xi \doteqdot \mathbf{X}$, and we have approximately

$$V_{np}=\int d\mathbf{R}2\rho_p\int 8d\mathbf{X}J(\mathbf{X},\mathbf{X}) \qquad (5)$$

under two conditions:

(A) that the neutron and proton densities do not vary greatly within distances of the order of the range of action of J; and

(B) that $J(\mathbf{X}, \xi)$ shall not be too narrow a function in its dependence on $\mathbf{X}-\xi$; or more precisely, that for a fixed ξ, J shall not vary rapidly when $\mathbf{X}-\xi$ is varied in the range 0 to $\sim 2\hbar/P_n$ (width of the mixed density function (*b*)).

Condition (A) is the usual requirement for the accuracy of the statistical method. Condition (B), however, is definitely not satisfied by an interaction of the Wigner type, $J(\mathbf{X}, \xi) = V(\mathbf{X})\delta(\mathbf{X}-\xi)$. In this case, as is well known, we obtain instead of (5) the expression

$$V_{np}=\int\int d\mathbf{R}d\mathbf{X}\rho_p(\mathbf{R}+\mathbf{X}/2)V(\mathbf{X})\rho_n(\mathbf{R}-\mathbf{X}/2),$$

in contradiction with the saturation character of nuclear binding. On the other hand, the Majorana potential, $J(\mathbf{X}, \xi) = V(\mathbf{X})\delta(\mathbf{X}+\xi)$, is in agreement with (B), and (5) gives the often demonstrated result:

$$V_{np}=\int d\mathbf{R}2\rho_p V(0).$$

At the same time we see from (5) that the Majorana force is a very special one, and that *any interaction depending upon* $\mathbf{X}$ *and* ξ *in accordance with condition B will equally well account for the saturation effect in nuclear binding.*

How this result comes about is most easily visualized by analyzing into groups of different relative momenta all the neutrons which interact with a given proton in a heavy nucleus. On the Fermi-Thomas statistical model, there are in the small element of volume $d\tau_p$ just $N_p = 2h^{-3}(4\pi/3)P_p^3 d\tau_p$ protons, distributed uniformly in momentum and direction of motion up to a certain maximum momentum, P_p, and similarly there are in $d\tau_n$, $N_n = 2h^{-3}(4\pi/3)P_n^3 d\tau_n$ neutrons. The number of protons in $d\tau_p$ which are in interaction with neutrons at a given distance r, having with respect to them relative momenta p_r parallel to r and p_a perpendicular to r, is determined by the volume common to two spheres of radii $P_p/2$ and $P_n/2$ separated by a distance $p=(p_r^2+p_a^2)^{\frac{1}{2}}$. On expressing p_a in terms of the quantum number L giving the mutual angular momentum of neutron and proton, we find (provided that the neutron density does not vary appreciably with r) that the average number of neutrons at a distance between r and $r+dr$ from a given proton, having with respect to it an angular momentum $L\hbar$ and a radial momentum in the range p_r to p_r+dp_r, is given by

$$\rho_L(p_r, r)dp_r dr = (2L+1)(dp_r dr/h)16f(P_p^{-1}[p_r^2+(L+\tfrac{1}{2})^2\hbar^2/r^2]^{\frac{1}{2}}), \qquad (6)$$

where $f(x)=1$ if $x\leqslant P_n/2P_p-\frac{1}{2}$,

$$f(x)=\frac{x^3}{2}-\frac{3x}{4}\left(1+\frac{P_n^2}{P_p^2}\right)+\tfrac{1}{2}\left(1+\frac{P_n^2}{P_p^3}\right)-\frac{3}{32x}\left(\frac{P_n^2}{P_p^2}-1\right)^2 \quad \text{if } x \text{ is between limits,}$$

$f(x)=0$ if $x\geqslant P_n/2P_p+\frac{1}{2}$.

A neutron-proton potential $V_L(r, p_r)$ dependent on velocity and angular momentum gives rise to an interaction energy

$$\sum_L \int V_L(r, p_r)\rho_L(p_r, r)dp_r dr$$

between the given proton and all neutrons. However, to avoid complications arising from the operator nature of a quantum-mechanical momentum, we transfer this expression to the form

$$\sum_L \int J_L(r, \rho)\sigma_L(\rho, r)drdp, \tag{7}$$

where $J_L(r, \rho)$ is the interaction kernel, related to $V_L(r, p_r)$ by an equation similar to (3), and $\sigma_L(\rho, r)$ is a mixed density matrix, connected with $\rho_L(p_r, r)$ by an analogous relation.[4] In particular, the diagonal values of the density matrix determine the number of neutrons of a given L in a range of distance, dr:

$$\sigma_L(r, r)dr=\int \rho_L(p_r, r)dp_r dr.$$

Fig. 1 shows the radial density, $\sigma_L(r, r)$, of neutrons of various angular momenta. (For definiteness, we have taken the density of neutrons equal to the density of protons and the volume of a nucleus of atomic weight A as $(4\pi/3)(1.48\times10^{-13})^3A$.) As a check, the density summed over all angular momenta (heavy curve) is compared with the expected value $4\pi r^2\rho_n$ (lower dotted curve).

Let us suppose we have a Wigner type of interaction between neutrons and protons; it has the same dependence on r for all values of the angular momentum, and expression (7) for the potential energy of the given protons becomes

$$\sum_L \int V(r)\sigma_L(r, r)dr.$$

If we increase the density of neutrons in the nucleus, all the curves in Fig. 1 are increased in height and move in to smaller values of r, so that the interaction energy is increased in proportion to the neutron density. On the other hand, a Majorana interaction gives attraction for the neutrons of angular momentum $L=0$, repulsion for $L=1$, attraction for $L=2$, etc. Thus the total potential energy per proton is an alternating sum,

$$\sum_L (-1)^L \int V(r)\sigma_L(r, r)dr,$$

whose value is not changed by an increase in the neutron density, essentially because the greater magnitude of the densities, σ_L, is balanced by the increased cancelation of terms of opposite sign which occurs as the curves move in to smaller values of r. This is, of course, only another way of putting Eq. (5), which states that in the general non-Wignerian case the interaction energy per proton is

$$16\int J(\mathbf{X}, \mathbf{X})d\mathbf{X}=16\sum_L (2L+1)\int J_L(r, r)dr, \tag{8}$$

a result independent of the neutron density.

[4] The value of the mixed density matrix $\sigma_L(\rho, r)$ may also be obtained from the equation just before (5) by expressing J in terms of its components J_L and carrying out the integration over θ_{12}. Otherwise the mixed density matrix is not uniquely defined in the text (unless the neutron and proton densities are everywhere constant). In the general case, where these densities depend on distance, $\sigma_L(r, \rho)$ should be regarded as giving, not the density of neutrons referred to a given point in proton space, but the density of neutron-proton pairs of a given mutual angular momentum referred to a given position, $\mathbf{R}$, of the center of gravity of the pairs. Then the σ_L's may be consistently defined. The total mixed density matrix $\sigma(\mathbf{X}, \boldsymbol{\xi}; \mathbf{R})$ is given by

$$\{\sum_i^P \varphi_i^*(\mathbf{R}+\mathbf{X}/2)\varphi_i(\mathbf{R}+\boldsymbol{\xi}/2)\} \times \{\sum_{k=1}^N \psi_k^*(\mathbf{R}-\mathbf{X}/2)\psi_k(\mathbf{R}-\boldsymbol{\xi}/2)\},$$

and the σ_L's may be found from this by inverting an equation very similar to Eq. (9) below.

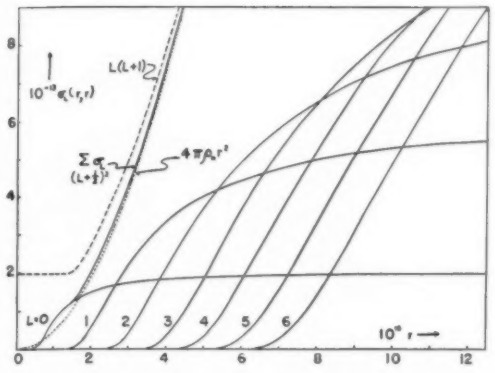

FIG. 1. Density of neutrons of various angular momenta around a given proton, using $(L+1/2)^2\hbar^2$ for the square of the angular momentum. Use of $L(L+1)\hbar^2$ gives the upper dotted curve, in disagreement with the expected value $4\pi\rho_0 r^2$ (lower dotted curve) for the total density.

The Majorana force, which is independent of the relative radial momentum p_r of the two interacting particles, since it depends on ρ as $\delta(r-\rho)$, is nevertheless a very singular type of interaction, for it relies entirely upon the $(-1)^L$ dependence of potential upon angular momentum to bring about the saturation effect in neutron-proton binding. This is seen in the fact that it gives a divergent result for the right-hand side of (8) although the left-hand side converges. Indeed, any dependence of interaction upon angular momentum alone, other than the Majorana type, must make the energy per proton dependent on the density of neutrons.

In other words, any interaction which is to give saturation binding, and is not to be of the Majorana type, must depend on radial momentum; only then does the right-hand side of Eq. (8) exist. The criterion which we have now developed for a satisfactory interaction, that the right-hand side of (8) shall converge, may seem to add restrictions to the earlier condition B (following Eq. (5)), but in fact it causes difficulties only for the Majorana force, which is a special singular case, and would have been realized as such if we had not interpreted condition B liberally above. The dependence of the general interaction on radial momentum makes it clear that if the nuclear density is increased, resulting in greater mean velocities of neutrons and protons, constancy of the energy per proton is ensured by the change of potential with velocity. Indeed, if the interaction kernel, $J(\mathbf{X}, \xi)$, is not of the singular Majorana type, we can conclude that the potential $V(\mathbf{X}, \mathbf{P})$ must decrease in magnitude for sufficiently high velocities, for it represents the Fourier transform of a regular function.

We obtain more detailed information as to the neutron-proton interaction by considering the simple two-body problem involved in the stability of the deuteron and the scattering of neutrons by protons. Referred to a frame of reference in which the center of gravity of the two particles is at rest, the wave equation is

$$(\hbar^2/2\mu)\nabla^2\psi + E\psi - \int J(\mathbf{X}, \xi)\psi(\xi)d\xi = 0.$$

This equation may be separated in polar coordinates, r, θ, φ, by writing ψ as a spherical harmonic $Y_L(\theta, \varphi)$ of order L ($L\hbar$ being the angular momentum of the system) times an undetermined function, $f_L(r)/r$, and by analyzing the total interaction $J(\mathbf{X}, \xi) = J(r, \rho, \theta_{12})$ into parts referring to the interaction of two particles of definite angular momentum, thus:

$$J(r, \rho, \theta_{12}) = \sum_L (2L+1)P_L(\cos\theta_{12})J_L(r, \rho)/4\pi r\rho. \quad (9)$$

The result is that $f_L(r)$ satisfies the equation

$$(\hbar^2/2\mu)f''(r) + [E - L(L+1)\hbar^2/2\mu r^2]f(r) = \int J_L(r, \rho)f(\rho)d\rho. \quad (10)$$

One fact at once emerges of interest in connection with the analysis of scattering experiments: From the behavior of two particles with angular momentum $L\hbar$ we cannot in general, without further information, draw conclusions as to the behavior of the same two particles moving with some other angular momentum.

Now we know from the binding energies of H^2 and He^4 that neutrons and protons of zero angular momentum form stable configurations. Furthermore we have indications that the nuclear forces fall off rather rapidly with distance. Consequently, the first component, $J_0(r, \rho)$, of the neutron-proton interaction must be negative, and a reasonable assumption is that it varies with distance as e^{-br}. To give J the proper

symmetry with respect to interchange of r and ρ, we might now take $J_0(r, \rho)$ equal to $-Ae^{-br}\delta(r-\rho)$, which represents a force independent of radial velocity. We have seen, however, that such a force is only consistent with the binding energies of heavy nuclei if it is of the Majorana type. If we do not wish to restrict ourselves to this form of interaction, we must bring in dependence on velocity, keeping J_0 symmetrical; our simplest possibility is to assume that J_0 has the form $-ae^{-b(r+\rho)}$.

For a velocity dependent interaction of the form just mentioned, the wave equation has an extremely simple solution, and there is found to be never more than one stable S state of the deuteron, whatever the values of a and b. Identifying the energy of this state with the experimental binding energy, D, of H^2, we obtain an equation giving the magnitude of the interaction in terms of its narrowness, b:

$$a/2b=(\hbar^2/M)(\kappa+b)^2, \tag{11}$$

where $$(\hbar^2/M)\kappa^2=D.$$

The cross section, σ_0, for the collision of neutrons and protons of zero angular momentum may also be calculated exactly:

$$\sigma_0=16\pi b^2\{4k^2b^2+[b^2-k^2-(b^2+k^2)^2/(b+\kappa)^2]^2\}^{-1}, \tag{12}$$

where

$$(\hbar^2/M)k^2=E=E_0/2,$$

E_0 being the energy of the incident neutron. To calculate the total cross section σ, we must make some assumption as to the forces acting when $L>0$; the simplest possible assumption is $J_L(r, \rho)=0$ for $L>0$ (i.e., $J(r, \rho, \theta_{12})$ independent of θ_{12}). σ is then exactly equal to σ_0; however, even if J_1, J_2, etc., do not vanish, σ will be closely equal to σ_0 for neutron energies of several million volts and lower. Fig. 2 shows the dependence of cross section on neutron velocity for several values of b. The recent experiments of Fermi (capture of slow neutrons) give support for a ^3S level at $\sim+130{,}000$ ev; there is therefore little doubt that we can only obtain a complete account of neutron scattering by bringing in a spin dependence of J as is done in the Majorana theory. From binding energies of other nuclei, also, there seems to be evidence[5] for the dependence of nuclear forces on spin.

[5] E. Feenberg and J. K. Knipp, Phys. Rev. **48**, 906 (1935).

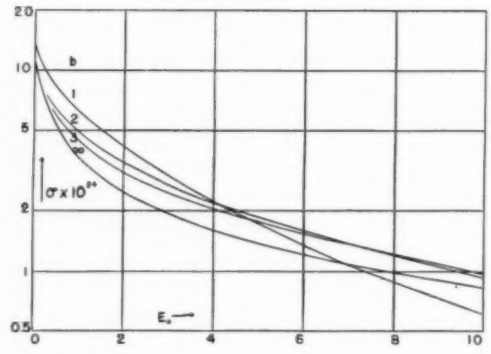

FIG. 2. Cross section for elastic scattering of neutrons in hydrogen as a function of neutron energy. Calculated on the basis of spin-dependent force of the type $-ae^{-b(r+\rho)}$ with constants adjusted to give singlet level of deuteron at 0.13 MEV, triplet level at -2.15 MEV. The curve $b=\infty$ is the same as that given on the Majorana-Heisenberg or Wigner theory.

Application of the interaction $J_0=-ae^{-b(r+\rho)}$ to the treatment of the alpha-particle also gives results not essentially different from those of the corresponding Majorana theory; we have therefore in this interaction a simple illustration of a velocity dependent force which gives quite reasonable physical results.

We bring this discussion to a close by investigating what is the most general dependence of the neutron-proton interaction kernel, $J(\mathbf{X}, \xi)$ on spin, position, and velocity consistent with the conservation laws. We denote by 1_p and $\mathbf{n}_p=(\xi_p, \eta_p, \zeta_p)$ the unit matrix and the three anticommuting spin matrices of the proton and use 1_n and $\mathbf{n}_n=(\xi_n, \eta_n, \zeta_n)$ for the corresponding neutron operators. Any function of the spins of the two particles is a matrix representable as a sum of the sixteen product matrices of the type $1_n\zeta_p$, with suitably chosen coefficients. In the case of the interaction operator, these coefficients must be such as to give invariance with respect to any rotation of the axes of reference; in other words, J must have the form

$$\begin{aligned}&1_p1_n\cdot(\text{scalar functions, } s, \text{ of } \mathbf{X} \text{ and } \xi)\\ &+1_p\mathbf{n}_n\cdot(\text{vector function, } t, \text{ or } \mathbf{X} \text{ and } \xi)\\ &+\mathbf{n}_p1_n\cdot(\text{another vector function, } u)\\ &+\mathbf{n}_p\cdot(\text{a tensor function, } w, \text{ of } \mathbf{X} \text{ and } \xi)\cdot\mathbf{n}_n.\end{aligned}$$

We have already in Eq. (9) expressed the fact that the most general scalar invariant depends only on $|\mathbf{X}|$, $|\xi|$, and $\mathbf{X}\cdot\xi$, or r, ρ, and θ_{12};

similarly, the most arbitrary vector function may be written

$$t_x\mathbf{X}+it_0[\mathbf{X},\,\boldsymbol{\xi}]+t_\xi\boldsymbol{\xi},$$

and the general tensor is

$$w_{xx}\mathbf{X}\mathbf{X}+iw_{x0}\mathbf{X}[\mathbf{X},\,\boldsymbol{\xi}]+w_{x\xi}\mathbf{X}\boldsymbol{\xi}+iw_{0x}[\mathbf{X},\,\boldsymbol{\xi}]\mathbf{X}-w_{00}[\mathbf{X},\,\boldsymbol{\xi}][\mathbf{X},\,\boldsymbol{\xi}]+iw_{0\xi}[\mathbf{X},\,\boldsymbol{\xi}]\boldsymbol{\xi}+w_{\xi x}\boldsymbol{\xi}\mathbf{X}+iw_{\xi 0}\boldsymbol{\xi}[\mathbf{X},\,\boldsymbol{\xi}]+w_{\xi\xi}\boldsymbol{\xi}\boldsymbol{\xi},$$

where the t's and w's are functions only of r, ρ and θ_{12}, and $\mathbf{X}\boldsymbol{\xi}$ is a tensor in the sense that it gives the scalar $(\mathbf{X}\cdot\mathbf{n}_p)(\boldsymbol{\xi}\cdot\mathbf{n}_n)$ when operating on the two vectors $\mathbf{n}_p$ and $\mathbf{n}_n$. The rotational invariance of the interaction obtained in this way insures constancy of angular momentum. The conservation of total linear momentum is assured because J depends on the separation of the particles but not the position of their center of gravity; and energy is conserved if (and only if) the following conditions for the self-adjoint nature of J are satisfied:

(a), $s(\rho,\,r,\,\theta_{12})=s^*(r,\,\rho,\,\theta_{12})$, with similar relations on t_0, u_0, w_{xx}, w_{00}, and $w_{\xi\xi}$; and

(b), $t_x(\rho,\,r,\,\theta_{12})=t_\xi^*(r,\,\rho,\,\theta_{12})$, and corresponding connections between u_x and u_ξ, w_{x0} and $w_{\xi 0}$, $w_{x\xi}$ and $w_{\xi x}$; and w_{0x} and $w_{0\xi}$.

Eleven functions of r, ρ, and θ_{12} are therefore required to describe the spin interaction in the general case. In contrast with this is the situation when the interaction is restricted to depend on $\mathbf{X}$ and $\boldsymbol{\xi}$ as $\delta(\mathbf{X}+\epsilon\boldsymbol{\xi})$. $J(\mathbf{X},\,\boldsymbol{\xi})$ reduces to

$$\{s(r)+(\mathbf{X}\cdot\mathbf{n}_n)t(r)+(\mathbf{X}\cdot\mathbf{n}_p)u(r)+(\mathbf{X}\cdot\mathbf{n}_p)(\mathbf{X}\cdot\mathbf{n}_n)w_{xx}(r)+(\mathbf{X}\cdot[\mathbf{n}_p,\,\mathbf{n}_n])w_A(r)+(\mathbf{n}_p\cdot\mathbf{n}_n)w_S(r)\}\,\delta(\mathbf{X}+\epsilon\boldsymbol{\xi})$$

because we have only one vector instead of three with which to form invariants. Various special cases are summarized as follows:

(1) $\epsilon=-1$; only $s(r)$ different from zero (Wigner);
(2) $\epsilon=\ \ 1$; all functions vanish except $s(r)=w_S(r)$ (Heisenberg);
(3) $\epsilon=\ \ 1$; only $s(r)$ nonvanishing (Majorana);
(4) $\epsilon=-1$; all functions zero except $s(r)=w_S(r)$ (Bartlett);
(5) $\epsilon=-1$; $w_{xx}(r)=-3\mu_p\mu_n r^{-5}$; $w_S(r)=\mu_p\mu_n r^{-3}$; all other functions zero (magnetic spin forces).

The magnetic interaction between proton velocity and neutron spin requires for its representation a more general dependence of $J(\mathbf{X},\,\boldsymbol{\xi})$ on $\boldsymbol{\xi}$ than that given by $\delta(\mathbf{X}+\epsilon\boldsymbol{\xi})$.

The proper value of the kernel, $J(\mathbf{X},\,\boldsymbol{\xi})$, required to account for the interaction between neutrons and protons (or between protons and protons, and neutrons and neutrons) is of course not arbitrary, but fixed by general physical principles of which we have not as yet a proper understanding. The fact that present treatments of nuclear binding point to neutron and proton velocities in the nucleus of the order of $c/4$ suggest a question as to whether the simple mathematical forms of the kernel given by (2) and (3) really give correctly the interaction between two nuclear particles, at distances smaller than the classical electron radius, moving with high relative velocities. In this connection it may be mentioned that, in a paper now in preparation for publication, it is shown on the basis of present theory that the interaction between two normal alpha-particles of not too high energy is representable in terms of an equivalent potential $J(\mathbf{X},\,\boldsymbol{\xi})$. This kernel, whether derived on the assumption of Wigner or Majorana forces between neutrons and protons or the more general type of interaction we have considered in this paper, is itself definitely not representable in its dependence on $\boldsymbol{\xi}$ by $\delta(\mathbf{X}+\epsilon\boldsymbol{\xi})$, and consequently is not a force of the Wigner or Majorana type.

In summary, we have found:

(1) that the most general interaction between two particles consistent with the conservation laws requires for its specification ∞^3 numbers (dependence of force on distance, relative velocity, and angular momentum) in contrast with a Wigner or Majorana potential, which is described by only ∞ numbers (dependence on distance);

(2) that a simple form of the interaction, dependent on velocity, and acting only between neutrons and protons of zero mutual angular momentum, is well adapted to the treatment of the binding energies of light nuclei; and

(3) that this particular interaction is only one instance of a whole group of non-Wignerian potentials, any one of which will account for the saturation effect in nuclear binding.

A decision between the Majorana force and a force of the more general nature considered above would appear possible as follows:

(1) from the dependence of the neutron-proton collision cross section upon velocity for high energy neutrons. A swifter falling off is to be expected for velocity dependent forces.

(2) the consequences of the Majorana interaction for the detailed structure of heavy nuclei are somewhat different from those given by the general non-singular type of force. Detailed calculations are needed to show which features of nuclear structure are most sensitive to the characteristic differences between the two kinds of interaction.

The Townsend Coefficients and Spark Discharge

DANIEL Q. POSIN, *Department of Physics, University of California, Berkeley, California*

(Received June 29, 1936)

A quantitative study has been made of the prespark current between plane parallel electrodes in purified N_2. The results yield the relationship between (X/p) (X in volts/cm, p pressure in mm of Hg) and (α/p) (α is the number of new pairs of ions created by one electron in advancing one cm in the direction of the field). The range in values of X/p covered is from 20 to 1000. The portion of the data between $X/p=20$ and $X/p=38$ may be represented at 22°C by

$$\alpha/p=(5.76\pm1.56)\times10^{-7}e^{(0.248\pm0.003)X/p}.$$

In this region the Townsend equation $i=i_0e^{\alpha d}$ for electron ionization alone was found to hold up to the passage of a spark. Between $X/p=44$ and 176 the curve $\alpha/p=F(X/p)$ is represented by

$$\alpha/p=(1.166\pm0.022)\times10^{-4}(X/p-32.1\pm1.4)^2.$$

The portion of the curve between $X/p=200$ and 1000 may be represented by $(\alpha/p+3.65)^2=0.21X/p$. These results are in excellent agreement with those of Masch but differ by an order of magnitude and more from those of Ayres below $X/p=70$. The deviations from $i=i_0e^{\alpha d}$ (due to a secondary process of ionization) were first observed at $X/p=100$. These deviations yield values of a coefficient β due to the secondary ionization mechanism in terms of Townsend's equation

$$i=i_0(\alpha-\beta)e^{(\alpha-\beta)d}/(\alpha-\beta e^{(\alpha-\beta)d})$$

which extend from $X/p=100$ to $X/p=1000$. To obtain consistent values of β it was found necessary to reduce the initial photoelectric current density from the cathode to less than 10^{-13} amp./cm². Current densities of magnitude greater than 10^{-12} amp./cm² give rise to space charge field distortion and consequently falsify values of the secondary coefficient. The values of α/p and β/p as functions of X/p are applied to the Townsend criterion for spark breakdown between plane parallel electrodes and yield a curve for sparking potential plotted against the product of pressure and electrode separation in agreement with the experimental data of Strutt and Hurst. Since the quantity β cannot be due to ionization by positive ions in the gas it must be ascribed to electron liberation at the cathode either by positive ion impact or by a photoelectric effect. The character of the variation of α/p and β/p as functions of X/p lends support to the hypothesis that it is the photoelectric effect at the cathode which is the effective secondary mechanism under these conditions.

INTRODUCTION

RECENT investigations involving the phenomena of spark breakdown in gases have indicated a need for adequate data on certain fundamental constants involved in the theory of these phenomena; the investigations have also revealed a lack of agreement between the results of several investigators. The constants referred to describe the primary and secondary mechanisms which play a role in spark discharge. These are the Townsend coefficients α and β, ascribed[1] by him to impact ionization of molecules by electrons and by positive ions in the gas. Lately,[2–8] the recognition of the fact that the secondary ionization (measured by β) could not be due to positive ion impact in the gas has accentuated the interest in the problem as a whole. A number of proposed alternate mechanisms have been shown[9] to give an equation of *type* similar to that holding for α and β.

The majority of the studies undertaken in recent times to fulfill the need have been made on air, inasmuch as this is the gas of most immediate practical importance in the field of applied electrical engineering. The earlier investigations made on other gases have been confined to rather narrow limits of the field strength and pressure.

The purpose of the present work was to make a detailed study of the ionization processes in a pure diatomic gas. Such a study should yield data for computing sparking characteristics for a gas which does not offer complications due to the presence of molecules of various ionizing potentials. It was also desirable to use a gas in which electrons remain relatively free (i.e., in which negative ion formation is rare). Furthermore, it was necessary to use a gas which did not react with the electrodes, as it was the intention

[1] Townsend, *Electricity in Gases*, Chaps. 8, 9.
[2] A. Von Hippel, Ann. d. Physik **81**, 1053 (1926).
[3] W. Rogowski, Archiv. f. Elek. **16**, 761 (1926).
[4] L. B. Loeb, Science **66**, 627 (1927).
[5] R. M. Sutton, Phys. Rev. **34**, 547 (1929).
[6] Mouzon, Phys. Rev. **35**, 695 (1930).
[7] O. Beeck, Phys. Rev. **38**, 967 (1931).
[8] R. N. Varney, Phys. Rev. **47**, 483 (1935).
[9] L. B. Loeb, Rev. Mod. Phys. **8**, 267 (1936).

to investigate the dependence of the secondary mechanism upon the cathode material. Purified N_2 fulfills the above conditions and was therefore selected for the present investigations.

Method and Experimental Procedure

The apparatus used was essentially that set up by Sanders.[10, 11] The condensers employed in the rectification of the high potential were of much greater capacity than those used by him. Each bank of condensers had a value of 0.25 mf. whereas those of Sanders were of value 0.02 mf. The general technique was that of Sanders and will not be described here.

A photoelectric emission of about 10^{-12} amp./cm^2 was attained by focusing a small, very bright section of a quartz mercury arc on the cathode. During the course of the experiments it became desirable to control the current density thus liberated from the cathode. (Sanders had not considered this as essential.) To obtain a smaller current density a less intense section of the arc was employed. The initial current density thereby obtained was about 10^{-14} amp./cm^2.

The N_2, taken from a tank, was passed through a purifying train of heated copper filings, $CaCl_2$, and P_2O_5. Gas temperature and pressure were reduced to a standard temperature (22°C) in admitting a given *amount* of N_2 to the chamber. Thus all data here given refer to 22°C.

Experimental Results

At given field strengths (X volts/cm) and pressures (mm of Hg), with ultraviolet light liberating an initial electron current i_0 from the cathode, the current i reaching the anode was studied as a function of the electrode separation d. Fig. 1, in which $(1/p)\log i/i_0$ is plotted against d, illustrates the fact that for the range in values of X/p from 20 to 46 the equation

$$i = i_0 e^{\alpha d} \qquad (1)$$

for electron impacts alone holds very well. For this work pressures between 100 and 700 mm were used, requiring the high tension set. Fig. 2, also drawn from data taken with the high tension set and depicting data analogous to those in Fig.

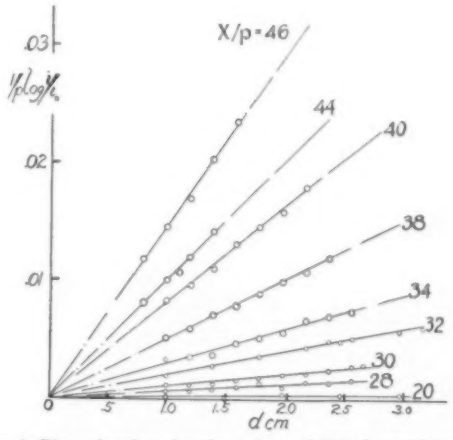

Fig. 1. Plots showing that for values of X/p from 20 to 46 the relation $i = i_0 e^{\alpha d}$ is valid.

1, but at higher X/p, illustrates the deviation of the current growth from the simple relation $i = i_0 e^{\alpha d}$. This figure shows that the deviations begin at $X/p = 100$. The fact that at $X/p = 88$ the simple equation appeared to be accurately obeyed up to a spark whereas at $X/p = 100$ a very great deviation from this law was observed may be explained by assuming that at $X/p = 88$ and lower, small surges of potential sufficed to lead to accidental breakdown before the deviations could become manifest. At higher X/p, on the contrary, the small surges though occurring did not lead to breakdown owing to a greater range of values in d between the appearance of a deviation and breakdown.

The slopes of the straight portions of these curves are the values of α/p. These were evaluated from the data by least squares reduction. Fig. 3 shows the entire α/p, X/p curve obtained by the writer indicated as circled points. The data of Townsend[1] are represented by a dashed curve, while Ayres'[12] data are given by the triangles and Masch's[13] results by the crosses. For values of X/p above 70 there is a fair agreement in values of α/p among all the investigators. The differences between the values of Ayres and the writer at X/p above 600 are of the order of a few percent. However, for values of X/p in the neighborhood of breakdown at atmospheric pressure (about 40 and lower) there is excellent

[10] F. H. Sanders, Phys. Rev. **41**, 667 (1932).
[11] F. H. Sanders, Phys. Rev. **44**, 1020 (1933).
[12] T. L. R. Ayres, Phil. Mag. **45**, 353 (1923).
[13] K. Masch, Archiv. f. Elek. **26**, 589 (1932).

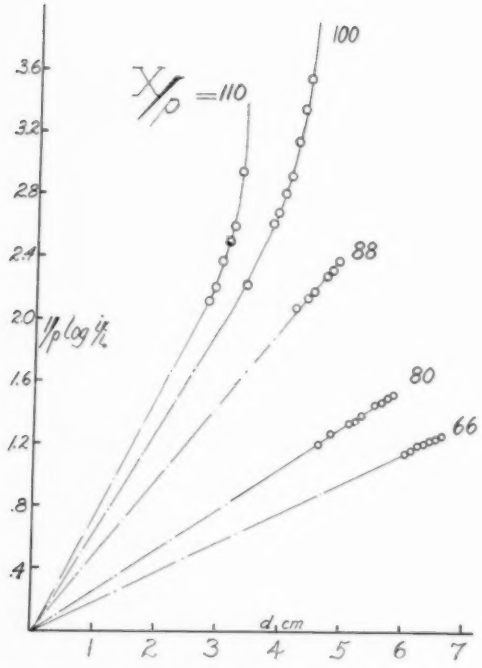

FIG. 2. Plots showing that at high values of X/p the simple exponential relation is not valid.

agreement between the results of Masch and the writer, whereas the results of Ayres are of the order of 100 times greater. The writer has great confidence in his own low X/p values in view of the very great resolving power of his apparatus with the large values of d. (See Sanders' papers for details.) Since the scale of Fig. 3 is such that an $\alpha/p \sim 10^{-2}$ cannot be distinguished from an $\alpha/p \sim 10^{-4}$ comparison must be made by a study of Table I in which the writer's least-squares valuation of α/p as $f(X/p)$ and the probable error in α/p are listed together with the values of Ayres[12] and Masch.[13]

It was found possible to fit almost the entire α/p, X/p curve (Fig. 3) by three simple equations. Fig. 4 shows that in the lower X/p range (20 to 38) the writer's data yield $\alpha/p = Ae^{BX/p}$ since $\log_e \alpha/p$ plotted against X/p fits a fairly straight line. The actual relation is

$$\alpha/p = (5.76 \pm 1.56) \times 10^{-7} e^{(0.245 \pm 0.003) X/p}$$

at 22°C. These data are of value in computations involving the development of the spark in N_2 at

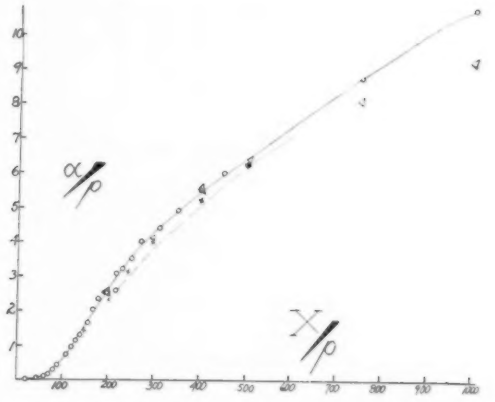

FIG. 3. Variation of α/p with X/p. Circled points—writer; dot-dash curve—Townsend; crosses—Masch; and triangles—Ayres.

low X/p, as will be seen later in this paper when sparking equations are derived. For air in a similar region Sanders[10] obtained

$$\alpha/p = (2.67 \pm 0.26) \times 10^{-8} e^{(0.350 \pm 0.002) X/p}.$$

In the present investigations in N_2 it was found possible to fit the curve of Fig. 3 from $X/p = 44$ to 176 by the equation

$$\alpha/p = (1.166 \pm 0.022) \times 10^{-4} (X/p - 32.1 \pm 1.4)^2$$

at 22°C. (From $X/p = 40$ to 120 Jodlbauer found the equation $\alpha/p = 1.35 \times 10^{-4} (X/p - 28.8)^2$ to fit Sanders'[11] results in air.) The fit of the experimental points to this curve is shown in the plot of $(\alpha/p)^{\frac{1}{2}}$ against X/p in Fig. 5. From $X/p = 200$ to 1000 it was found that the following relationship could be established:

$$(\alpha/p + 3.65)^2 = 0.21 X/p.$$

The fit of the inverted parabolic curve to the experimental data is shown in Fig. 6 where α/p is plotted against $(X/p)^{\frac{1}{2}}$. From $X/p = 176$ to 200 it was not possible to find a simple function conveniently representing α/p as an $f(X/p)$.

As indicated previously the deviations of the current from $i = i_0 e^{\alpha d}$ were first observed at $X/p = 100$. An extensive study of the deviations was made at $X/p = 120$ where current-distance curves were obtained for a series of pressures. As was to be expected from Paschen's law, the higher the pressure the smaller the value of d at which deviation set in. In order to analyze

these deviations an attempt was made to fit them to Townsend's equation

$$i = i_0(\alpha-\beta)e^{(\alpha-\beta)d}/(\alpha-\beta e^{(\alpha-\beta)d}), \qquad (2)$$

taking into account the primary *and* secondary ionization mechanisms. It was found that the equation could not be made to fit a given curve if β were to be constant as required by Eq. (2). A study of the deviations and their behavior eventually led to the suspicion that the relatively large photoelectric current densities $\sim 10^{-12}$ amp./cm² used were creating space charges which distorted the field between the plates at sufficiently large d. This proved to be correct. The curves obtained with the large ($\sim 10^{-12}$ amp./cm²) initial current densities are shown in Fig. 7 as *full* lines. Curves obtained with lower current densities ($\sim 10^{-14}$ amp./cm²) were found to fit Townsend's Eq. (2) satisfactorily. These curves are shown in Fig. 7 as *broken* lines. It is seen that the rate of current rise after the turning point depends on the initial current density; the curve with the higher initial current density leads more readily to the spark.

It was in fact this discovery that led the writer and others to the theoretical interpretation of the appearance of space charges in these experiments. This interpretation has already been published.[14] The study[14] shows that space charges can cause a more rapid current increase than the equation $i = i_0 e^{\alpha d}$ warrants, by distorting the effective α to higher values when the current density (i_0 per cm²) is sufficiently great. That is, an α distorted by space charges may be mistaken for a secondary ionization mechanism. This, however, can occur only in the first two regions of variation of α/p with X/p discussed above, not in the third. Moreover, the deviation of α from a constant value occurs very sharply as d increases; this is especially true in the first region. Thus, in this region, for large initial current density the space charge effect may possibly be the primary cause of the spark breakdown.[9, 14] In the second region the effect of space charge is separable only with difficulty from the true *secondary* ionization mechanism. In the third region α is not increased by a space charge effect. With sufficient ultraviolet inten-

[14] R. N. Varney, H. J. White, L. B. Loeb and D. Q. Posin, Phys. Rev. **48**, 818 (1935).

TABLE I. *Values of α/p for nitrogen (α is the number of new pairs of ions created by one electron in advancing 1 cm in the direction of the field).*

	α/p			Probable Error in α/p	Pressure Used
X/p	Ayres	Masch	Posin	Posin	
10	0.0110				
15	.0170				
20	.0239		0.000087	0.000008	700
25	.0305	0.00009			
26		.00022	.000258	.00002	500
27		.00041			
28		.00060	.000456	.000036	500
29		.00081			
30	.0382	.00112	.000911	.000040	250
31		.00150			
32		.00190	.00199	.000048	250
33		.00245			
34		.00315	.00281	.000108	250
35		.00385	.00305	.000076	250
36		.00475	.00441	.000160	250
38		.0071	.00521	.000120	150
40	.0550	.0100	.00734	.000330	100
44			.01070	.001100	100
45		.0208	.01353	.000900	100
50	.0820	.0373			
59			.09340	.007110	0.985
60	.121	.087			
68			.14500	.007110	.985
70		.162			
78			.28300	.009450	.635
80	.257	.260			
88			.41200	.025200	.635
90		.375			
100	.471	.505	.70000		
108			.72900	.053500	
110		.65	.73000		
120		.80	.95000	.007000	1.000
125	.850				
127			1.13500	.102000	0.490
130		.98			
137			1.272	.0160	.425
140		1.15	1.400	.0140	.720
142			1.451	.0145	.345
150	1.32	1.32			
156			1.635	.0170	.420
160		1.50			
166			2.020	.0241	.290
175	1.84				
176			2.350	.1500	.425
180		1.95			
196			2.522	.0304	.230
200	2.50	2.25			
215			3.07		.330
230			3.20		.25
250		3.15	3.50		.25
270			4.00		.25
300	4.10	3.90			
310			4.40		.18
350		4.55	4.93		.18
400	5.43	5.2	5.50		.14
450		5.7	6.00		.125
500	6.29	6.1	6.23		.125
750	7.91		8.78		.075
1000	9.02		10.8		.075
2000	11.24				
3000	12.10				

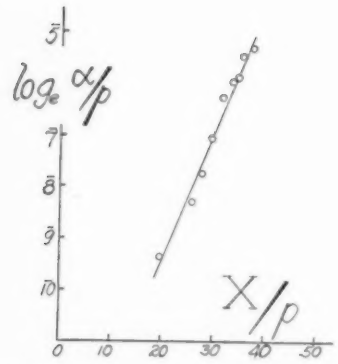

FIG. 4. Plot showing that in the range X/p from 20 to 38 $\alpha/p = ae^{bX/p}$.

sity, therefore, field distortion can and does occur and has in the past affected some of the results of the investigations of Townsend coefficients (e.g., the results of Sanders in air and apparently those of Paavola[15] in air at low X/p).

When sufficiently low current densities were used, the currents fitted the Townsend Eq. (2) for the entire X/p range. Fig. 8 shows the relation between β/p obtained from these curves and X/p for a range in X/p of 100 to 1000. The data obtained by the writer (circled points) are shown together with those of Townsend (full curve no points) and Ayres (dashed curve). The β/p values of Ayres are considerably higher than those of the writer in the region of low X/p (~ 100) as was also the case with Ayres' values of α/p. The disagreement is not serious at the higher values. (This was likewise the case for α/p.) The comparison of the data can be made with greater advantage by referring to Table II in which are listed the β/p values in N_2 of both Ayres and the writer.

Inasmuch as the energy gained by a positive ion between impacts is hardly more than five or six volts in N_2 even at $X/p = 1000$, it is certain that the additional ionization observed in the region under discussion ($X/p = 100$ to 1000) *is not due to positive ion impact with the gas molecules*, i.e., to a β as interpreted by Townsend. The alternate Townsend mechanism which accounts for the ionization, *viz.*, the electron liberation due to positive ion bombardment of the cathode, may possibly be the active mechanism leading to values of β. Inasmuch as very little is known about the efficiency of positive ions of energy ~ 10 volts and less in liberating electrons from metal as a function of energy, little can be concluded from the data on β/p in this connection except that such a liberation is possible. As has been pointed out in this laboratory by Cravath, there is evidence that one may find some help in explaining the Townsend coefficient β by considering photoelectric effects. That is, one may look to photoelectric ionization of the gas itself for mixed gases and electron liberation from the cathode by the excitation radiation produced in the gas by primary electron impact. The existence of appreciable photoelectric effects of this character in corona discharge has been recently demonstrated by Cravath. His work was confined to atmospheric pressure, where he found the existence of two components of excitation radiation, one easily absorbed by the gas and having an absorption coefficient of 10 cm^{-1}, the other penetrating to the cathode and having an absorption coefficient of 2 cm^{-1}. At higher $X/p \sim 500$, where lower pressures ~ 0.5 mm are used, a minimum of such radiation would be absorbed by the gas; the rest would liberate photoelectrons from the cathode. As a consequence of the above findings a new prespark

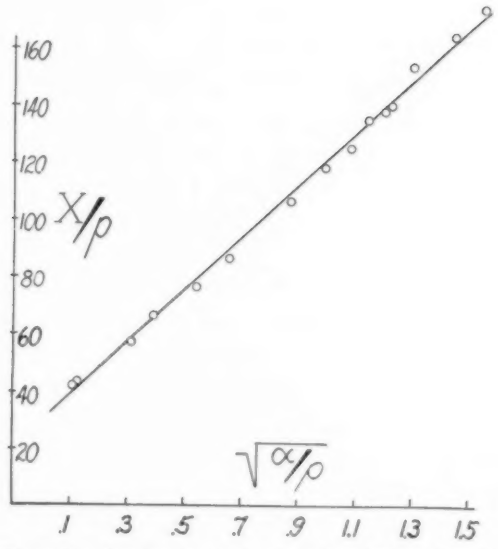

FIG. 5. Plot showing that in the range from $X/p = 44$ to 176 the values of α/p satisfy the relation $\alpha/p = A(X/p - B)^2$.

[15] M. Paavola, Archiv. f. Elek. **22**, 443, 450 (1929).

current equation may be derived[9] which turns out to be of the Townsend *type* (see Eq. (2)). The approximate form of this new equation (i.e., when absorption of radiation by the gas is neglected) is

$$i = i_0 \alpha e^{\alpha d} / (\alpha - \theta\eta g(e^{\alpha d} - 1)).$$

Here β is replaced by $\theta\eta g$ where θ is the number of photons produced by one electron in one cm of path in the field direction, η is the number (fraction) of photoelectrons liberated from the cathode by one photon, g is a geometrical factor (fraction of photons, created in the gas, that can reach the cathode). It is of interest now to consider how β, or its equivalent, $\theta\eta g$, compares with α as X/p increases. In Fig. 9 β/α is plotted against X/p. It is seen that β/α *flattens out for* $X/p > 500$ (the same characteristics are revealed by an examination of Ayres' values of α and β). If β were truly the Townsend coefficient giving the production of new ions by positive ion impact with gas molecules (which is quite impossible, as shown by Varney), then it is difficult to understand why the rate of increase of β with respect to α should fall off as X/p increases. There is also at present no reason for believing that the liberation of electrons from the cathode by positive ions, having 0 to 10 volts energy varies in the fashion indicated by $\gamma \leqq \beta/\alpha$ as a function of X/p. On the other hand, ascribing the secondary emission to a photoelectric effect at the cathode caused by electron impact in the gas would lead one to expect that $\beta/\alpha = \phi(X/p) = \theta\eta g/\alpha$ would vary in the manner represented in Fig. 9, as pointed out by Loeb.[9] For, assuming that in the region of X/p used (100 to 1000) η and g are nearly constant (η may increase at high X/p due to higher energy photons), the efficiency of photon production by electrons as a function of velocity (excitation function for electron impact) relative to the ionization function for electrons is such that photon production begins at lower electron energies than ionization; it then rises more steeply and reaches a maximum of efficiency before the ionization curve has done so. Hence, since the curves for probabilities of excitation and ionization in a gas as a function of electron energy have the form described above it is clear that in the region of terminal electron energies of 10 to 100 volts the ratio of $\theta\eta g/\alpha$ or β/α will have just about the form observed.

The *values* of β or $\theta\eta g$ together with α now permit one to test the simple criterion for a spark early laid down by Townsend. If in the Townsend Eq. (2) the denominator vanishes, that is,

$$\alpha - \beta e^{(\alpha-\beta)d} = 0 \qquad (3)$$

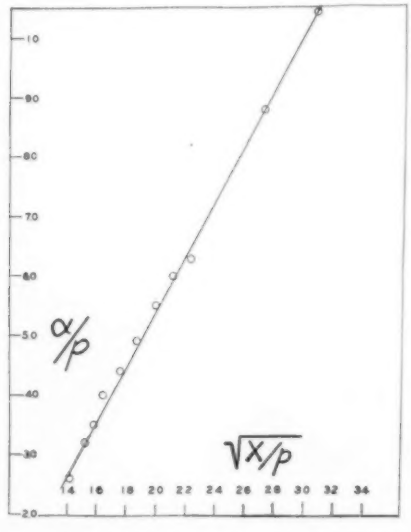

FIG. 6. Plot showing that in the range from $X/p = 200$ to 1000 the values of α/p satisfy the relation $(\alpha/p + C)^2 = DX/p$.

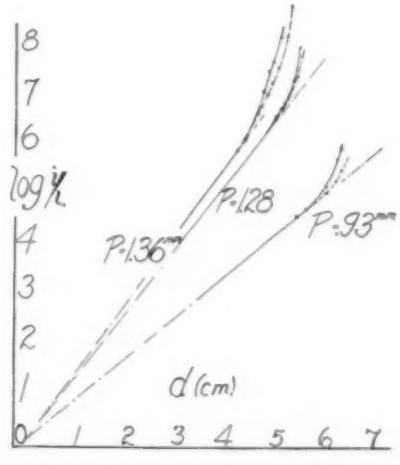

FIG. 7. Values of $\log i/i_0$ as a function of d for 3 different pressures. Full curves are for current density approximately 10^{-12} amp./cm²; dotted curves for current density approximately 10^{-11} amp./cm².

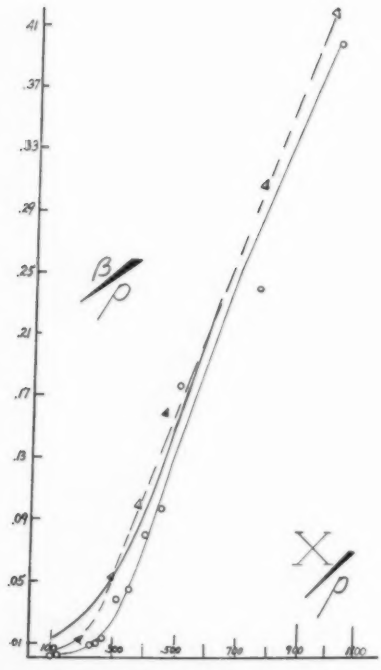

FIG. 8. Values of β/p as a function of X/p. Full curve, circled points—writer; full curve—Townsend; dashed curve, triangles—Ayres.

then i will become indefinitely large, regardless of the value of i_0. One can then interpret this as the condition leading to a spark. Such an unstable condition takes place if one increases d at a constant α and β (constant X/p and p) until the critical value δ for which the spark passes. If β be neglected in the exponent of (3) relative to α (β/α at $X/p=100$ is 5×10^{-4}, β/α at $X/p=1000$ is 3.9×10^{-2}) then $\beta/\alpha=e^{\alpha\delta}$. Thus $\log(\beta/\alpha)=\alpha\delta$, or $\log F(X/p)=p\delta f(X/p)$, and $\log F(X\delta/p\delta)=p\delta f(X\delta/p\delta)$. Here $X\delta$ is the sparking potential V_s, assuming uniform fields. As a result one can write $V_s=F(p\delta)$. This is merely the well-known Paschen law long ago deduced in this form by Townsend and tested by him over a limited range of values. As a result of the present work α/p as $f(X/p)$ and β/p as $\phi(X/p)$ are now known for N_2 over a wide range of values: $X/p=20$ to 1000. It is thus possible to insert the proper functions expressing α/p and β/p in terms of X/p into the relation (3) above and determine $V_s=F(p\delta)$. These values of V_s may be compared with those obtainable from the well-known sparking curves in which V_s is plotted against $p\delta$. Strictly, one should insert the values of β/α as $\phi(X/p)$ (empirical equations) into Eq. (3). (For α in the exponent this *is* done.) However, β/α as $\phi(X/p)$ would be a very involved formulation and thus in Eq. (3) the value of the important parameter V_s could not be obtained explicitly. Furthermore it happens that Eq. (3) is quite insensitive to changes in β/α of 100 percent or more. This follows since one or more logarithms are taken of the relatively small β/α in order to obtain V_s explicitly. In the following study, therefore, use will be made of an average β/α for a substantial range in X/p. The critical feature in formulations of V_s as $F(p\delta)$ is the nature of the relationship α/p as an $f(X/p)$. Since this relationship depends on the region of X/p used, the formulation of $V_s=F(p\delta)$ must be given in at least three parts [corresponding to at least three laws of $\alpha/p=f(X/p)$].

Region I:

For $X/p=20$ to 38, $\alpha/p=5.76\times10^{-7}e^{0.245X/p}$. The value of β/α may be taken as 10^{-5} by extrapolating from the data of Table II. Substitution into $\alpha/\beta=e^{\alpha\delta}$ yields $V_s=69p\delta-4.08\ p\delta\log p\delta$, which is to hold so long as the ratio of $V_s/p\delta\equiv X/p$ ranges between 20 and 38. This corresponds to the limits of $p\delta$ (mm×cm) of ~800 to >10,000 and V_s (volts) 33,400 to 314,000.

Region II:

For $X/p=44$ to 176, $\alpha/p=1.17\times10^{-4}(X/p-32.2)^2$. Here β/α is taken as 10^{-3}; these yield $V_s=32.2p\delta+244(p\delta)^{\frac{1}{2}}$ which holds for the stated X/p region, the range in $p\delta$ being 3 to 600 (mm×cm) and in volts 520 to 25,320.

Region III:

For $X/p=200$ to 1000, $(\alpha/p+3.65)^2=0.21X/p$. For the range $X/p=320$ to 1000, β/α is chosen

TABLE II. *Values of β/p for nitrogen.*

X/p	β/p Ayres	β/p Posin	X/p	β/p Ayres	β/p Posin
100	0.0002	0.000016	250		.0105
110		.000016	270		.0138
120		.00054	300	.058	
125	.0013		310		.0389
150	.0048		350		.0455
175	.0084		400	.103	.0792
200	.013		450		.0963
210			500	.157	.176
215		.008	750	.301	.24
230		.0094	1000	.422	.40

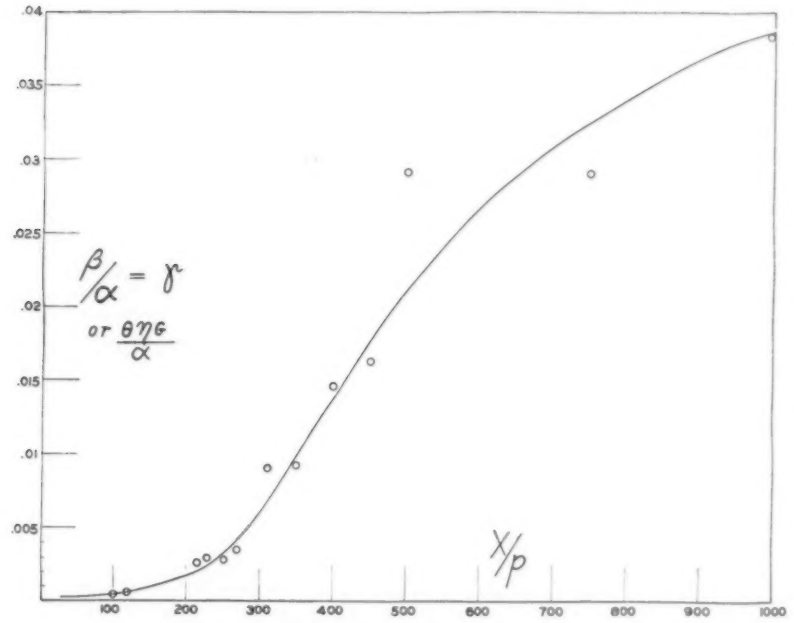

FIG. 9. β/α as a function of X/p.

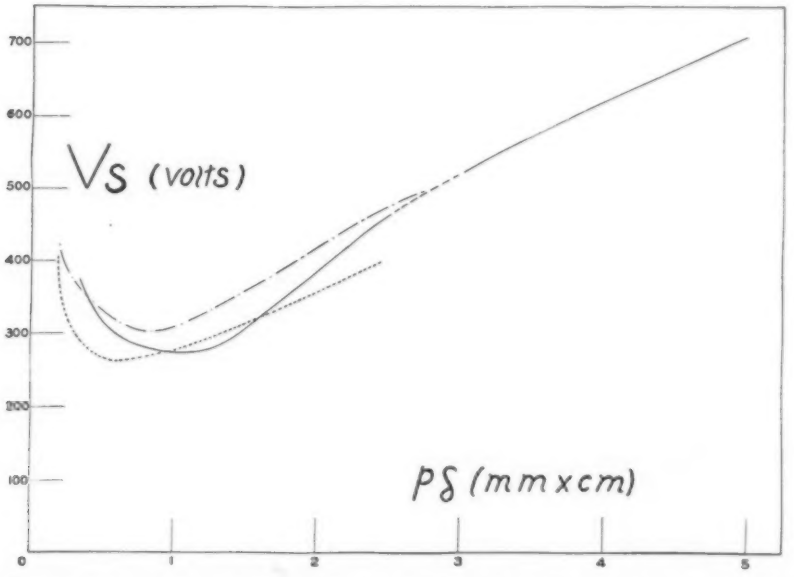

FIG. 10. Values of the sparking potential as a function of $p\delta$ for values of $p\delta$ up to 5 mm cm. The dot-dashed curve is from Strutt, experimental; the dashed curve, Hurst, experimental; full curve is calculated from the writer's equations.

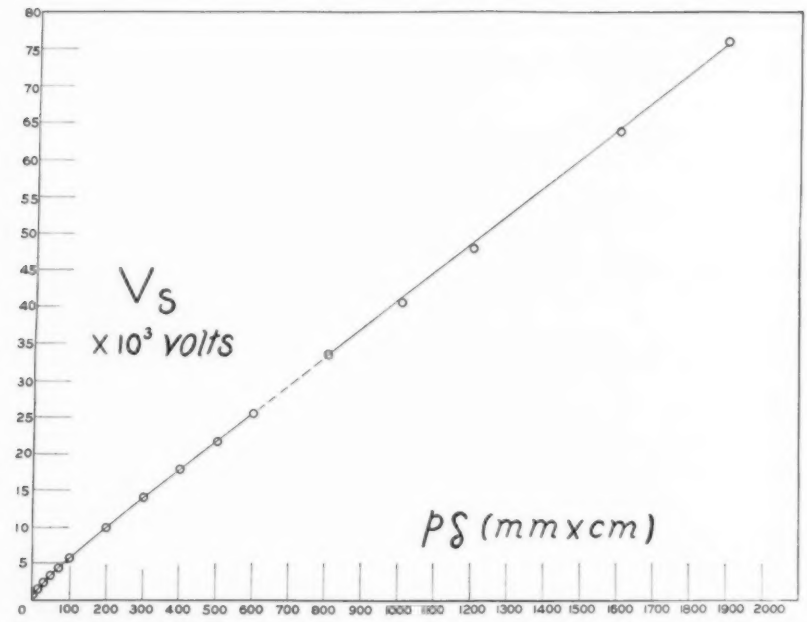

FIG. 11. Values of sparking potential as a function of $p\delta$ for values of $p\delta$ up to 1900 mm cm calculated from the writer's equations.

as 0.02; these give $V_s = 63.5p\delta + 73.5/p\delta + 137$ for $p\delta = 0.4$ to 1.2. The minimum sparking potential, obtained by differentiating the above equation, is found to be 274 volts. The corresponding value of $p\delta$ is 1.07. The average minimum sparking potential in N_2, as obtainable from the Paschen law curves of Hurst and Strutt, is about 270 volts, the $p\delta$ (average) is about 0.8. For $X/p \sim 200$, β/α is about 0.0015. Using this value instead of 0.02, the equation obtained is $V_s = 63.4p\delta + 203/p\delta + 226$, which holds from $X/p = 200$ to 280, $p\delta = 1.6$ to 2.5.

Fig. 10 shows the relation between V_s and $p\delta$ as found many years ago by Hurst and Strutt.[16] This figure also shows the plot of the equation for V_s against $p\delta$ found by the writer. It is seen that the latter curve falls between those of the investigators named where the ranges are common. No reliable sparking data in N_2 are available for ranges of $p\delta$ greater than 2.5 (mm×cm). Thus, although Fig. 11 shows the computed relation between V_s and $p\delta$ from $p\delta = 2.5$ to $p\delta > 10{,}000$, the relation cannot be at present verified beyond the limits already indicated. It is hoped that a full curve will be obtained for N_2 in this laboratory in the near future.

The hope of ultimately using the present apparatus[10] to study the effect of cathode material on the values of β was abandoned owing to the contamination of the large chamber with mercury vapor.

In conclusion, the writer wishes to express his gratitude to Dr. R. N. Varney and Professor R. T. Birge for a number of valuable suggestions. The writer is especially appreciative of the help of Professor L. B. Loeb, who proposed the investigations and supervised them throughout.

[16] See W. O. Schumann, *Elektrische Durchbruchsfeldstärke von Gasen*.

Electron Diffraction Experiments Upon Crystals of Galena

L. H. GERMER, *Bell Telephone Laboratories, New York, N. Y.*

(Received July 22, 1936)

Cleaved surfaces of galena crystals yield electron diffraction patterns made up of Kikuchi lines, and spots which are drawn out into streaks by refraction. After etching, the spot pattern predominates and the individual spots are sharp. The lines are then rather diffuse and ill-defined. Rocking curves upon various Bragg reflections from the surface plane prove that the imperfection of a certain crystal does not exceed about 15 minutes, and that the projections through which the electrons pass are relatively thick. Estimates of imperfection and thickness made from rocking curves are in approximate agreement with those obtained from widths of Kikuchi lines.

A galena crystal which has been filed or ground parallel to a cube face exhibits two different sorts of surfaces. There are smooth "mirror" surfaces from which large blocks of the crystal have been mechanically torn, and there are very deeply scratched portions of the surface. The "mirror" surfaces give diffraction patterns which are qualitatively similar to patterns from cleaved surfaces, although there are notable differences. From mirror surfaces produced by filing Kikuchi lines are very diffuse or are entirely missing, and diffraction spots form an extended array. The diffuseness of the lines and the extent of the array of spots correspond to great crystal imperfection, or to exceedingly thin projections. Reasons are advanced for believing in imperfection rather than extreme thinness.

The deeply scratched portions of the surface of a galena crystal give diffraction patterns which are entirely unlike patterns from cleaved surfaces. Before etching, Debye-Scherrer rings are produced. After a light or moderate etch a complex pattern appears, the nature of which is related to the angle between primary beam and direction of filing. The pattern is that of a mass of minute crystallites which have been rotated about an axis in the surface normal to the direction of filing, and in the sense determined by imaginary rollers which would be turned by slipping on the (0 1 0) plane. The magnitude of the rotation varies for different crystallites over a range from 5 to about 35 degrees. By alternate etching and examination by electron diffraction it is found that this layer of rotated crystallites extends beneath the surface to a depth of 0.003 mm.

Rotation of crystallites accompanying slip along slip planes is the mechanism reported to account for strain hardening in metals. This same rotation is observed in the present experiments on galena. It seems altogether possible that the simple technique of these experiments can be applied directly to study the disturbance in surface layers of metal crystals produced by abrasion. It may thus be a useful way of studying strain hardening in metals

GALENA crystals were chosen for examination by electron diffraction because of the simplicity of the crystal structure of galena, because the crystals are fairly good electrical conductors, and because they cleave readily. The testing of such a simple crystal as galena seemed desirable after unexplained and complex phenomena had been discovered in the investigation of less simple crystals. It was thought that experiments upon galena might aid in clarifying our views.

The simple experiments recorded here have fulfilled this purpose. At the same time they have revealed a type of strain in these crystals which is of interest in itself, and which seems to be related to the mechanism believed to account for strain hardening in metals. They suggest, in fact, a possible means of investigating slip and strain hardening.

Diffraction by Mirror Surfaces Produced on Galena Crystals by Abrasion

Galena is the mineralogical name for lead sulphide (PbS) occurring in nature as cubic crystals of the rocksalt type. These crystals cleave very easily. The cube face, {100}, is both the cleavage plane and the slip plane.

The crystals upon which the first experiments were carried out were cut to expose {100} faces. The final mechanical operation upon one of these faces was filing or grinding parallel to a cube edge, and in one direction only. After this abrasion the appearance of a crystal is similar to that shown in the photomicrograph, Fig. 1. There are frequently occurring areas from which large blocks of the mineral have been torn out to expose mirror surfaces which have the appearance of cleavage surfaces. Between these are areas which have been plowed up by the filing or grinding and are covered by very deep scratches. Electron diffraction examinations show that these two areas, which have such different appearances, differ also in other interesting ways.

By abrasion with a coarse file, it is easy to tear out a block of galena so large that a mirror

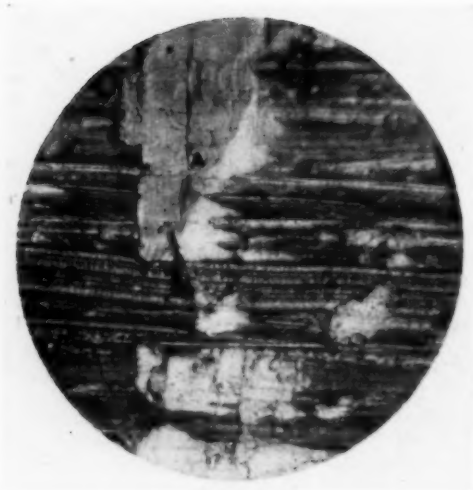

FIG. 1. Cube face of a galena crystal which has been filed from left to right, parallel to a cube edge. Magnification 90×.

surface of two or three square millimeters is exposed. A surface of this sort, after being brushed with a camel's hair brush to remove powdered galena, gave the electron diffraction pattern shown in Fig. 2. The crystal was then etched very lightly in a mixture composed of two parts HCl and one part HNO_3, then boiled vigorously in water to remove deposited lead salts, washed in absolute alcohol, and dried quickly in a stream of dry nitrogen. Following this treatment it was remounted in the camera and the diffraction pattern shown in Fig. 3 obtained from its surface.[1]

The spots of Fig. 3 constitute the diffraction pattern which one expects to observe from the surface of a galena crystal oriented, as is this crystal, with a cube edge parallel to the electron beam. The elongation of the spots of Fig. 2 is apparently due to refraction and appears because the unetched surface of the crystal is very flat, but not perfectly so.[2]

Some mirror surfaces produced by abrasion give, before etching, traces of diffuse Kikuchi lines in addition to the elongated spots of Fig. 2. *Cleaved* galena surfaces produce patterns in which the Kikuchi lines are very much stronger. Such a pattern is shown in Fig. 4. A light etch changes a cleaved surface, or a mirror surface formed by abrasion. After etching, Kikuchi lines are no longer prominent in the diffraction pattern. The pattern is then always rather similar to that of Fig. 3, although cleaved surfaces usually still show Kikuchi lines.

These experiments indicate a marked similarity between cleaved galena surfaces and mirror surfaces produced by abrasion; diffraction patterns are formed which are essentially alike, although differences exist which indicate that cleaved surfaces are more nearly perfect. Entirely different patterns are produced by those parts of an abraded surface which show the roughnesses and scratches appearing in Fig. 1. These different, and more interesting, patterns will be described in later sections of this paper. It is desirable first to give more consideration to square arrays of diffraction spots such as that shown in Fig. 3.

THE SPOT PATTERN

One cannot say from casual inspection whether the pattern of spots shown in Fig. 3 is due to diffraction by extremely thin projections from a perfect crystal, or to diffraction from many relatively thick crystals which are well but not perfectly aligned; whether, that is, we have a "cross grating" pattern or a pattern due to crystal imperfection.

If the roughnesses extending above the surface of a perfect crystal were sufficiently thin they would give rise to a pattern of diffraction spots the positions of which, in the neighborhood of the primary beam, could be calculated by assuming the crystal to consist of a single plane of scattering centers normal to the direction of this beam.[3] This equivalent plane of scattering centers is not necessarily a physical plane of atoms in the crystal, but it is obtained from the structure of the physical crystal by projecting upon a plane at right angles to the electron beam all of the atoms in one of the very thin projections. An absolutely perfect crystal would produce this

[1] The rectangular light patch which appears strongly in Figs. 2 and 3, and weakly in some later figures, is without important significance; it is due to electrons scattered from the slit system.

[2] See French, Proc. Roy. Soc. **A140**, 637 (1933); Darbyshire, Phil. Mag. **16**, 761 (1933); Kikuchi and Nakagawa, Sci. P.I.P. & C.R. (Japan) **21**, 256 (1933); Germer, Phys. Rev. **49**, 165 (1936).

[3] Bragg and Kirchner, Nature **127**, 738 (1931).

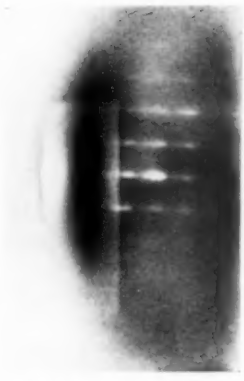

FIG. 2. Electron diffraction pattern from such a mirror surface of galena as that marked *A* in Fig. 1. Surface brushed to remove powdered galena, but not etched. Primary beam nearly parallel to a cube edge.

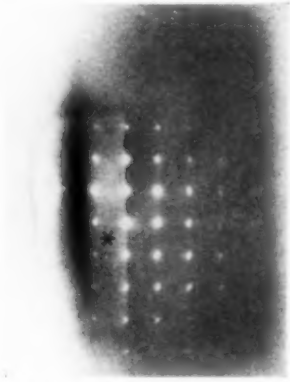

FIG. 3. Diffraction pattern from the surface which gave the pattern of Fig. 2 after a very light etch.

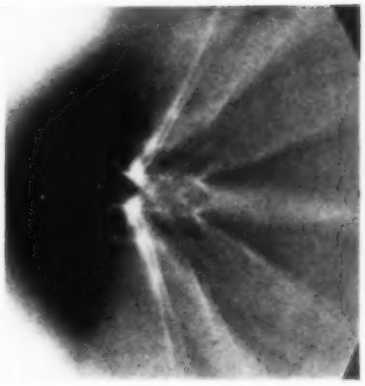

FIG. 4. Pattern from a cleaved surface of galena.

pattern of diffraction spots, if only the crystal were sufficiently thin in the direction parallel to the electron beam. The actual thickness determines only the *extent* of the "cross grating" pattern of spots, the radius of the pattern R being related to the thickness T, the electron wave-length λ and the separation L between crystal and photographic plate by the formula

$$R = L(2\lambda T)^{\frac{1}{2}}. \qquad (1)$$

If the crystal is aligned with an important crystallographic direction parallel to the primary electron beam this radius of the pattern is measured out from the intersection of the primary beam with the photographic plate. For slightly imperfect alignment this formula may still hold approximately with R measured out from the intersection of the important direction.

The alternative interpretation of such patterns as that of Fig. 3 as due to crystal imperfection rather than thinness was first given by W. L. Bragg.[4] He showed that substantially the same diffraction pattern would be produced by a slightly imperfect single crystal in which the electron paths need not necessarily be sufficiently short to give rise to the cross grating effect. If the spots of the square array are due to crystal imperfection they can be regarded as Bragg reflections from all of those crystal planes which pass through the cube edge, which is nearly parallel to the primary beam, as a common zone axis. In order that reflections from these planes appear it is necessary only that the imperfection be so great that cube edges of various crystallites are inclined to the direction of the primary beam by angles equal to the Bragg angles of the various planes. For the planes giving rise to the outermost spots which are clearly visible along the center line in Fig. 3 these angles are about 3°.

It is interesting and important to note that this angle of 3° is somewhat larger than the Bragg angles of several crystal planes which are inclined by approximately these angles to the common crystallographic zone axis of those planes which produce the square array of spots. Diffraction spots from these other planes do not appear near the center line, although some of them can be seen clearly along the upper edge of the pattern. From the unsymmetrical distribution of these "additional" spots we conclude that, due to imperfect alignment of the crystal, the cube edge of the mean orientation is not exactly parallel to the primary beam direction. It must intersect the photographic plate at a point somewhere in the square array of spots and below the center line. (The same conclusion is reached when one attempts to explain the

[4] W. L. Bragg, Nature **124**, 125 (1929).

square array of spots as due to a crystal which is perfect but extremely thin.)

Use of the Ewald Reciprocal Lattice

A more critical analysis and some further experimentation seem necessary to discriminate between these two possible explanations of the diffraction pattern shown in Fig. 3. The analysis is best supplied by an application of Ewald's conception of a reciprocal lattice.[5] As this will be almost indispensable later, it will be developed at once.

A vector is drawn from a fixed origin normal to each of any three pairs of planes which enclose a smallest possible unit of structure in a crystal lattice, the lengths of the three vectors being made numerically equal to the reciprocals of the separations of their corresponding planes. These vectors chosen as primitive translations define a new point lattice which is said to be reciprocal to the original physical lattice. The vector from the origin to any point of this new lattice can be written as

$$\mathbf{F}=h\mathbf{A}+k\mathbf{B}+l\mathbf{C},$$

where **A**, **B** and **C** are the primitive translations and h, k and l are whole numbers. The fundamental Laue conditions for coherent scattering are very simply expressed in terms of the vector **F**. These conditions are contained in the single equation

$$\mathbf{S}-\mathbf{S}_0=\lambda\mathbf{F}, \qquad (2)$$

where $\mathbf{S}_0$ is a unit vector in the direction of the primary beam and **S** a unit vector in the direction of a diffraction beam. Every unit vector **S** which can satisfy Eq. (2) represents the direction of a diffraction beam, and conversely all diffraction beams are included in this assemblage. Eq. (2) has a simple geometrical interpretation which is very useful. Choosing any point of the reciprocal lattice as origin, we draw the vector $-\mathbf{S}_0/\lambda$ (which is of length $1/\lambda$ and opposite in direction to the primary beam direction). A sphere is constructed of radius $1/\lambda$ about the endpoint of this vector as center. This sphere is called the sphere of reflection ("Ausbreitungskugel"). Eq. (2) states that the directions of all diffraction beams are obtained by drawing vectors from the center of the sphere to those points of the reciprocal lattice which fall upon its surface.

In the case of the galena crystal, we need consider scattering from the lead atoms only. These form a cubic face-centered structure with cube edge $a=5.93$A. It is easy to show that the lattice reciprocal to this is body centered with a cube edge b numerically equal to $2/a=0.337$. A cross section of this lattice is represented in Fig. 5. The plane of the paper is a cube face, which was approximately the plane of incidence of the primary electron beam upon the crystal when the pattern of Fig. 3 was produced. The large arc is the intersection of this plane with the sphere of reflection, assuming the primary beam to lie accurately along a cube edge. (The electron wave-lengths was 0.054A, which makes the radius of this sphere numerically equal to 18.5.) The solid circles are points of the reciprocal lattice of the galena crystal (lead atoms only) which fall in the plane of the paper, and the hollow circles are points which fall above and below this plane by distances equal to half the smallest separations of the solid circles. It is convenient to designate the points of the reciprocal lattice by the indices of corresponding planes of the physical crystal. If the direction of the primary electron beam is [100] and the normal to the crystal surface [010], then the points of Fig. 5 directly above the origin (000) are (020), (040), etc. and other points have the indices which appear in the figure.

This construction, which corresponds to a large perfect crystal, can be readily modified to indicate the pattern to be expected when the crystal is not perfect and is not large. In particular, to represent diffraction from a powder we image a great number of reciprocal lattices all with common center (000) but oriented entirely at random. The points of these lattices are scattered over a family of spherical surfaces about the point (000). The sphere of reflection cuts these other spheres in circles, and the diffraction beams form continuous circular cones, the apex angles of which are readily calculated from this construction.

[5] Similar applications to electron diffraction have been made by: Kirchner, Ann. d. Physik **13**, 38 (1932); Aminoff and Broomé, Zeits. f. Krist. **89**, 80 (1934); **91**, 71 (1935); Darbyshire and Cooper, Proc. Roy. Soc. **A152**, 104 (1935); and by others.

If the diffracting material is a collection of small (but not too small) crystals with nearly the same orientation—the case of an imperfect single crystal—then instead of the single reciprocal lattice of Fig. 5 one has a collection of such lattices with the same distribution of orientations as the crystals. The points of given indices form a cluster which occupies a small cap on the corresponding lattice sphere. If the distribution is random all such caps subtend the same solid angle at (000). The sphere of reflection may cut through many caps, thus giving rise to such a considerable array of diffraction spots as that exhibited in Fig. 3.

To represent diffraction by a number of perfectly aligned but extremely thin crystals, the simple reciprocal lattice is altered in a different manner. Kirchner has pointed out[5] that thinness in the direction of the primary beam can be represented by making each point of the lattice the center of a line segment parallel to the beam direction and of length inversely proportional to the thickness. It is easy to show that the line segments have a common length equal numerically to twice the reciprocal of the thickness. This modified reciprocal lattice is generated by moving the original lattice back and forth parallel to the primary beam direction through a total distance numerically equal to $2/T$. One sees that, in this case also, the sphere of reflection will intersect many reciprocal lattice line segments if their common length is comparable to the constant of the lattice—that is, if the crystals are sufficiently thin. Thus thinness is also capable of accounting for such an array of spots as that shown in Fig. 3.

With the designation of crystal axes given in Fig. 5, the spots of the principal array of Fig. 3 have indices of the form $(0\ k\ l)$, with k and l even and k having positive values only. It is easy to estimate from Fig. 5 the degree of imperfection required to explain the extent of the pattern in Fig. 3. The rotation of the lattice of Fig. 5 required to bring to the sphere of reflection a point of the form $(0\ k\ 0)$ is readily estimated from the figure, and it is easy to show that the rotation required to bring in the $(0\ k\ l)$ reflection is

$$\theta=\sin^{-1}((\lambda/2a)(k^2+l^2)^{\frac{1}{2}}).$$

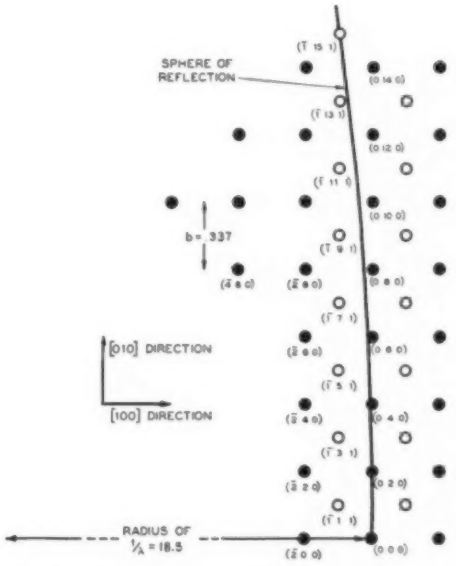

FIG. 5. Cross section of the reciprocal lattice of galena and the sphere of reflection, with the primary electron beam in the [100] direction.

Still more generally, the reflection $(h\ k\ l)$ requires a rotation of

$$\theta=\tan^{-1}(h/(k^2+l^2)^{\frac{1}{2}}) +\sin^{-1}((\lambda/2a)(h^2+k^2+l^2)^{\frac{1}{2}}). \quad (3)$$

(The correct sign must be assigned to the number h.)

From Eq. (3) one calculates that the reflection (0 12 0) requires a rotation of about 3.1° and the reflection ($\bar{1}$ 11 1) about −2.3°. The former reflection appears clearly in Fig. 3 although the latter, which should lie nearby, is entirely missing. Other diffraction spots with high odd indices, which one expects to find near the center line in Fig. 3, also are missing. Those spots with odd indices which actually appear are located in the upper part of the figure. The obvious interpretation of the unsymmetrical occurrence of odd-ordered diffraction spots is that Fig. 5 does not correctly represent the reciprocal lattice corresponding to the mean orientation of the crystal. For this mean orientation the lattice of Fig. 5 should be turned slightly. In Fig. 6, for example, is represented the same lattice rotated by an angle of 3° about an axis through (0 0 0) and normal to the plane of the paper. One sees that, if this lattice represented the mean orien-

tation of the crystal, a very slight imperfection, or equally well a small elongation of lattice points due to thinness, could account for the appearance of even-ordered diffraction spots of the form $(0\ k\ 0)$ and the odd-ordered spots $(\bar{1}\ k\ 1)$ would not appear unless the imperfection were quite large, or elongation of lattice points due to thinness very great.

It is not difficult to determine the actual orientation of the crystal required to account for the pattern of Fig. 3. If, for example, one goes out from the primary beam position along the 45° line in the upper half of Fig. 3 one comes first to the position of the missing $(0\ 2\ \bar{2})$ diffraction spot, then successively to the spots $(0\ 4\ \bar{4})$, $(0\ 6\ \bar{6})$, $(\bar{1}\ 7\ \bar{7})$, $(\bar{1}\ 9\ \bar{9})$ and $(\bar{1}\ 11\ \bar{1}\bar{1})$. The weak spots $(0\ 6\ \bar{6})$ and $(\bar{1}\ 7\ \bar{7})$ seem to be equally intense. This equality means that the sphere of reflection passes between the corresponding reciprocal lattice points, and that these points are located at equal distances from the sphere. It can be shown that this is sufficient to locate the intersection of the [100] axis with the photographic plate upon a straight line normal to the line of diffraction spots just considered and passing very close to the primary beam position, but slightly on the other side from the $(0\ 6\ \bar{6})$ and $(\bar{1}\ 7\ \bar{7})$ diffraction spots. Other simple considerations modify the indicated position of this line slightly, and finally locate the intersection of the [100] axis at about the position of the star in Fig. 3.

Although these considerations seem to show that the extended array of spots in the pattern of Fig. 3 can appear as a result of imperfection or as a result of thinness, it is of course true that a pattern due to thinness cannot be identical with one which results from imperfection. Yet the differences are not so marked that one can by inspection always attribute a pattern to one cause or the other.

It should, in principle, be possible to reach a conclusion regarding the state of the material producing the pattern shown in Fig. 3 from a study of widths of rocking curves.

Rocking Curves from a Cleaved Galena Crystal

A crucial experiment from which one might distinguish between imperfection and thinness is suggested by the ways in which the simple reciprocal lattice must be modified to represent these different conditions. If one rotates the crystal its reciprocal lattice rotates with it, and one sees that a given diffraction beam will persist through whatever angle the lattice feature representing this beam remains in contact with the sphere of reflection. For a slightly imperfect crystal each lattice feature is the small cluster of points already described. Each of these clusters subtends the same angle at the origin. If the crystal is rotated about an axis normal to the plane of incidence the clusters which represent the $(0\ k\ 0)$ beams will remain in contact with the sphere through equal angles; the "rocking curves" of these beams will have equal widths. For a thin perfect crystal the case is different. The lattice features are line segments of equal lengths. These do not subtend equal angles at the origin, and if the crystal is rotated about an axis normal to the plane of incidence the "rocking curves" of different beams of the form $(0\ k\ 0)$ will not have equal widths.

These two cases are illustrated by the lattice features of Fig. 7. In 7A are drawn the reciprocal lattice line segments of the form $(0\ k\ 0)$ corresponding to a perfect crystal only $3a = 17.8$A in thickness. To compare with this are drawn in 7B arcs representing the loci of reciprocal lattice points of the form $(0\ k\ 0)$ corresponding to the various crystallites of a thick crystal of which the maximum imperfection is 3°. It is evident that, if one attempts to measure "crystal imperfection" by the rocking crystal method, he will obtain results which are dependent upon which of these figures represents the true condition of the crystal. If the condition is that represented by Fig. 7B one will obtain 3° for the total width of rocking curve, quite independently of the diffraction spot upon which the measurements are made. If, however, the condition is that represented by Fig. 7A one will also obtain 3° if the measurements are carried out upon the diffraction spot $(0\ 12\ 0)$, but a larger value will be found if a lower ordered spot is chosen for measurements. In general, for a crystal of thickness $T = na$, a spot of the form $(0\ k\ 0)$ will give a total rocking curve width equal to

$$W = 2a/kT = 2/kn \qquad (4)$$

in circular measure.

Unfortunately rocking curves of various dif-

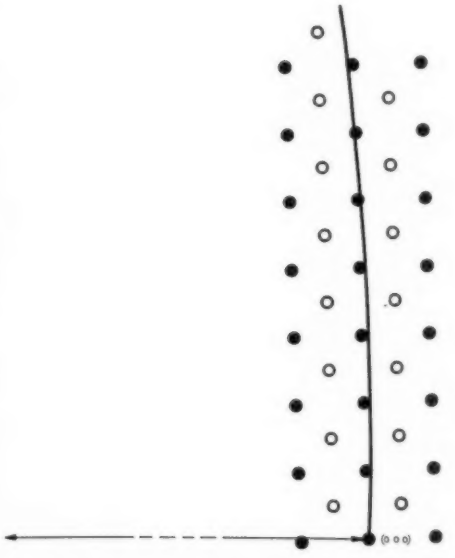

FIG. 6. The reciprocal lattice and sphere of reflection of Fig. 5, with the primary electron beam lying in the (001) plane of the galena crystal and inclined by 3° to the [100] direction.

fraction spots appearing in Fig. 3 cannot be obtained; the widths of these curves would be so great that the crystal itself would intercept the primary electron beam on one side, and the diffraction beam under examination on the other. The proposed crucial experiment could be carried out only by the transmission method.

Although this investigation of the variation of rocking curve width with order cannot be made upon the crystal which produced the pattern of Fig. 3 it can be carried out upon a crystal which gives rise to *narrower* rocking curves. The cleaved surface of a galena crystal does give curves which are sufficiently narrow to permit direct measurements. But unfortunately the curves are so narrow and exhibit such anomalies that no certain conclusion can be drawn from them concerning the condition of the surface. They do, however, supply us with data from which we can decide regarding the condition of material on the surface of a filed crystal. The conclusion is that such an extended pattern of spots as that shown in Fig. 3 is due to imperfection, and not to thinness.

In Fig. 8 are reproduced nine rocking curves for a cleaved and etched crystal. These curves represent the variation of intensity with angular crystal setting, respectively, of the diffraction spots (0 2 0), (0 4 0), (0 6 0), (0 8 0), (0 10 0), (0 12 0), (0 14 0), (0 16 0), and (0 18 0). The abscissae are the angular positions of the crystal, measured from the position of grazing incidence, as determined by a lamp and scale and a mirror attached to the crystal holder.[6]

The first five of the curves of Fig. 8 were obtained by measuring directly the intensities of diffraction spots upon the fluorescent screen by means of a Macbeth illuminometer manufactured by the Leeds and Northrup Company. Because of the small size of the fluorescent screen, spots beyond (0 10 0) could not be observed directly. Rocking curves of the spots beyond this were obtained photographically as described below. The spot (0 18 0) fell near the edge of the photographic plate, and higher ordered spots were beyond the range of observation.

In using the illuminometer a color match was established by the use of suitable filters. The ordinates of the first five rocking curves are readings taken directly from the illuminometer. Nearly three hours were required to obtain the data of these curves; voltage, current and direction of the primary beam remained constant throughout this time.

The photographic method of obtaining rocking curves of diffraction spots beyond (0 10 0) consisted of several steps. With stops in front of the photographic plate so adjusted that 23 exposures could be made upon one plate, preliminary estimates of intensities and approximate widths were easily made. After such preliminary estimates a series of exposures at constant time shows clearly the variation of intensity of a diffraction spot with crystal position. Such a series of photographs is exhibited in Fig. 9. The electron beam current has been adjusted to a rather low value so that the uniform exposure time of 7 seconds gives suitable darkening of the photographic plate. On Fig. 9 the diffraction spots (0 12 0) and (0 14 0) reach their maximum intensities, and the spots (0 8 0), (0 10 0) and (0 16 0) can be observed. Various diffuse Kikuchi lines also appear weakly.

Each final rocking curve exhibited in Fig. 8, beyond the (0 10 0) curve, was obtained from a

[6] For the means of rotating the crystal see Germer, Rev. Sci. Inst. **6**, 138 (1935).

series of exposures in which approximately constant photographic intensities were maintained by varying exposure time with crystal position. In this way it was unnecessary to make estimates of relative blackness. A photographic comparison of intensities of different diffraction spots was also carried out, and all curves of Fig. 8 have been reduced to readings upon the illuminometer. The photographic estimations of rocking curves involved altogether a total of 424 exposures upon 19 plates.

In Fig. 10 are plotted the widths at half maximum of the various curves shown in Fig. 8 against the reciprocal of k, the order of reflection. If the diffracting material is an aggregate of "thick" crystals imperfectly aligned the points of Fig. 10 should fall along a straight line parallel to the axis of abscissae; if it is an aggregate of thin projections from an essentially perfect crystal they should fall along a straight line passing through the origin. The line drawn on the figure corresponds to a perfect crystal having a thickness of about 350A.[7] The range of the measurements is so small, and their anomalies are so great, that one cannot decide between imperfection and thinness. One can, however, at once conclude that the imperfection of the crystal is at least *as small as 10 or 15 minutes* and that the average thickness is *350A or more.*

In addition to measurements upon diffraction beams of the form (0 k 0) the rocking curve of the beam ($\bar{1}$ 15 1) also was determined. This beam was found to be about equal to (0 18 0) in intensity, and the rocking curve width at half maximum was measured to be 14′. This width is represented on Fig. 10 by an open circle at an abscissa of 1/15, which is approximately the correct value to make this point comparable with the others.

The maximum of the ($\bar{1}$ 15 1) rocking curve occurred at glancing angle 0.49°. From Eq. (3) one calculates that this should come at 0.27°. Slightly incorrect azimuth adjustment of the crystal is undoubtedly responsible for the discrepancy. The calculation assumes that, at zero glancing angle, the primary beam lies accurately along the [100] direction. It is easy to show from the lattice of Fig. 5 that an azimuth rotation of the crystal through a small angle θ will result in changing the glancing angle of a diffraction beam of the form ($\bar{1}$ k 1) by an amount equal to θ/k. If the glancing angle of the beam ($\bar{1}$ k 1) is increased, the angle of the beam ($\bar{1}$ k $\bar{1}$) will be decreased by an equal amount. Thus we might expect to find the beam ($\bar{1}$ 15 $\bar{1}$) at 0.05° glancing angle. It was not looked for. The *positions* at which diffraction beams occur are not perceptibly changed by slight rotation of the crystal in azimuth.

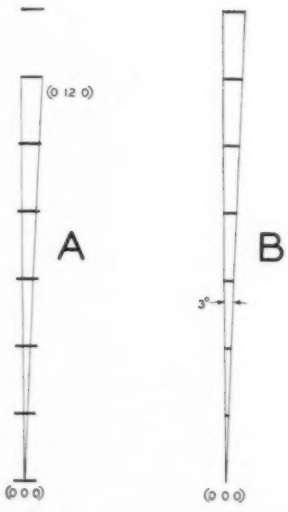

FIG. 7. Reciprocal lattice line segments of the form (0 k 0). *A*. For a perfect crystal having a thickness of only 17.8A in the direction of the primary beam. *B*. For a thick crystal with a total imperfection of 3°.

No explanation has been given of the curious relative intensities of the beams of Fig. 8, or of the anomalous broadness of the (0 4 0) curve. (This broadness is so striking that it could be readily observed on the fluorescent screen, entirely without the aid of the illuminometer.) Other anomalies were also observed. For example, rocking curves of beams of the form (0 k 0) were not the same for different crystal azimuths. Several such curves were obtained with the crystal rotated 180° about the normal to its face. In this position the (0 4 0) beam was considerably more intense than in the original azimuth, and its rocking curve was not unusually

[7] The value 350A is not obtained by direct substitution of the slope of the line of Fig. 10 into Eq. (4). The quantity W in this expression is total rocking curve width, whereas the ordinates of Fig. 10 represent widths at half maximum. From the latter, estimates are made of total widths, under the simplifying assumption of uniform thickness for all the projections from a perfect crystal.

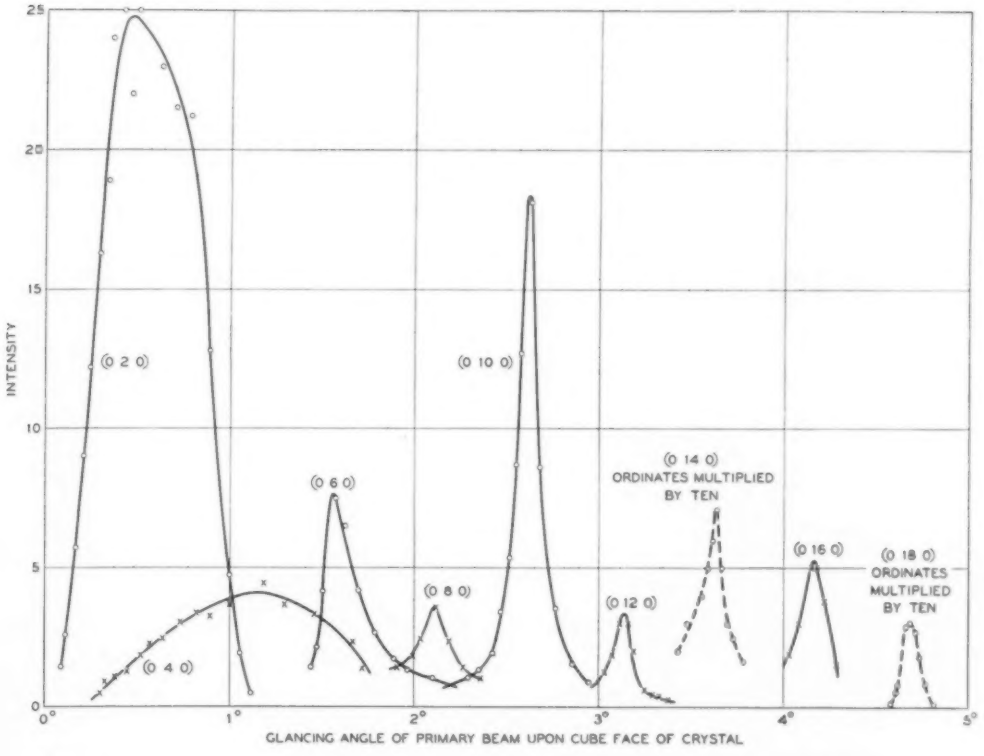

FIG. 8. Rocking curves of various Bragg reflections from the cube face of a cleaved and etched crystal.

broad. In the new azimuth it was found, however, that the (0 12 0) beam was very weak and had a rocking curve which was broad. This curve had, in fact, two maxima the stronger of which occurred at the correct glancing angle.

GENERAL CONCLUSIONS CONCERNING THINNESS AND IMPERFECTION

In the above section two conclusions have been drawn from rocking curve measurements upon a cleaved galena crystal: (1) The imperfection of the surface of this crystal does not exceed about 10 or 15 minutes. (2) Those projections from its surface, which are most effective in scattering electrons of 0.054A wave-length, are not thinner than about 350A. Less extensive measurements upon a number of other cleaved crystals of galena have indicated that for these also the general surface imperfection does not exceed a small fraction of one degree, and that effective projecting portions are quite thick. The rather good definition of Kikuchi lines from cleaved, but unetched, crystals supports this conclusion regarding relative perfection of cleaved surfaces.

On the other hand, galena crystals which have been filed, and which have subsequently been deeply etched, show *extended* spot patterns. Clearly defined Kikuchi lines are not found even before etching.

All of these data are consistent with the hypothesis that the surface of a galena crystal which has been filed is, even after very deep etching, much more imperfect than the surface of a cleaved crystal. On the other hand, the data can also be understood if we are willing to believe that projections are always thinner upon the surface of a filed and deeply etched crystal than upon the surface of a crystal which has been

FIG. 9. Series of exposures at progressively varied glancing angles, showing the (0 12 0) and (0 14 0) diffraction spots.

cleaved and etched.[8] This latter hypothesis seems so unlikely that the former can be regarded as thoroughly established. It seems altogether reasonable to generalize further. Any extended spot pattern from a galena crystal, which would correspond to an indicated imperfection as large as 2 or 3 degrees, is really due predominantly to imperfection and not to thinness.

In some earlier experiments[9] upon metal crystals diffraction patterns of this sort were explained in this manner, but G. P. Thomson[10] has taken exception to this explanation and believes that these patterns should be attributed mainly to thinness. Further study of spot patterns from metal crystals seems desirable.

One predicted feature of the considerable imperfection indicated by the extent of the diffraction pattern of Fig. 3 does not appear in this figure, and requires explanation. One might expect that the total indicated imperfection of over 4° would result in diffraction spots drawn out into arcs of this length. *Such arced spots are actually found in many cases.* It seems probable that the imperfection is not uniform around different axes, but that it is related to the direction in which a crystal was filed. The experiments of the next section are concerned with this matter.

Diffraction by Deeply Scratched Surfaces

All of the diffraction patterns which have already been described were obtained from "mirror" surfaces of galena. Entirely different patterns are obtained from abraded areas, either before etching or after moderate etching.

The diffraction pattern of Fig. 11 was produced by a filed but unetched galena crystal so adjusted that the electron beam was nearly parallel to a cube edge and was scattered mainly by deeply scratched portions of the surface, of the type marked *B* in Fig. 1. The predominant part of the pattern consists of Debye-Scherrer rings. Thirty-one of these rings are observable on the plate from which the figure was made. Their radii and, as far as one can estimate easily, their intensities have the values predicted for randomly oriented

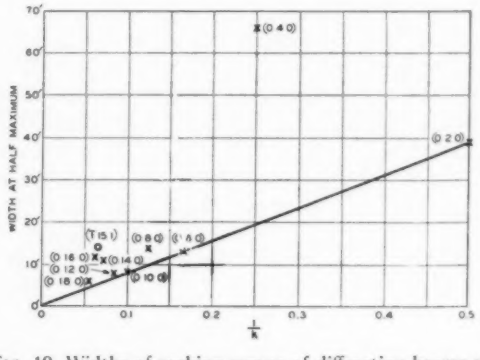

FIG. 10. Widths of rocking curves of diffraction beams of the form (0 *k* 0), as taken from Fig. 8.

[8] If this second hypothesis is correct the projections upon the surface of a filed and deeply etched crystal must quite generally be of the order of 20Å in thickness.

[9] L. H. Germer, Phys. Rev. **44**, 1012 (1933).

[10] G. P. Thomson, Phil. Mag. **18**, 640 (1934).

crystals of galena. The rings are very sharp. One estimates that the average linear dimensions of the small galena crystals cannot be less than about 100A, and that the individual crystals are not greatly strained. Superposed on this ring pattern is a weak pattern of the type shown in Fig. 2. From this one infers that a small fraction of the *B*-type surface is really of type *A*.

Etching a crystal, which gives a pattern like that of Fig. 11, changes the surface in such a way that a subsequent diffraction pattern shows an array of spots in place of the weak streaks of Fig. 11. If the etch is rather light the Debye-Scherrer rings persist. Examples of these "combination" patterns showing diffraction from two different sorts of galena surfaces are shown in Fig. 12. The relative intensities of the two patterns depend upon a number of factors, dominant among which are, of course, the relative extents of the two sorts of surfaces in the area upon which the beam strikes. (See, for example, Figs. 12A and 12B.) Other factors are the depth of the etch, the glancing angle of the primary electron beam upon the surface, the amount by which the surface of the crystal deviates from a cube face, and the direction in azimuth of the plane of incidence. Some of these factors are of importance because the galena surface is extremely rough, and the mirror surfaces from which the spot patterns come are below the general plane of the abraded areas. The difference in level is of the order of 0.02 mm.

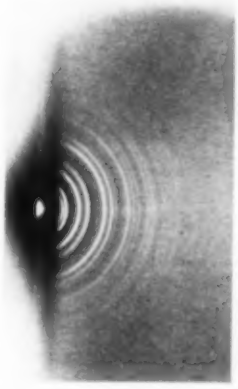

FIG. 11. Diffraction pattern from such a filed galena surface as that marked *B* in Fig. 1.

The higher parts cast shadows upon the photographic plate. A clear example of this is shown in Fig. 12C. Here the spot pattern fails to come up to the general shadow of the galena surface by a distance which corresponds to an angle at the specimen of about 2°. Various "shadowing" effects of this nature have been observed, some of which are not entirely understood.

Deeper etching of a crystal, which gives diffraction patterns more or less like those of Fig. 12, results in a surface from which strikingly different patterns are obtained. Two of these are reproduced in Figs. 13 and 14. These two patterns were produced by the same crystal without

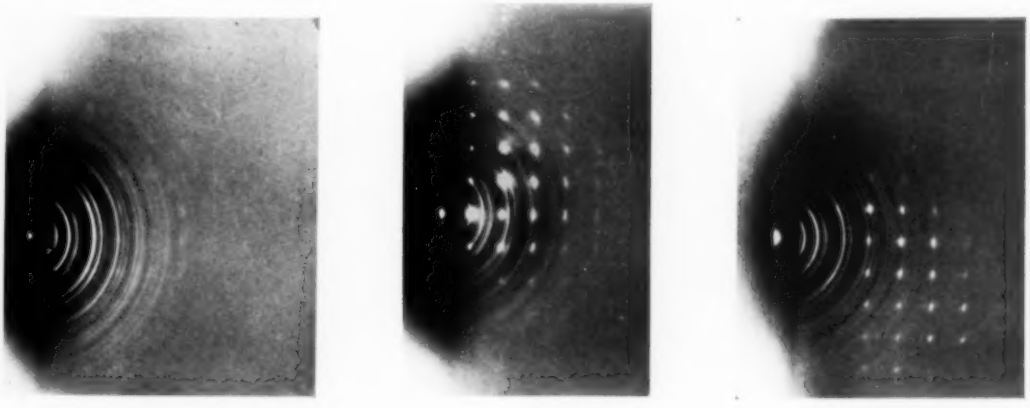

A B C

FIG. 12. Combination patterns from galena crystals which have been first filed, then very lightly etched.

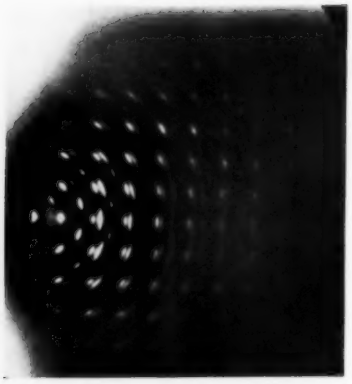

FIG. 13. Pattern from a crystal which has been filed and moderately etched. The primary electron beam was approximately parallel to the direction of filing.

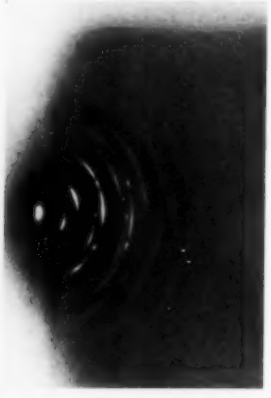

FIG. 14. Another pattern from the crystal which produced Fig. 13, after rotating the crystal so that the electron beam direction lay normal to the direction of filing.

alteration of its surface condition. In both cases the electron beam direction was approximately parallel to a cube edge. In the former the beam direction was the direction of grinding, while in the latter the crystal had been rotated so that the grinding direction was normal to the beam direction.

Both in Fig. 13 and in Fig. 14 we recognize two different sorts of diffraction patterns. The square array of spots which arises mainly, if not entirely, from the etched mirror surfaces has remained unchanged; the Debye-Scherrer rings from the deeply scratched areas have been replaced by new diffraction spots in Fig. 13 and

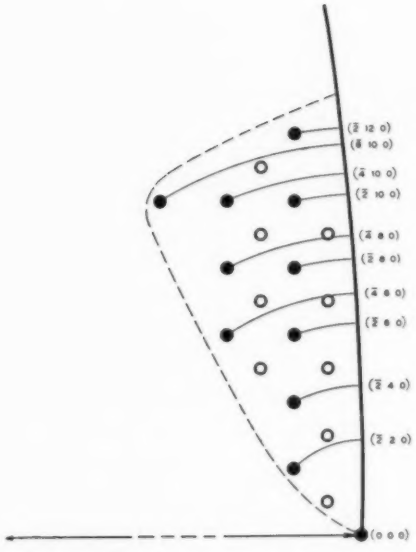

FIG. 15. Reciprocal lattice of the lead atoms of galena, representing only those points of the form $(0\ k\ 0)$ and $(1\ k\ 1)$ which correspond to reflections observed in Fig. 13.

by arcs in Fig. 14. It is easy to see that the latter correspond to crystallites which have been rotated from the orientation of the galena crystal about an axis approximately parallel to the primary beam and by amounts varying from 5 to about 35 degrees. The sense of the rotation is that of imaginary rollers on the surface of the crystal which have been rotated by motion of the grinding wheel. The new spots of Fig. 13 are also attributed to these same rotated crystallites.

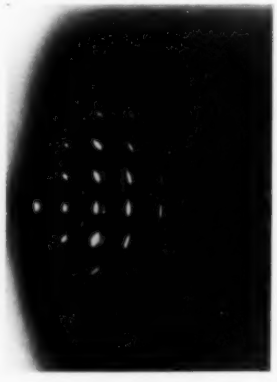

FIG. 16. Pattern like that of Fig. 13, from a crystal which has been more deeply etched.

The axis of rotation is now normal to the electron beam. The sense of the rotation is not readily determined from Fig. 13.

Fig. 15 represents again the reciprocal lattice of the galena crystal and the sphere of reflection. The solid circles are those points of the reciprocal lattice which lie in the plane of incidence and the open circles points located at the distance $1/a$ either side of this plane. Only those points are drawn which correspond to reflections actually observed in Fig. 13 among the *new* array of diffraction spots. (Lattice points corresponding to the square array of spots are not indicated.) The rotations of the original crystal about an axis normal to the plane of incidence required to bring various reciprocal lattice points to the sphere of reflection are immediately estimated from Fig. 15. Arcs are drawn from those lattice points which lie in the plane of incidence. The intersections of these arcs with the sphere of reflection represent the locations of the corresponding diffraction points on the photographic plate, and the lengths of the arcs, the rotations of the crystallites from the mean orientation of the large galena crystal. Indices of those diffraction spots appearing in the plane of incidence are marked on the figure. The dashed curve represents an approximate envelope of the reciprocal lattice points which correspond to observed diffraction spots.

Repeated etching of the crystal which produced the patterns of Figs. 13 and 14 resulted in further modifications of these patterns. The new spots became relatively much weaker, as in Fig. 16, and finally disappeared entirely indicating that the etching had at last removed all of the material which had been disturbed by the abrasion. A crude estimate of the depth of this disturbed layer was obtained in a series of experiments in which a crystal was alternately etched and examined by electron diffraction until, after ten etchings, only the square array of diffraction spots was produced. The amount of material removed was estimated by chemical analysis of the etching solutions for amount of dissolved lead. These experiments indicated that the rotated crystallites extended to a depth of about 0.00^3 mm below the surface. The mean rotation, as estimated from patterns like those of Figs. 13 and 14, was about 20°. The interesting observation was made that this mean rotation was about the same after different amounts of material had been removed.

In Fig. 13 one observes clearly that the "spots" due to the rotated crystallites are actually arcs extending several degrees along the corresponding Debye-Scherrer rings. This means that, in addition to the considerable rotation about an axis normal to the direction of grinding, the crystallites have suffered also slight rotations about other axes.

A Possible Application to Metallurgy

It is known from x-ray examinations that when the surface of a metal crystal is filed, or polished on abrasive material, the regular arrangement of atoms near the surface is profoundly disturbed; but, so far as I am aware, no systematic investigation of the nature of this disturbance has been made.

The results of the present experiments suggest that a similar investigation of metallic crystals might be interesting and valuable. The observed rotation of crystallites is similar to the mechanism postulated to account for strain hardening of metals,[11] and it seems possible that the simple experimental technique used here could be applied to metal crystals and might yield readily important data regarding slip and strain hardening.

I am glad to thank Dr. C. J. Davisson for his interest and advice throughout the course of these experiments, and Mr. K. H. Storks for doing a great deal of the experimental work and helping considerably with the interpretation of data.

[11] See e.g. Burgers, *Int. Conf. Physics*, London, 1934, Vol. 2, pp. 139–160.

LETTERS TO THE EDITOR

Prompt publication of brief reports of important discoveries in physics may be secured by addressing them to this department. Closing dates for this department are, for the first issue of the month, the eighteenth of the preceding month, for the second issue, the third of the month. The Board of Editors does not hold itself responsible for the opinions expressed by the correspondents.

Communications should not in general exceed 600 words in length.

Intensity of the Central Spot Produced by X-Rays Penetrating Piezoelectrically Oscillating Quartz Crystals

In an investigation of the increase in the intensity of the Laue spots when a quartz crystal oscillates piezoelectrically, Fox and Fraser[1] observed an increase both in the area and in the blackness of the central spot produced by the primary beam of x-rays when the crystal was oscillating. On the other hand, Jauncey and Deming,[2] who were investigating the effect of piezoelectric oscillations on the intensity of the diffuse scattering of x-rays from quartz, found no increase in the intensity of the primary rays penetrating the crystal. It seemed worth while to examine this matter further.

Now, Bertsch[3] finds that the increase in the intensity of the Laue spots depends upon whether or not the primary beam passes through a nodal or antinodal portion of the crystal. Hence a sideways displacement of the crystal plate may remove the effect of the oscillations on the Laue spots and may possibly have an effect on the central spot. In our experiments we passed the primary beam from a tungsten target tube operated at 42 kv peak through various portions of both X-cut (1741 kc short dimension) and Y-cut (1763 kc short dimension) crystals. We measured the intensity of the central spot by means of both an ionization chamber and a photographic film.

In a typical set of readings with the ionization chamber, the average of the "oscillating" readings differed by 0.5 percent from the average of the "not oscillating" readings with a probable error in each average of about 0.3 percent. The ionization chamber method therefore shows no change in the total primary beam penetrating the crystal. Now, although the total intensity of the primary beam entering the ionization chamber window remains unchanged, the width of the beam penetrating the crystal and the area of the central spot on a photographic film may be changed when the crystal goes from "oscillating" to "not oscillating." Photographic reversal, which we obtained quite easily, may produce peculiar effects.[4] It is possible with two beams of the same true total intensity but of different areas for the broader beam to produce a blacker and bigger spot on a photographic film if the time of exposure is just right. Also with long exposure there is halation, the blackening of the film in the vicinity of the true spot by x-rays scattered from the film itself. We have found that halation combined with reversal can give a spot consisting of a black periphery with a light center. In the photographic experiments, we were careful to avoid the effects of reversal and halation by making the time of exposure short. Further, the "oscillating" and "not oscillating" spots were produced on the same strip of film. The blackness and width of each spot on the developed film were measured by means of a microphotometer. We found no certain change either in the blackness or the width from "oscillating" to "not oscillating."

The accepted explanation for the increase in the intensity of the Laue spots is that the oscillations cause a decrease in the extinction coefficient. This explanation is supported by Jauncey and Deming's result that the oscillations have no effect on the diffuse scattering. We may look upon calcite, a crystal of high perfection, as having a high extinction coefficient and upon rocksalt, a mosaic crystal, as having a low extinction coefficient. We therefore made plates of calcite and rocksalt of equivalent thicknesses with respect to absorption of x-rays and looked for a change in the width of the central spot produced by the primary rays penetrating the crystal when rocksalt was substituted for calcite. It was just possible that there might be such an effect. However, no such effect was found and so the extinction coefficient has no effect on the width of the central spot.

We conclude that the effect reported by Fox and Fraser was due to an accidental combination of photographic reversal and halation and not to a change in the primary beam penetrating the quartz.

G. E. M. JAUNCEY
A. T. JAQUES

Wayman Crow Hall of Physics,
Washington University, St. Louis,
September 6, 1936.

[1] G. W. Fox and W. A. Fraser, Phys. Rev. **47**, 899 (1935).
[2] G. E. M. Jauncey and J. H. Deming, Phys. Rev. **48**, 462 (1935).
[3] C. V. Bertsch, Phys. Rev. **49**, 128 (1936).
[4] A. E. Garrett, *The Advance of Photography*, p. 358.

Electron Velocity Distribution in Gases

Specification of electron velocity distributions in ionized gases of medium conductivity is at present one of the most interesting problems of discharge physics. We wish to report briefly some results obtained by applying Druyvesteyn's method of analysis[1] to representative probe data which have been accumulated in this laboratory for arcs and glows with electron concentrations of about 10^7-10^9 cc^{-1}.

The outstanding result is the frequent existence of a wide depression in the distribution function for electron velocities rather greater than the mean, taking the Maxwellian distribution as standard. This modified form of the distribution function has been predicted by (amongst others) Morse, Allis and Lamar,[2] for electrons drifting

through a gas in a uniform field and losing energy in elastic collisions with molecules. Although it is difficult to trace down the exact origin of any particular feature of a complicated discharge, it appears that conditions in our tubes have often been such as to make loss of energy in this way an important factor. Further, the ratio of random and drift currents has in many instances about the predicted value. With increase in electron concentration, the distribution function tends to the Maxwellian.

The second, less definite result, is the common occurrence of a fairly distinct group of electrons with a mean energy of the order of 5–10 electron volts, under conditions when much ionization was certainly due to fast primary electrons. If we suppose this group consists of electrons ejected from molecules by the primary electrons, its roughly constant energy receives an explanation on the quantum theory of ionization, which predicts that many of the ejected electrons should have an energy of this order, whatever the primary energy.[3]

It has been assumed in this investigation that the ideal conditions postulated in the usual theory of probes have been satisfied sufficiently well for the results to have meaning in relation to the undisturbed plasma. It would be very difficult to go into this theoretically for the complex discharges which have been studied, although the lines on which such calculations could be made have been laid down.[4] It is however at least certain that the main features of the results are independent of probe size over a wide range of this.[1, 5]

K. G. Emeleus
R. J. Ballantine

Queen's University,
Belfast, Ireland,
August 21, 1936.

[1] Sloane and Emeleus, Phys. Rev. **44**, 333 (1933).
[2] Morse, Allis and Lamar, Phys. Rev. **48**, 412 (1935).
[3] Mott and Massey, *The Theory of Atomic Collisions* (Oxford 1933), p. 171.
[4] Tonks and Langmuir, Phys. Rev. **34**, 876 (1929).
[5] Greeves and Johnston, Phil. Mag. **21**, 659 (1936).

Attempt to Observe the Spectrum of Doubly Excited Helium

According to the calculations of Massey and Mohr,[1] the excitation cross sections of the doubly excited states of helium by electron impact are very small for low electron energy and reach their maximum values for electron energy of the order 500–600 volts. Hence an attempt is made to excite the spectrum of doubly excited helium by electrons of these energies. Electrons emitted by a hot cathode consisting of an oxide coated spiral tungsten filament are accelerated through a glass tube to a hollow nickel anode at a distance of 2 cm from the cathode. The pressure of helium in the tube is kept within 0.07 and 0.12 mm of mercury so that the electron mean free path is of the order of 1 cm. The accelerating voltage is varied between 1100 and 1800 volts so that the electron energy on impact with the helium atoms would be of the order of 500–700 volts. A tube of 3 mm bore extends from the hollow anode and confines the excitation process within it in order to increase the intensity of the radiation which is observed end-on in the direction of accelerating field. The strongest lines of the spectrum $2s^2\,{}^1S-2s2p\,{}^1P$, $2s2p\,{}^1P-2s3s\,{}^1S$ and $2s2p\,{}^3P-2s3s\,{}^3S$, whose positions are calculated from the energy states obtained by the variational method[2] to be at 6329A, 5840A, and 2670A, respectively, are looked for. But prolonged exposures fail to reveal any faint lines at the expected positions.

In a way, this failure to observe the spectrum is understandable when one considers the widths of the levels of doubly excited helium. The lifetime of a doubly excited state is mainly determined by the process of autoionization, i.e., a radiationless transition in which one electron goes to $1s$ state while the other is ejected with the proper energy. The transition probabilities between a doubly excited state and the singly excited states and those between doubly excited states are small compared with that due to autoionization and hence can be neglected in estimating the lifetime of the doubly excited state. Calculation of the probability of autoionization has been carried out for $2s3s\,{}^3S$ by Kreisler[3] using for the ejected electron the continuous wave function of hydrogen. To ascertain the order of magnitude of Kreisler's result, we calculate the probability of autoionization using our variational wave function for $2s3s\,{}^3S$ and Wentzel's spherical wave[4] for the ejected electron and obtain a result agreeing with Kreisler's in the order of magnitude, namely, $P\sim10^{14}$ sec.$^{-1}$. The lifetime is then $\sim10^{-14}$ sec. and the width of the level is ~3000 cm^{-1}. The widths of other doubly excited levels would certainly be of the same order of magnitude. Thus transitions between two doubly excited states would give rise to a continuous band extending over hundreds of angstroms, if they are observed at all. This seems to show that the suggestion that the corona spectrum may be due to doubly excited helium is untenable.[5]

The lines observed by Compton and Boyce[6] and Kruger[7] in the region of 300A, if they arise from transitions between doubly and singly excited states, would according to these calculations have a width of 3A, or 1 mm at the dispersion employed by Kruger. This does not agree with the observation of Compton, Boyce and Kruger; for although the width of the line 329.4A is not explicitly mentioned, it appears to be quite sharp in the reproduction in their papers. Thus we may regard the question as to the origin of the lines at 320.4 and 357.5A still unsettled.

We are grateful to Mr. K. T. Chao for his help during the experiment.

A. T. Kiang
S. T. Ma
Ta-You Wu

Physics Department,
National University of Peking,
August 8, 1936.

[1] Massey and Mohr, Proc. Camb. Phil. Soc. **31**, 604 (1935).
[2] T. Y. Wu, Phys. Rev. **46**, 293 (1934). The corrected energies and eigenfunctions are given in T. Y. Wu and S. T. Ma, J. Chinese Chem. Soc. **4**, 344 (1936).
[3] Kreisler, Phys. Acta Polonica **4**, 1–2, 151 (1935).
[4] G. Wentzel, Zeits. f. Physik **40**, 574 (1926); **43**, 524 (1927).
[5] Rosenthal, Zeits. f. Astrophys. **1**, 115 (1930); Goudsmit and Wu, Astrophys. J. **80**, 154 (1934).
[6] K. T. Compton and Boyce, J. Frank. Inst. **205**, 497 (1928).
[7] P. G. Kruger, Phys. Rev. **36**, 855 (1930).

Energy Distribution of Cosmic Rays

Anderson and Neddermeyer's[1] list of the energies of 78 of the individual rays in a "sample" of 104 vertical cosmic rays provides the energy distribution of any sample and has been used as such by Street, Woodward and Stevenson.[2]

An attempt to reproduce Anderson and Neddermeyer's distribution curve led to confusion as to how they had eliminated the rather large statistical variations in the number of rays for each energy increment. The sum of all rays greater than a given energy, however, ought to be largely independent of such variations. From their list it is possible to obtain a list of N's where $N=\sum_E^\infty \phi(E)dE$ and a corresponding list of E's for 3×10^8 ev$<E<6\times10^9$ ev. Fig. 1 shows a plot of log N against E where it is seen that a linear relation might well connect these two quantities. This leads to an exponential energy distribution $dN=34e^{-0.34E}dE$ for a sample of 100 rays where E is measured in units of 10^9 ev. Similar independent treatments of the positive and negative rays lead to distributions with the same modulus where there are 52 positive rays in a sample of 100. Since both of these distributions are found to have the same modulus, the apparent predominance of positives in the higher energy ranges would have to be due to statistical fluctuations.

It is, however, possible to analyze the data in terms of possible Maxwellian distributions. This led to the equation

$$N=58\int_E^\infty 1.1E^{\frac{1}{2}}e^{-E}dE+47\int_E^\infty 0.13E^{\frac{1}{2}}e^{-0.25E}dE$$

which has been included as a smooth curve in the figure. Thus there are two energy groups, the first of 55 percent with a mean energy of 10^9 ev and the second of 45 percent with a mean energy of 4×10^9 ev. The energy distribution for a sample of 100 rays is $dN=62E^{\frac{1}{2}}e^{-E}dE+5.8E^{\frac{1}{2}}e^{-0.25E}dE$.

An analysis of the negative rays shows them to have only a low energy component which amounts to 67 percent of that group in the combined distribution. The positive rays, however, show the presence of both energy groups, and thus must include all of the higher energy group for the combined distribution as well as most of the 20 rays which Anderson and Neddermeyer[1] mention as having energies too high to measure.

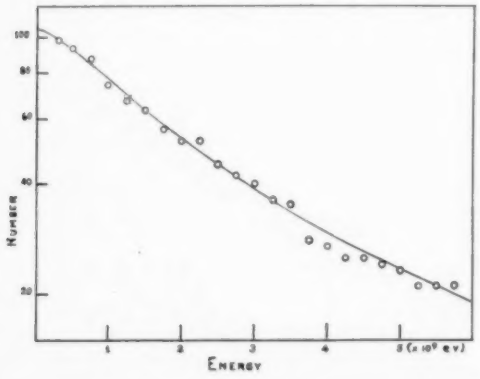

FIG. 1. Plot of log N against energy.

Thus a sample of 100 vertical cosmic rays will consist of 37 negative rays and 63 positive rays, the latter being divided into two groups of 18 in a low energy distribution and 45 in a higher energy distribution.

ANDREW LONGACRE

Phillips Exeter Academy,
Exeter, New Hampshire,
October 14, 1935.

[1] Anderson and Neddermeyer, Proc. London Conf. on Nuclear Physics (1934).
[2] Street, Woodward and Stephenson, Phys. Rev. **47**, 891 (1935).

On Relativity Corrections in the Theory of the Deuteron

Recently attempts have been made to compute the relativity correction in the theory of the deuteron.[1, 2] The calculations are based on the Gordon-Klein quadratic relativistic wave equation for a single particle with mass equal to the reduced mass of the deuteron. This equation should give correctly the order of magnitude of the relativity correction to the depth of the neutron-proton potential well; nothing more has been claimed for it. Actually a relativity correction can be computed in a straight-forward manner without recourse to an artificial single particle model.

From the classical relativistic kinetic energy

$$Mc^2\{(1+(P_1/Mc)^2)+(1+(P_2/Mc)^2)-2\} \cong(P_1^2+P_2^2)/2M-(P_1^4+P_2^4)/8M^3c^2 \quad (1)$$

we obtain the modified Schroedinger equation

$$\{\Delta_1+\Delta_2+(2M/\hbar^2)(E+J(r_{12})) +(\hbar/2Mc)^2(\Delta_1\Delta_1+\Delta_2\Delta_2)\}\psi=0, \quad (2)$$

in which the last term is the relativity correction to the kinetic energy correct to terms in $1/c^2$. Introducing the obvious assumption that the center of gravity is at rest, Eq. (2) becomes

$$\{\Delta+(M/\hbar^2)(E+J(r))+(\hbar/2Mc)^2\Delta\Delta\}\psi=0. \quad (3)$$

To estimate the effect of the correction term we make use of the Hermitian property of the operator Δ:

$$(\hbar^4/4M^2c^2)\iiint\psi\Delta\Delta\psi d\tau=(\hbar^4/4M^2c^2)\iiint(\Delta\psi)^2d\tau \cong(1/4Mc^2)\iiint\psi(E-J)^2\psi d\tau. \quad (4)$$

Thus the energy correction has the same form, but is only one-fourth as large as in the quadratic relativistic wave equation for the artificial single particle model. If this factor of one-fourth is considered in connection with the actual numerical estimates[1, 2] of the relativity correction given by the single particle model, it is evident that the energy correction is entirely negligible for the effective range of the forces (about 2.25×10^{-13} cm) which appears to fit best the binding energies of H^3 and He^4. It is not difficult to compute the corresponding energy corrections in the 3 and 4 particle problems. The numerical results are $\Delta E(H^3)\sim-0.2mc^2$, $\Delta E(He^4)\sim-0.9mc^2$.

EUGENE FEENBERG

Institute for Advanced Study,
Princeton University,
September 14, 1936.

[1] D. Blochinzew, Physik Zeits. Sowjetunion **8**, 270 (1935).
[2] H. Margenau, Phys. Rev. **50**, 342 (1936).

Comparison of Majorana-Heisenberg and Velocity-Dependent Forces

Breit has recently shown[1] that the specific interaction between like particles required to account for proton scattering is substantially equal to the neutron-proton interaction in ^1S states and has the magnitude which one deduces independently from the energies of the ^1S (virtual) and ^3S states of the deuteron and the binding energies of H^3 and He^4. That three constants, a, B_1, and B_3 (giving the range of nuclear forces and the strength of the interaction in singlet and triplet states) can be adjusted to give a satisfactory fit to the four experimental values $E_1(H^2)=-2.15$, $E_3(H^2)=+0.13$, $E(H^3)=-8.3$, $E(He^4)=-27.6$, furnishes the best available support for present nuclear theory.

We wish to point out that this agreement with experiment does not furnish a specific argument for the Majorana-Heisenberg type of force on which the derivation was based. This fact is illustrated most simply by assuming that the heavy particle interaction is not of the M-H form but has a different dependence on velocity, given by[2] $J_0(r,\rho)=-B(2/a)e^{-(r+\rho)/a}$ ($B=B_1$ or B_3 according as the wave function is symmetric or antisymmetric in the spins of the two particles). B_1 and B_3 in the table are obtained for various values of a by exact solution of the wave equation which determines $E_1(H^2)$ and $E_3(H^2)$. With these values of the B's, the binding energies of $E(H^3)$ and $E(He^4)$ are calculated by a modified equivalent two-body method.[3] We obtain the best agreement with experiment for $a=1.17\times10^{-13}$ cm, $B_1=26.2$ MEV, $B_3=48.3$ MEV. The fit (to five percent for H^3, three percent for He^4) is of the same order as given by the Majorana-Heisenberg theory for an interaction $-\mathrm{Be}^{-r^2/a^2}$ (with $a=2.32\times10^{-13}$, $B_1=21.0$ MEV, $B_3=34.1$[4]), and is within the probable error of the equivalent two-body method.

The order-of-magnitude agreement of the constants derived on the M-H theory and on the basis of a simple form of velocity dependent interaction, gives some justification for concluding that estimates of the magnitude (and to a lesser extent, the range) of nuclear forces are essentially independent of the special assumption one makes as to the *type* of these forces.

TABLE I. *Strength and range of velocity-dependent forces required to account for the virtual and stable levels of H^2 and the binding energies of H^3 and He^4.* Energies in MEV; E', uncorrected for Coulomb forces; C, Coulomb correction; a in units of 10^{-13} cm.

				$-E(He^4)$ (27.6 exp.)		
a	B_1	B_3	$-E(H^3)$ (8.3 exp.)	$-E'$	C	$-E$
2.86	3.52	13.7	3.7	11.1	0.55	10.5
2.33	5.66	17.8	4.2	13.2	.67	12.5
2.03	7.85	21.5	4.7	15.2	.76	14.4
1.66	12.3	28.5	5.6	19.2	.92	18.3
1.44	16.9	35.3	6.4	22.7	1.04	21.7
1.28	21.5	41.8	7.1	26.0	1.15	24.8
1.17	26.2	48.3	7.9	29.7	1.22	28.5
1.08	31.0	54.5	8.7	33.2	1.28	31.9
1.01	35.6	60.9	9.4	36.8	1.34	35.5

K. WAY
JOHN A. WHEELER

University of North Carolina,
Chapel Hill, North Carolina,
July 25, 1936.

[1] Reported at the Gibson Island Conference on Nuclear Structure, June, 1936.
[2] Cf. John A. Wheeler, this issue for notation and discussion of velocity dependent forces.
[3] Cf. Bethe and Bacher, Rev. Mod. Phys. **8**, 143 (1936) for a description of the general procedure. We follow a method similar to method (a), p. 144.
[4] Bethe and Bacher, reference 3, Table III p. 111 and Eq. (128) (these values are based on the value $E=0$ for the virtual level of H^2 and do not assume exact equality of the like particle ($B_1=21.0$) and unlike particle ($B_1=20.5$) interaction in singlet states).

Energy Levels in Crystals of Samarium Salts

It was reported at the Washington meeting of the Physical Society in April that many of the absorption lines of solutions and crystals containing rare earth ions may be identified as forbidden transitions from the ground states to higher multiplets of the normal electronic configurations, ($4f^6$). It was further shown that the *structure* of the Gd groups ($^8S_{3\frac{1}{2}}$–^6I) observable in crystal absorption[1] is interpretable in terms of the expected splitting of the atomic levels by the internal crystal field.

An analysis of the published data[2] on the absorption of salts of Sm has now been partially completed. The more than fourfold increase in the number of lines in a close group in Sm over the number in similar groups of Gd, especially at liquid hydrogen temperatures, at once suggests that some other agency is here effective in addition to crystal field splitting. The successive repetition of the pattern of the strong lines at the bottom of a group as sets of weaker lines displaced about 20, 40, 60, 80 and 100 cm^{-1} to the violet points to the coupling of a set of vibrational (?) levels to the crystal field levels. Evidence for this fundamental frequency of about 20 cm^{-1} is to be found in each of the four Gd salts for which data are available and also in europium sulphate.[3] Its origin is still uncertain. In addition, higher coupling frequencies are present which seem to be different for each compound. Thus the strongest of these for samarium ethylsulphate (hydrated) is about 345 cm^{-1}. In a given group of the spectrum only certain ones of the coupling frequencies are observable; rarely is the complete set present at once.

A detailed discussion of the absorption of the Gd, Sm and Eu ions in crystals will be presented shortly.

CECIL B. ELLIS

University of Michigan,
Ann Arbor, Michigan,
September 1, 1936.

[1] Spedding and Nutting, J. Am. Chem. Soc. **55**, 496 (1933).
[2] Spedding and Bear, Phys. Rev. **46**, 308 (1934).
[3] Meehan, J. Chem. Phys. **3**, 621 (1935).

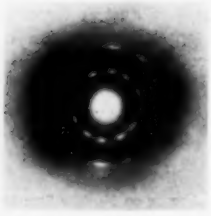

FIG. 1. Diffraction pattern from a foil consisting of 50 compressed layers of stearic acid. Electron beam direction normal to foil. ($\lambda = 0.072$A.)

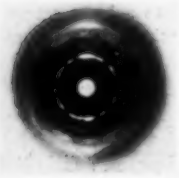

FIG. 2. Pattern from a foil of 21 compressed layers of barium-copper stearate. Beam direction normal to foil. ($\lambda = 0.064$A.)

FIG. 3. Foil of Fig. 2 inclined 45° to beam direction. ($\lambda = 0.064$A.)

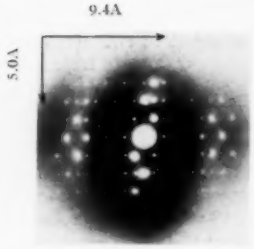

FIG. 4. Pattern from a single crystal of stearic acid about 1.5×10^{-5} cm thick. ($\lambda = 0.054$A.)

Electron Diffraction by Films Built from Many Monomolecular Layers

Dr. Irving Langmuir and Dr. Katharine Blodgett have kindly supplied us with films consisting of multiple compressed layers of stearic acid and of mixed barium and copper stearates[1] for examination by electron diffraction. Each of these films was loosened from its glass slide by a drop of dilute sulphuric acid according to a technique described to us by Mr. Vincent J. Schaefer. A loosened film was floated upon a water surface, and mounted from the water over a slit 0.05 mm in width.

Electron diffraction patterns produced by films prepared in this manner are shown in Figs. 1, 2 and 3. The fact that Figs. 1 and 2 are symmetrical spot patterns is proof that the molecules in the compressed layers are regularly arranged—that they form two-dimensional crystals. It is proof also that the orientations of these crystals, which together form the film, are not random—that they form, perhaps, a single three-dimensional crystal. This is not, however, the normal crystal of stearic acid.

For purposes of comparison we have reproduced in Fig. 4 a diffraction pattern produced by a single crystal of stearic acid obtained by evaporation from dilute benzene solution. From the locations of the spots of this figure we have discovered that the structure of the crystal is that of the monoclinic alpha modification, and we have determined precisely the orientation with respect to the photographic plate. It turns out that the (001) plane is inclined to the plate by only 8°, the arrows in Fig. 4 representing the projections of the *a* and *b* axes.

The patterns produced by the films of compressed layers are entirely different. We are as yet unable to interpret them.

K. H. STORKS
L. H. GERMER

Bell Telephone Laboratories, Inc.,
New York, N. Y.,
September 2, 1936.

[1] Blodgett, J. Am. Chem. Soc. **57**, 1007–1022 (1935). Examination of these films by x-rays has been described by Holley and Bernstein, Phys. Rev. **49**, 403 (1936).